Master's Theses and Capstones   Student Scholarship

Winter 2009

Are the world's oceans optically different?

Mimi Szeto
University of New Hampshire, Durham

Follow this and additional works at: https://scholars.unh.edu/thesis

ARE THE WORLD'S OCEANS OPTICALLY DIFFERENT?

BY

MIMI SZETO

B. A., Wellesley College, 2007

THESIS

Submitted to the University of New Hampshire
in partial fulfillment of
the requirements for the Degree of

Master of Science

in

Earth Sciences: Oceanography

December 2009

UMI Number: 1481722
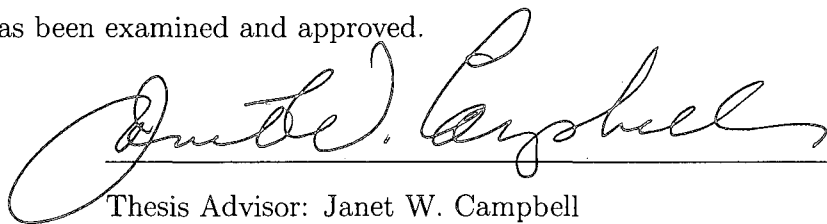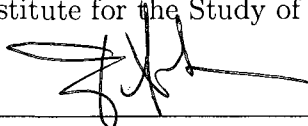
This thesis has been examined and approved.

Thesis Advisor: Janet W. Campbell

Research Professor of Earth Sciences

Institute for the Study of Earth, Oceans, and Space

Timothy S. Moore

Research Scientist

Institute for the Study of Earth, Oceans, and Space

John Ruairidh Morrison

Assistant Research Professor

Institute for the Study of Earth, Oceans, and Space

P. Jeremy Werdell

Oceanographer & Programmer Analyst

Ocean Biology Processing Group at NASA, Goddard
Space Flight Center

13 Nov 2009

Date

DEDICATION

This work is dedicated to my mom, my dad, and my sister Daisy.

ACKNOWLEDGMENTS

I am greatly indebted to the many people who have helped me along the way. I am very much grateful to have enjoyed the guidance of my main advisor Janet Campbell. Janet exposed me to the field of bio-optical oceanography by providing me with key literature and data as well introducing me to leading scholars. She has helped me see research's critical importance in society and has given me tremendous insight around what it means to be a scientist. She has always provided tactfully candid advice to me, and I am blessed for the opportunity to train under her supervision.

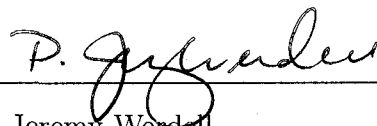I would also like to give much thanks to my advisor Tim Moore for his help with all the details, for his friendship, and for his constant reminders to go at my own pace and enjoy the journey. Additionally, I am grateful for his patience in teaching me Matlab, which has since become my favorite muse. I could not have completed this thesis without his tutelage.

In addition, I would like to thank my advisor Jeremy Werdell for his energetic guidance during my internship with the Ocean Biology Processing Group at NASA and his mentorship even after I left. Jeremy has constantly helped maintain my positive attitude despite some setbacks; one of the first pieces of advice he offered me was to never forget how far we've come along. In addition, he is responsible for consolidating the dataset I used.

I'd like to give thanks to my advisor Ru Morrison for instilling in me the significance of collecting data out at sea. From him, I have begun to understand the great deal of effort and funding required to take just a few samples of measurements from the ocean. Ru has also been crucial to strengthening my experience in Matlab programming.

Along with my advisors, special thanks goes to the OPAL faculty and staff for their companionship, and for the collection of the COOA dataset, a complicated

iv

TABLE OF CONTENTS

List of Tables

List of Figures

ABSTRACT

ARE THE WORLD'S OCEANS OPTICALLY DIFFERENT?

by

Mimi Szeto

University of New Hampshire, December, 2009

With satellite technology, the dynamics of oceanic photosynthesis can be analyzed on a global scale using remotely sensed estimates of chlorophyll concentration. Such work is dependent on the performance of empirical ocean color algorithms that produce the chlorophyll estimates. In hopes to understand the sources of algorithm uncertainty, the NASA bio-Optical Marine Algorithm Data set (NOMAD) was analyzed. The OC4v.4 algorithm estimates were compared to NOMAD's *in situ* measurements, and a bias was apparent when the data were sorted by ocean (Atlantic, Pacific, and Southern). Several instrumental artifacts were found to be insignificant to the oceanic algorithm bias. Using a subset of NOMAD that contained absorption measurements with each observation, the oceanic bias was independently verified, and explained through differences in the concentration of non-algal organic matter and the phytoplankton community structure. Ultimately, the world's oceans were found to be optically different as a result of differences in biogeochemical processes.

CHAPTER 1

INTRODUCTION

As primary producers of biomass in the ocean, phytoplankton serve an important role in the biosphere. Through photosynthesis, they transform the sun's energy into chemical energy that can be consumed in marine ecosystems. In this manner, they maintain the livelihood of heterotrophic marine organisms and influence the chemistry of the surface waters, thereby impacting the biogeochemical processes in the oceans. With the aim of understanding the ocean's contribution to the global carbon cycle and the dynamics of marine ecosystems, oceanographers have developed global models for primary productivity (the rate at which phytoplankton perform photosynthesis), all of which currently require a quantity for the autotrophic biomass standing stock in the ocean. Using satellite sensors and ocean color algorithms, oceanographers measure the reflected light from the ocean surface and translate it to estimate the biomass standing stock. Consequently, consistent satellite measurements of ocean color across the planet have enabled our ability to quantitatively estimate primary production through these models.

Such satellite technology is founded on the principles of light propagation through the surface layer of the ocean and the inherent manner in which the materials in the ocean absorb or scatter the incidental light. Absorption converts light into other forms of energy such as heat or chemical energy, and scattering changes the direction of light. The unique optical behavior of different constituents in the water depends on the particular material's composition and abundance.

From the influx of visible light propagating through seawater, most of it is either absorbed or scattered downward by phytoplankton, detritus, or dissolved organic matter, and only a small portion returns to the surface (scattering upward). The

1

light reflected through the surface can then be measured both at sea with radiometers and from space with a satellite sensor.

Through decades of research, oceanographers have developed the mathematical groundwork at sea for relating the light reflected at the surface to the absorption and scattering of light by the ocean water and all its components. With the goal of estimating primary productivity, efforts have been made to empirically relate the amount of reflected light to near-surface chlorophyll-a concentration (Chl). The chlorophyll-a pigment, ubiquitous in all species of phytoplankton, reflects green light in a predictable manner, and so it serves as the indicator for phytoplankton biomass in primary production models. Coincident observations of the amount of reflected light and Chl from the world's oceans then form the basis for global empirical ocean color algorithms such as the OC4v.4 and the OC3M, used for the SeaWiFS and MODIS Aqua sensors, respectively (O'Reilly et al., 2002). Additionally, satellite-derived estimates for the absorption and scattering properties are currently approached via semi-analytical algorithms, established from theoretical assumptions of the relationship between the reflected light and the scattering and absorption properties (e.g., Garver and Siegel (1997)).

Satellite technology has transformed our understanding of the ocean's surface processes, but much work has yet to be done to improve the accuracy of the satellite-derived bio-optical properties. An assessment of the accuracy of empirical algorithms contributes to an assessment of the accuracy of higher order productivity algorithms as well as for time-series evaluations based on satellite data from the past three decades (Moore et al., 2009). Empirical global algorithms currently offer the best performance for global analyses, but they are criticized for having minimal theoretical foundation (O'Reilly et al., 2002). Semi-analytical algorithms rely on a theoretical framework, but perform no better and sometimes worse than empirical algorithms (O'Reilly et al., 2002).

Current empirical algorithms were developed to perform only in open-ocean waters where it is probable that the biomass co-varies with the non-living matter. Moore et al. (2009) have recently validated the algorithm performance, claiming that the bio-optics community's desired 35% accuracy (Mcclain et al., 2006; Bailey and

2

Werdell, 2006; Hooker et al., 1992) has been met for much of the world's open-ocean waters containing low levels of biomass. Inaccuracies remain in coastal waters and high-latitude regions where the assumption that biomass co-varies with non-living matter does not hold, where seasonal variability affects the surface ocean's optical behavior, and where the 35% accuracy threshold is not met.

This study entails the evaluation of NOMAD (NASA bio-Optical Marine Algorithm Data set), a global bio-optics *in situ* dataset, with the goal of improving our understanding of the global empirical algorithm uncertainty. In particular, this work aims to explain the mismatch between *in situ* and satellite-based measurements using corresponding measurements of absorption now available in the second version of NOMAD. Based on the community's literature and an analysis of the NOMAD dataset (Szeto et al., 2006), I hypothesize that an ocean bias exists in the empirical algorithms, and that it can be explained by systematic variation in the abundance of non-algal dissolved and particulate matter, and the phytoplankton community structure as described by the dominant cell size and pigment packaging. This hypothesis is consistent with the past literature on regional-scale studies, but it has never before been tested on a global scale.

CHAPTER 2

BACKGROUND

2.1 A brief history of U.S. ocean color satellites

The first global ocean color data (in 1978) from the Coastal Zone Color Scanner (CZCS), on the NASA NIMBUS-7 satellite, provided bio-optical oceanographers with an unimaginable wealth of observations (Gordon et al., 1983; Hovis et al., 1980). Subtle but detectable variations in ocean color changed the simple notions oceanographers had about meso-scale eddies in the open ocean, thermal and shelf-edge fronts, and large-scale patchiness in algal blooms (Hovis et al., 1980). With a correction for the atmospheric influence, the first satellite measurements translated to estimates of *Chl* were within 0.5 log *Chl* of corresponding *in situ* measurements (Gordon et al., 1983). CZCS observations continued until sensor degradation interfered in 1986 (Evans and Gordon, 1994).

In 1997, the Sea-viewing Wide Field-of-view Sensor (SeaWiFS) (Figure 2-1) was launched on the OrbView-2 satellite, allowing ocean color observations to resume (Hooker et al., 1992). NASA also launched the Moderate Resolution Imaging Spectroradiometer (MODIS) sensors in 1999 on the Terra satellite and in 2002 on the Aqua satellite (Lee and Carder, 2002). Both sensors have 1 km^2 resolution (for Sea-WiFS it is actually 1.1 km^2 at the nadir-viewing angle) and measure reflectance at specific bands centered at the wavelengths shown in Table 2.1. These wavelengths were chosen to specifically capture certain absorption and scattering properties of the organic matter in the surface ocean and the atmosphere above it. Previous research had shown that algorithm performance is not improved by including other wavelengths in the detection scheme (Sathyendranath et al., 1989; Lee and Carder, 2002).

The development of satellite-derived *Chl* has led to global estimates of primary production ranging from 36.5 to 48.5 Gt C yr^{-1}, depending on different assumptions and models (Palmer and Totterdell, 2001). Figure 2-1 shows a climatological mean *Chl* from SeaWiFS (1997-2008). Besides primary productivity (Behrenfeld and Falkowski, 1997a), ocean color has been used to estimate other properties including the global euphotic depth, the diffuse attenuation coefficient for downwelling irradiance (Loisel and Stramski, 2000), and the abundance and character of non-algal matter in the oceans (Garver and Siegel, 1997).

2.2   The foundation of ocean color algorithms

It is instructive to explain the fundamentals of radiative transfer theory in order to discuss ocean color algorithms in detail. Along with the references specifically cited, the explanation is adapted from Kirk (1994b).

Radiation from the sun consists of electromagnetic (EM) packets of radiant energy, called photons or quanta. These photons exhibit the properties of waves, and so they vary by wavelength (λ), which describes the distance per cycle. The amount of energy within each packet varies inversely with the wavelength. In the EM spectrum, wavelengths range from 10^{-3} to 10^{12} nm per cycle, and from high to low energy yield per photon, respectively. Photons traveling between 400 and 700 nm per cycle are visible as colors following the order of a rainbow, from violet to red, respectively.

Photons reaching the Earth's atmosphere and ocean surface interact with constituents in the respective media. These constituents either absorb or scatter the radiant energy. In absorption, the light energy changes to another form of energy such as heat or chemical energy. In scattering, the photons change in direction. Different wavelengths of light, and hence different colors, absorb at different intensities and scatter at different intensities into different directions. The unique composition and abundance of the medium's constituents govern these properties. Consequently, the light field in the particular medium indirectly reveals the absorption and scattering processes, and thereafter, the potential characterization of the constituents.

2.2.1 Terms to describe light in a medium

Models for quantifying the extant light and the absorption and scattering behaviors of the various types of matter in the atmosphere and sea have been developed to investigate this phenomenon mathematically. Apparent optical properties (AOP) describe the extant light, while inherent optical properties (IOP) describe the absorption and scattering behaviors (Preisendorfer, 1960). Note that all the following concepts are spectrally dependent, meaning they vary by wavelength, and so they are measured as spectra.

AOPs

The AOPs are derived from measured quantities for the radiant flux, which is the flux of photons. The radiant intensity is the radiant flux in a specified direction. The specified point is described as (z,θ,φ). The terms z, θ, and φ, describe the direction of the path with respect to the Earth's surface. The depth z defines the closest distance to the surface. The zenith angle θ defines the direction from the vertical axis at depth z, and the azimuth angle φ defines the direction from a specified horizontal axis. See Figure 2-2.

Consider the radiant intensity towards a certain point (z,θ,φ). In constraining the space around the direction of flow with a solid angle (ω) at that point, the radiant flux within the space is defined as the radiance (L). See Figure 2-3. This value is measured as W steradian^{-1} nm^{-1} or quanta s^{-1} steradian^{-1} nm^{-1}. In considering the solid angle that covers an entire hemisphere (2π steradian), the radiance then essentially describes the radiant intensity traveling through the horizontal plane at point (z,θ,φ), and is referred to as irradiance, E. This value is measured as W m^{-2} nm^{-1} or quanta s^{-1} m^{-2} nm^{-1}.

Irradiance is often considered for the radiant intensity in the downwelling or upwelling directions, (denoted as E_d and E_u, respectively). Taking the ratio of E_u to E_d gives the reflectance (R), an AOP that describes the flux of light reflecting upward relative to the flux of light scattered downward from a point.

Another AOP is K_d, the diffuse attenuation coefficient for downwelling irradiance. It describes the strength in light attenuation, which varies with the turbidity of the medium. The following equation explains its derivation from radiometric quantities.

$$\frac{ln\frac{E_d(0)}{E_d(z_1)}}{z_1} = K_d \qquad (2.1)$$

where $E_d(0)$ is E_d at the surface and $E_d(z_1)$ is E_d at depth z_1.

IOPs

The IOPs are measured within a collimated beam of light with a quantifiable pathlength. The absorbance and scatterance indicate the intensity at which light is absorbed and scattered, respectively, relative to the radiant flux within the beam. Attenuance indicates the relative intensity at which the light is absorbed or scattered away from the beam. To relate these properties to the scale of L and E at a point in space, oceanographers consider the absorption (a), scattering (b), and beam attenuation (c) coefficients, which are the derivatives of absorbance, scatterance, and attenuance, respectively, with respect to the pathlength. The beam attenuation coefficient (c), is equivalent to the sum of the absorption (a) and scattering (b) coefficients.

In particular, the scattering in the backwards direction, b_b, is pertinent to ocean remote sensing. The backscattering coefficient b_b is rigorously defined in terms of the volume scattering function (VSF), $\beta(\theta,\lambda)$, where θ is the scattering angle, and λ is the wavelength (Mobley, 1994). For a collimated beam of light traveling through a thin layer of a medium, $\beta(\theta,\lambda)$ describes the scattered radiant intensity into the scattering angle θ per unit irradiance of the incident light within the layer per unit volume of the medium (Kirk, 1994b; Mobley, 1994; Stramski et al., 2004). The backscattering coefficient b_b is equivalent to the integration of $\beta(\theta,\lambda)$ over the backward directions, $\pi/2 \leq \theta \leq \pi$:

$$b_b(\lambda) = 2\pi \int_{\frac{\pi}{2}}^{\pi} \beta(\theta, \lambda) \sin\theta \, d\theta \qquad (2.2)$$

The terms 2π and $\sin\theta$ represent the integration over the azimuth angle, which is assumed to be symmetric about the incident direction of the collimated beam.

2.2.2 Application of the terms

These concepts then allow for the consolidation of the interactions between photons and the constituents of a medium within a linear narrow path of length r, as expressed in the equation of radiative transfer:

$$dL(z, \theta, \varphi)/dr = -c(z)L(z, \theta, \varphi) + L^*(z, \theta, \varphi) \qquad (2.3)$$

Here, the change in L with respect to the infinitesimal path of length dr, is defined as a linear combination of the reduction of light as it is scattered away from the path or absorbed, represented by c, and the addition of light as it is scattered into the path from all directions, denoted as $L^*(z, \theta, \varphi)$. The expression is also illustrated in Figure 2-4.

A third term representing chlorophyll fluorescence at approximately 685 nm and Raman scattering by seawater molecules can be added to the right-hand side for accuracy (Gordon, 1989; Stramski et al., 2004). Fluorescence refers to the process in which the chlorophyll-a pigments re-emit incoming photons at a wavelength near 685 nm. Raman scattering refers to scattering that changes the direction of a photon as well as its wavelength. Both fluorescence and Raman scattering are called inelastic scattering because they involve both a change in energy (equivalent to wavelength) and direction.

2.2.3 Application to remote sensing

Bio-optical oceanographers rely on Earth-observing satellites containing sensors that routinely measure radiance emanating from the atmosphere and the ocean.

The goal is to extract the water-leaving radiance (L_w), which is equivalent to L_u at z=0 just above the surface. Complicated evaluation processes are required to detect and remove other portions of the signal, including the radiance scattered from the atmosphere (a portion that often exceeds 90% of the signal) and the boundary surface between the ocean and the atmosphere. The water-leaving radiance, L_w, varies with viewing and solar zenith angle, and with atmospheric conditions. To correct or remove such variation, it is transformed to the normalized water-leaving radiance nL_w. For nL_w, the sun is considered directly overhead, and the atmosphere is considered non-existent. Originally, the normalization was performed using the work of Gordon and Clark (1981). This publication first introduced the term normalized-water-leaving radiance, defined as the following:

$$nL_w = \frac{L_w}{E_d(0_+)} F_0 \qquad (2.4)$$

where F_0 is the solar incident irradiance at the top of the atmosphere (or the mean extraterrestrial solar irradiance), and $E_d(0_+)$ refers to E_d at z=0 just above the surface, commonly denoted as E_s. Today, this normalization is based on the work of Morel and Gentili (1991, 1993, 1996) and Morel et al. (2002).

Various above- and in-water techniques are used to measure corresponding values of L_w at sea. Note that optical measurements often have subscripts u or d to represent the upward and downward direction, respectively. For above-water L_u, the measurement is made a small distance above the surface and includes the diffuse sky light reflected off the surface, which must be subtracted to derive L_w. For in-water L_u, measurements at several depths are collected and extrapolated to just below the surface; the extrapolated value is denoted as $L_u(0_-)$(Werdell and Bailey, 2005). Then to obtain L_w, $L_u(0_-)$ is multiplied by t_u and η^{-2}, where t_u is the upward Fresnel transmittance of the air-sea interface ($\sim$0.975), η is the refractive index of seawater (Austin, 1974).

Methods for measuring E_d are similar to those for measuring L_u. For in-water E_d, $E_d(0_-)$ is multiplied by t_d^{-1} to obtain E_s, where t_d is the downward Fresnel irradiance transmittance across the air-sea interface($\sim$ 0.96) (Mueller et al., 2003b).

L_u is normalized by a corresponding *in situ* measurement of downwelling irradiance, E_d, a calculation that implicitly accounts for the influences of the solar zenith angle. The end product is known as the remote sensing reflectance, R_{rs}, and is quantified in sr^{-1}. The ratio of nL_w at two wavelengths is approximately equal to the ratio of *in situ* R_{rs} at the same wavelengths. Slight differences are due to the wavelength dependence of F_0. Subsurface values for R_{rs} are denoted as r_{rs}, and the translation from below- to above-water is approximately non-spectral (Austin, 1974).

2.3 R_{rs} as a function of IOPs

In relating the remote sensing reflectance, an apparent optical property, to the IOPs, the following relationship is commonly used (Gordon et al., 1975; Gordon and Morel, 1983; Morel and Prieur, 1977).

$$r_{rs}(\lambda) \sim \frac{b_b(\lambda)}{a(\lambda) + b_b(\lambda)} \tag{2.5}$$

This can be viewed as an expression of the probability that a photon entering the ocean is backscattered to the surface, since the fate of any such photon is either to be absorbed within the medium, or backscattered to the surface. Equation 2.5 states that the subsurface remote sensing reflectance is proportional to this "probability." Assuming that sea-air transmittance is non-spectral, the same statement can be made about above-water reflectance, R_{rs}, and is often the basis for semi-analytic algorithms.

A proportionality factor, g, is used to relate the left- and right-hand sides. The term g depends on the radiance distribution over all directions and the VSF in the backward direction (Gordon et al., 1988). Zaneveld (1995) presents a thorough explanation of the theory behind the dependence, work that is based on the measurements and models of Gordon et al. (1988), Morel (1988), and Gordon (1989). Most models assume that the in-water materials absorb much more than they backscatter ($b_b \ll a$), and such models perform well mainly in oligotrophic regions in which

phytoplankton biomass co-vary with the non-algal matter (Morel and Prieur, 1977). Morel and Prieur (1977) label this type of water as *Case 1*, while *Case 2* refers to water that contains non-algal materials that do not covary with the algal matter. This type is usually found in coastal waters.

2.3.1 Partitioning the IOPs

The terms $a(\lambda)$ and $b_b(\lambda)$ of Eqn. 2.5 can be partitioned into absorption by seawater, phytoplankton, non-algal particles, and colored dissolved organic matter, and backscattering by seawater and particles. Each component is further defined by a magnitude and spectral shape (Hoepffner and Sathyendranath, 1993; Roesler and Perry, 1995; Roesler et al., 1989). The magnitude varies with the concentration, and the spectral shape describes how the material absorbs or scatters for all the visible wavelengths, based on its composition. For instance, the spectral shape of backscattering depends on the size distribution, the refractive index, the structure and the mean shape of the particles in a water sample (Loisel et al., 2007). See Figure 2-5 for the examples of the IOP spectra.

Absorption

Colored dissolved organic matter and non-algal particles. The category non-algal particles (NAP) is composed of bacteria, viruses, biological degradation products (including phytoplankton shells), inorganic particles (e.g., clay minerals, feldspars, quartz, calcite), and mixed organic-inorganic structures (Stramski et al., 2004). Colored dissolved organic matter (CDOM) is formed from the degradation of living organisms from both terrestrial and aquatic origins. The biological decay processes primarily include direct excretion from phytoplankton, zooplankton, and bacteria, release during zooplankton grazing due to sloppy feeding, and viral lysis (Nelson and Siegel, 2002), and less likely by percolation from zooplankton fecal pellets (Steinberg et al., 2004).

NAP and CDOM both absorb predominantly in the blue with an exponential decrease towards the red. The similar absorption behaviors of these two components

makes the separation of their absorption terms difficult when attempting to invert Eqn. 2.5, translating Rrs to the IOPs. While several different formulations have been developed (Twardowski et al., 2004), the absorption term has been commonly described as the following (Jerlov, 1976; Prieur and Sathyendranath, 1981; Bricaud et al., 1981; Mobley, 1994):

$$a_{comp}(\lambda) = a_{comp}(\lambda_0) \exp(-S(\lambda - \lambda_0)) \tag{2.6}$$

The subscript *comp* reflects that the equation applies for CDOM, NAP, or both combined (denoted as CDM). The term $a_{comp}(\lambda_0)$ describes the magnitude of absorption at a reference wavelength λ_0, and the exponential term S describes the spectral shape, which for CDOM, varies with the chemical composition (Kitidis et al., 2006; Stedmon and Markager, 2001). CDOM from open-ocean waters reflects a biological signature acquired over a long period of time (Bricaud et al., 1981). CDOM from coastal areas may better reflect a strong terrestrial input (Bricaud et al., 1981; Nelson and Siegel, 2002).

CDOM has been shown to serve several important roles in biogeochemical processes. It has influence on the steady-state concentrations of free radical species, and so it affects the photo-reactivity of surface waters (Dister and Zafiriou, 1993; Mopper and Zhou, 1990). It is subjected to photo-oxidation, a process that yields CO_2 and CO from the breakdown of dissolved organic carbon (Miller and Zepp, 1995; Riemer et al., 2000; Valentine and Zepp, 1993; Clark et al., 2002). CDOM chelates phytoplankton nutrients, such as ammonium and nitrite, and it is important in the photochemical cycling of Fe (Bushaw et al., 1996; Bushaw-Newton and Moran, 1999; Gao and Zepp, 1998; Kieber et al., 1989, 1999; Moran and Zepp, 1997). CDOM protects phytoplankton from damaging UV radiation at the surface (Arrigo and Brown, 1996), but reduces the light exposure to phytoplankton in deeper waters (Stedmon and Markager, 2001).

Phytoplankton. Phytoplankton contain photosynthetic and non-photosynthetic pigments that inherently absorb light at specific and distinct wavelength regions. The chlorophyll-a pigment resides in all phytoplankton, and so historically, it has

been used to indicate the phytoplankton biomass. The pigment absorbs efficiently in the blue and red regions of visible light (maxima at approximately 443 and 664 nm). Unlike the shape of CDM, the phytoplankton spectral shape cannot be universally defined by a simple parameter because pigment composition varies among phytoplankton species and with respect to nutrient and light availability. Variations among species are referred to as photoadaptation, in which the evolution of phenotypes have led to unique pigment-protein complexes for different species (Falkowski and Raven, 2007). Variations with respect to nutrient and light availability are referred to as photoacclimation (Falkowski and Raven, 2007). For instance, phytoplankton cells will utilize their accessory pigments to block their chlorophyll pigments from excess light in high irradiance conditions, and produce more chlorophyll pigments to increase their chances of absorbing light in low irradiance conditions (Falkowski and Raven, 2007).

The most common model to portray phytoplankton absorption is shown in the following equation (Mobley, 1994):

$$a_\phi(\lambda) = Chl\, a_\phi^*(\lambda) \tag{2.7}$$

Here, Chl represents the magnitude, and $a_\phi^*(\lambda)$, the chlorophyll-a-specific absorption coefficient, describes the spectral shape. Bricaud et al. (1995) defines $a_\phi^*(\lambda)$ as the following, with the unit as $m^2\ (mg\ Chl)^{-1}$.

$$a_\phi^*(\lambda) = A\, Chl^{-B} \tag{2.8}$$

A and B are spectrally-varying terms determined through a least-squares fit of measured Chl-normalized absorption and chlorophyll concentration. See Table 3 in Bricaud et al. (1995) for details. As a power-law function of Chl, this approach to modeling the spectral shape incorporates primarily the phenomenon of pigment packaging (Bricaud et al., 1995, 2004). Pigment packaging refers to the shading of pigments from light when confined in discrete cells as opposed to dispersed uniformly like in an *in vitro* solution (Morel and Bricaud, 1981). The shading causes absorption per chlorophyll pigment to diminish with increasing cell size, since a

sample with small cells better simulates a solution with uniform dispersion than a sample with large cells (Morel and Bricaud, 1981).

Seawater. Seawater, comprised of water molecules and ions, absorbs heavily in the red region and weakly in the blue region, due to different temperature-dependent intramolecular and intermolecular forces (Morel, 1974). Smith and Baker (1981) attempted to derive a maximum seawater absorption by subtracting, b_{bw}, measured backscattering due to seawater, from measured K_w, the diffuse attenuation coefficient for the clearest natural freshwaters. Sogandares and Fry (1997) and Pope and Fry (1997) updated that work using two independent techniques: the photothermal method (Sogandares and Fry, 1997), in which the energy removed from the incident light field is converted to thermal energy and then measured, and the integrating cavity method (Pope and Fry, 1997), in which all energy removed from the incident light field is directly measured using optical fibers. Figure 2-5 displays the results from Pope and Fry (1997).

Backscattering

Particles. Similar to CDM absorption, particle backscatter occurs strongest at 400 nm and decreases towards higher wavelengths. Morel (1974) modeled the relationship as the following.

$$b_{bp}(\lambda) = b_{bp}(\lambda_0)(\lambda/\lambda_0)^{-\eta} \tag{2.9}$$

The exponent, η, describes the spectral shape for the backscattering of particles and $b_{bp}(\lambda_0)$ describes the magnitude at a reference wavelength λ_0. The spectral shape flattens out for larger particles as η approaches 0, and approximates molecular scattering for smaller particles as η increases ($\eta = 4.322$ for seawater). η also varies with particle size distribution, which is characterized by an inverse relationship between particle size and the concentration of the given size (Stramski et al., 2004).

Morel and Ahn (1991) and Stramski and Kiefer (1991) initially suggested that under non-bloom conditions, the particulate backscattering is predominantly at-

tributed to detrital matter and not phytoplankton. However, their models utilized homogenous spheres, while more recent models incorporating layered spheres, proved that phytoplankton have the capability to backscatter as strongly as detrital matter in clear waters (Kitchen and Zaneveld, 1992; Zaneveld and Kitchen, 1995) and this statement has been validated with empirical evidence (Vaillancourt et al., 2004). Stramski et al. (2004) provides an extensive review of the various contributions (colloids, bacteria, phytoplankton, biogenic detritus, minerogenic particles, and bubbles) to particulate scattering in the ocean.

Seawater. Morel (1974) has examined previous studies and established the total scattering coefficient for pure sea-water with salinity between 35 ‰ and 39 ‰. The backscattering coefficient for seawater is defined as half the total scattering coefficient, and this value has been considered as known (Stramski et al., 2004; Twardowski et al., 2005). However, the uncertainty in scattering by seawater may be greater than 10% with a strong dependence on salinity (Twardowski et al., 2007). The current widely-used spectra is displayed in Figure 2-5. The spectral value can also be expressed using Eqn. 2.9 with η as 4.322 (Morel, 1974).

2.3.2 The transformation of seawater R_{rs} with increasing organic matter

The following explanation was introduced by Morel and Prieur (1977). See Figure 2-6 for the graphical description. According to the known behavior of IOPs, clear waters with low concentrations of organic matter such as phytoplankton cells would yield an r_{rs} spectrum generally dominated in the lower blue wavelengths, since seawater absorbs strongly in the red region and backscatters strongly in the blue region.

With the assumption that $b_b \ll a$, changes in a will affect the r_{rs} spectrum more strongly than changes in b_b. Consequently, at first approximation, the addition of organic matter to the water will change the r_{rs} spectra according to the absorption behaviors of that organic matter, whether it is phytoplankton or colored detrital matter. Phytoplankton pigments absorb predominantly in the blue and red, and

colored non-algal matter absorbs strongly in the blue region. Both types of matter cause the dominant reflectance to shift towards greener wavelengths. As a result, oligotrophic clear blue waters in the open ocean differ from the eutrophic green waters of the coastal regions, which have larger concentrations of organic matter.

2.4 Types of algorithms

Morel and Gordon (1980) claim that ocean color algorithms can exist in three forms: empirical, semi-empirical (also known as semi-analytic), and analytic, but Sathyendranath et al. (1989) explain that the non-linearity within the system and similarities between optical signatures reduce the feasibility of the analytic type. Therefore, most algorithms are either empirical or semi-analytic (IOCCG, 2006). However, analytical simulations of the light propagation in the water have been established that rely on the radiative transfer equation to associate the IOPs to the diffuse attenuation coefficient for downwelling irradiance, K_d, and irradiance reflectance, R (Loisel and Stramski, 2000). These two AOPs can be calculated from *in situ* measurements of E_d and E_u, and estimated from remote sensing (Loisel and Stramski, 2000). Additionally, developments have been made to solve the radiative transfer of sunlight in ocean-atmospheric systems using successive-orders of scattering that may be implemented in ocean color algorithms in the future (Zhai et al., 2009).

2.4.1 Empirical algorithms

Empirical algorithms include the OC4v.4 for the SeaWiFS sensor (O'Reilly et al., 2002), the OC3M for the MODIS Aqua (O'Reilly et al., 2002), and the MERIS neural network algorithm (Doerffer and Schiller, 2000; Schiller and Doerffer, 2005; Doerffer and Schiller, 2007). The OC4v.4 and the OC3M are ratio algorithms that relate the R_{rs} to *Chl*, and they were formed from empirical analyses of corresponding measurements of *Chl*, L_w, and E_s at various locations (O'Reilly et al., 2002). These algorithms require the ratio of R_{rs} at two wavelengths in order to minimize the sensitivity to absolute measurment errors (e.g., atmospheric correction).

The ratio of nL_w at two wavelengths is proportional to the ratio of R_{rs}, calculated as L_w/E_s, measured *in situ* at the same wavelengths. In the OC4v.4 and OC3M algorithms, *Chl* is approximated through a fourth-order polynomial function of the R_{rs} ratio. The following equations refer to the OC4v.4 algorithm for the SeaWiFS sensor (O'Reilly et al., 2002; Carder et al., 1999):

$$\log_{10}(Chla) = 0.366MBR - 3.067MBR + 1.930MBR^2$$
$$+ 0.649MBR^3 - 1.532MBR^4 \tag{2.10}$$

where MBR is the Maximum Band Ratio defined by the following.

$$MBR = \log 10(max\,[R_{rs}443, R_{rs}490, R_{rs}510]\,/R_{rs}555) \tag{2.11}$$

The maximum of R_{rs} at 443, 490, and 510 serves to detect a valid signal in the blue region as the signal at 443 nm may be too weak in green waters. This value is divided by the R_{rs} at 555 nm, a green wavelength, which tends to be insensitive to the chlorophyll level. Then the base-10 logarithm of the value is input to the fourth-order polynomial, Eqn 2.10. The OC3M algorithm used for MODIS, is similar, only it selects the maximum of R_{rs} from two blue wavelengths (443 and 490 nm), since MODIS lacks a band at 510 nm (Lee and Carder, 2002).

For the neural network algorithm, an extensive dataset of IOPs and AOPs is used to train and validate a neural network to produce IOP estimates from measured AOPs (Doerffer and Schiller, 2000; Schiller and Doerffer, 2005; Doerffer and Schiller, 2007). Although they are currently implemented for MERIS, the European ocean color satellite, neural network algorithms will not be discussed in this work.

2.4.2 Semi-analytic algorithms

Semi-analytic algorithms employ some inversion from AOPs to IOPs through Eqn. 2.5, and the empirical relationships for the decomposition of a and b_b. They include the GSM Semi-Analytical Bio-Optical Model (GSM) (Garver and Siegel,

1997; Maritorena et al., 2002), the Quasi-Analytical Algorithm (QAA) (Lee et al., 2002), and the linear matrix inversion algorithm (Hoge and Lyon, 1996). For the development of the GSM and the linear matrix inversion, *in situ* values of r_{rs} at several satellite wavelength bands and the empirical approximations for the spectral shapes S, η, and a_ϕ^* are used to approximate the magnitudes a_ϕ, a_{cdm}, and b_{bp}. The IOPs for water are considered known. Eqn. 2.5 at several satellite wavelength bands forms a system of over-determined equations, and several optimization schemes can be attempted to estimate the IOP magnitudes. *Chl* can then be extracted from the estimated magnitude for phytoplankton absorption at 443 nm. The GSM algorithm uses the Levenberg-Marquardt optimization (Garver and Siegel, 1997; Maritorena et al., 2002), and a simulated annealing technique to tune the process (Maritorena et al., 2002). The algorithm by Hoge and Lyon (1996) uses the matrix inversion optimization. To apply these algorithms, nL_w measurements from satellites are normalized by F_0 to retrieve R_{rs}, and this is translated to the sub-surface r_{rs}.

The Quasi-Analytic Algorithm, QAA (Lee et al., 2002), employs a manipulation of Eqn. 2.5 and empirical approximations for total absorption at 555 nm and the spectral shape η in order to obtain values for total absorption and particle backscattering at all wavelengths. Then empirical approximations for $a_\phi 410/a_\phi 440$ and the spectral shape, S, are used to deconvolve the total absorption into its different parts.

2.4.3 Analytical methods for the IOP-Irradiance relationship

The analytical methods involve the numerical simulation of the radiative transfer equation through various techniques including the invariant embedding method, the Monte Carlo method, the discrete ordinate method, and the matrix-operator method (Zhai et al., 2009; Albert and Mobley, 2003; Boynton and Gordon, 2002; Chami and Robilliard, 2002; Loisel and Stramski, 2000; Gordon et al., 1975; Gordon, 1991; Kirk, 1981, 1994a). This approach requires an estimate of the VSF (Stramski et al., 2004), can account for a non-homogenous depth profile (Loisel and Stramski, 2000), and does not include the decomposition of a (Loisel and Stramski, 2000).

2.5 Assumptions in the implementation of chlorophyll algorithms

Upon using remotely sensed *Chl* estimates in biogeochemical and primary productivity models, as attempted by many (Eppley et al., 1985; Sathyendranath et al., 1995; Longhurst et al., 1995; Antoine et al., 1996; Behrenfeld and Falkowski, 1997b), several considerations have been made.

First, I discuss the concerns for estimating the greatest depth above which phytoplankton have access to light, known as the euphotic depth (z_{eu}). Due to regional variability in seawater turbidity, this depth is defined in terms of the strength in light attenuation. Specifically, z_{eu} is equivalent to 4.6 optical depths, where the optical depth is defined as the ratio of 1 over K_d. At z_{eu}, the light level has attenuated to $\exp(-4.6) = 0.01$ (or 1%) of the level at the surface.

Although z_{eu} is exactly defined, approximately 90% of a satellite sensor's nL_w signal is detected from the first optical depth (z_{90}), known as the "e-folding" depth (Gordon and Mccluney, 1975). Here, the light level has attenuated to $\exp(-1)=36.8\%$ of the level at the surface (Gordon and Mccluney, 1975). Ocean color chlorophyll algorithms are tuned to z_{90}, but primary productivity models require *Chl* estimates covering the entire euphotic layer (down to z_{eu}). Consequently, empirical methods were developed to estimate the average *Chl* for the entire euphotic layer from the satellite-derived reflectance measurements that originated mainly from the first optical depth (Morel, 1988; Morel and Berthon, 1989).

As part of this extrapolation, an assumption was made to describe the chlorophyll profile. Often in open-ocean waters, there exists a deep chlorophyll maximum, the depth at which *Chl* is the greatest, that falls below the first optical depth. Such issues have been problematic for obtaining accurate estimates of primary production (Stramska and Stramski, 2005).

Second, the estimated chlorophyll biomass represents a net result of production and the loss terms: grazing and respiration. The loss terms have been difficult to account for empirically. Sverdrup's 1953 critical depth hypothesis (Sverdrup, 1953)

employs a constant rate of respiration, and some production models follow suit (Behrenfeld and Falkowski, 1997a), while more complex ones rely on oxygen consumption experiments using dark and light bottles (Williams, 1998). Additionally, a change in standing stock can be viewed as either an actual change in net production or a possible vertical or horizontal redistribution of chlorophyll (Menesguen and Gohin, 2006).

Table 2.1: Wavelength range for MODIS, SeaWiFS, and CZCS (nm) adapted from
Martin (2004)

MODIS	SeaWiFS	CZCS
405-420	402-422	–
438-448	433-453	433-453
483-493	480-500	–
–	500-520	510-530
526-536	–	–
546-556	545-565	540-560
662-672	660-680	660-680
673-683	–	–
743-753	745-785	–
862-877	845-885	700-800

[mg/m**3] (Sep1997-Jan2009)
SeaWiFS Chlorophyll a concentration

0.08 0.1 0.2 0.3 0.4 0.5 0.6 0.7 1 2.5 10 30

Generated by NASA's Giovanni (giovanni.gsfc.nasa.gov)
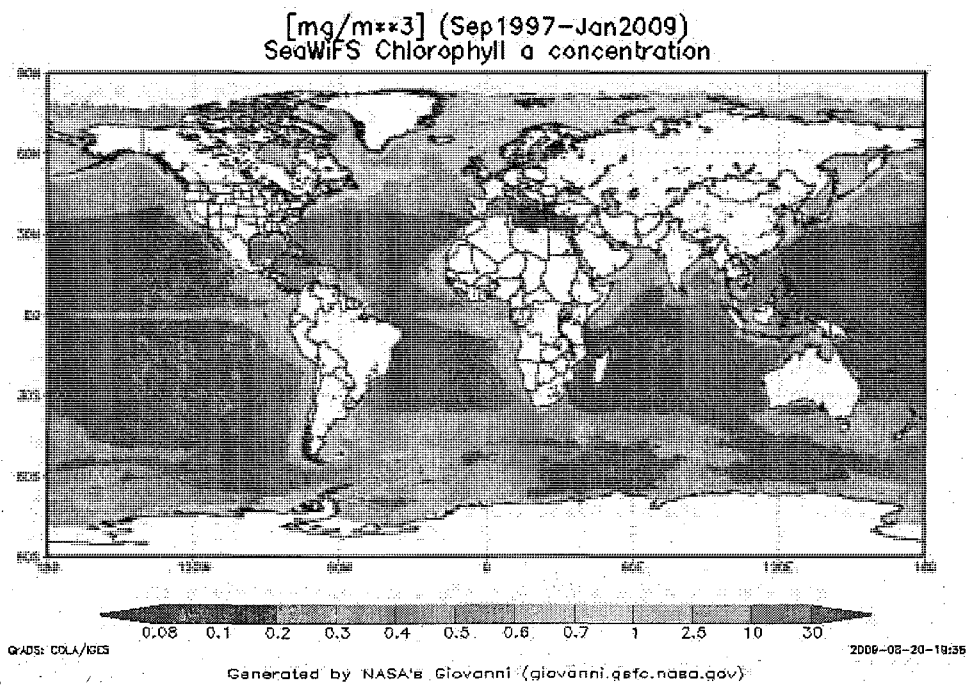
Figure 2-1: **Tools and products of ocean remote sensing.** Top: The SeaWiFS satellite sensor, Bottom: The SeaWiFS Global 9-km climatological mean estimate of *Chl*: September 1997-January 2009 (Both courtesy of NASA's Ocean Biology Processing Group).
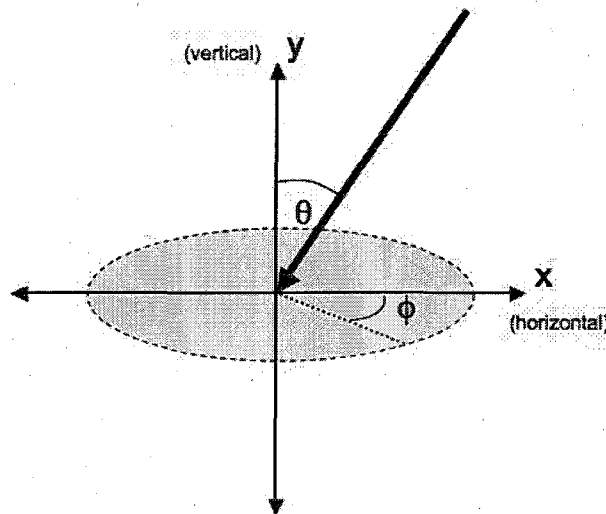
Figure 2-2: **The angles used to describe the geometrical structure of radiance.** The zenith angle, θ, describes the angle of a radiance path from the vector normal to the horizontal surface, and the azimuth angle, φ, describes the angle of the radiance path from a specified vector normal to the vertical plane. This schematic was adapted from Chapter 1 of Kirk (1994b).
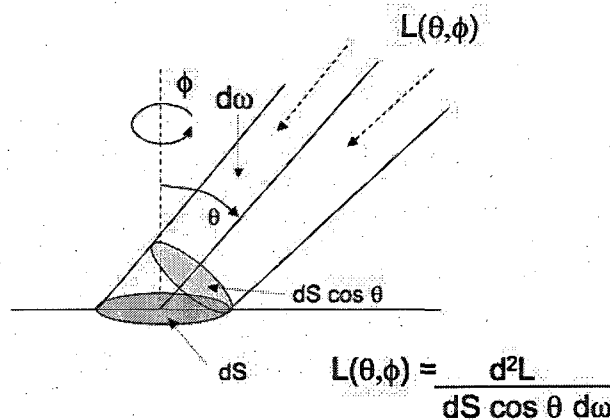
Figure 2-3: **The geometry for radiance at a point on a horizontal surface.** The radiance, $L(\theta,\varphi)$, is constrained within the solid angle, $d\omega$. $dS \cos \theta$ is the area within the solid angle normal to the radiance path's direction. dS is the projection of this area onto the horizontal surface. This schematic was adapted from Chapter 1 of Kirk (1994b).
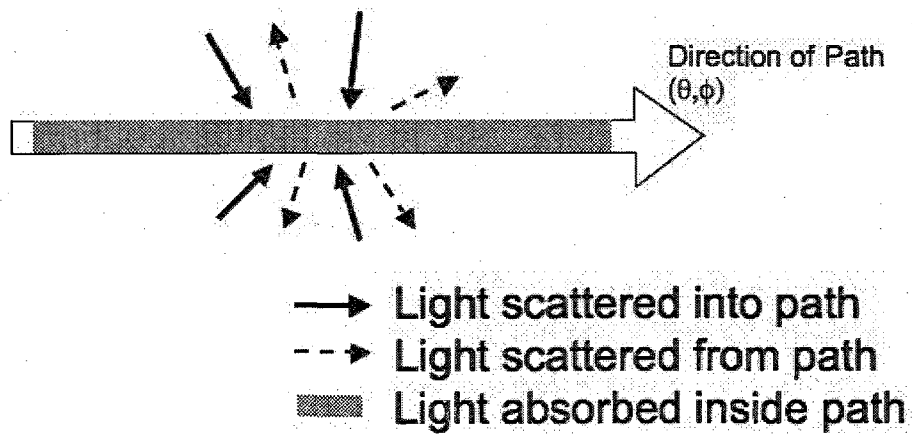
Figure 2-4: **A schematic of the radiative transfer of light through a narrow beam.** The change in radiance along the path is dependent on the scattering and absorption processes occurring within the path. This schematic was adapted from Chapter 1 of Kirk (1994b).
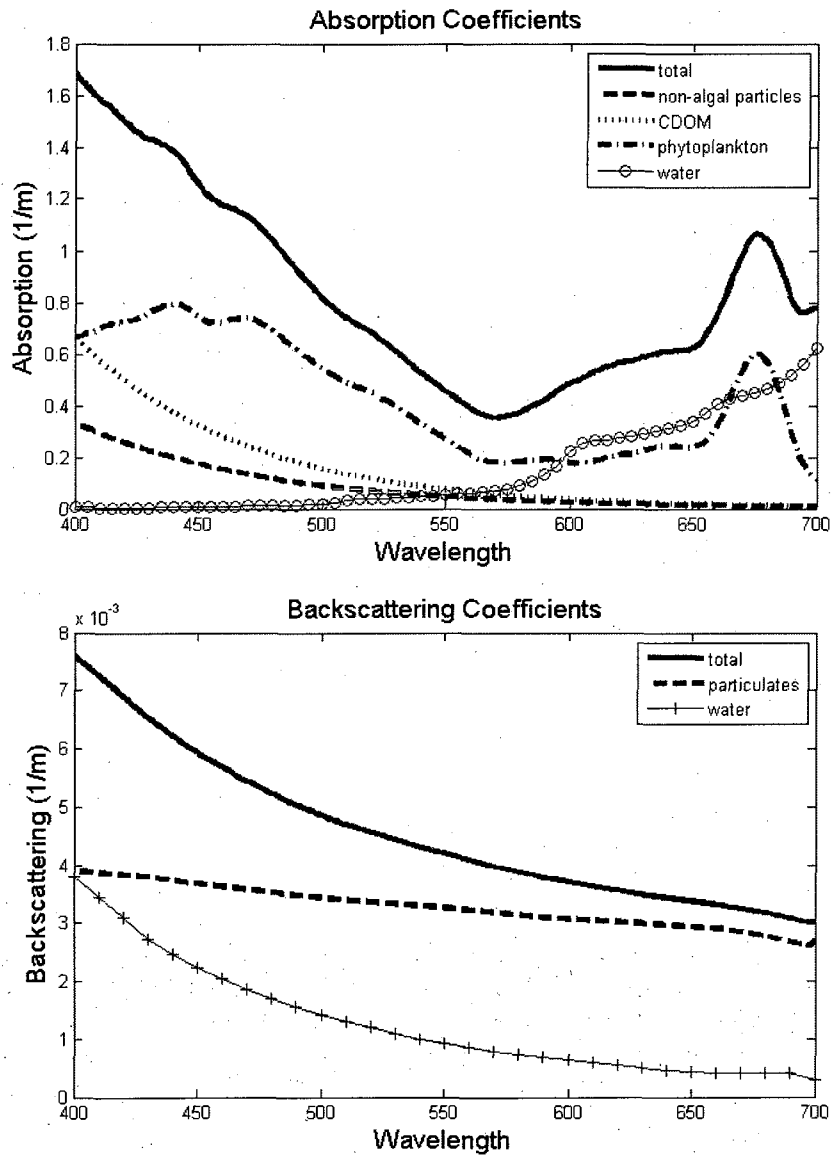
Figure 2-5: **An example of absorption and backscattering spectra.** Top: Absorption spectra for the total sample, non-algal particles, CDOM, phytoplankton, and water. Bottom: Backscattering spectra for the total sample, particles and water. The water spectra are constant, the rest change with alterations in composition and distribution.
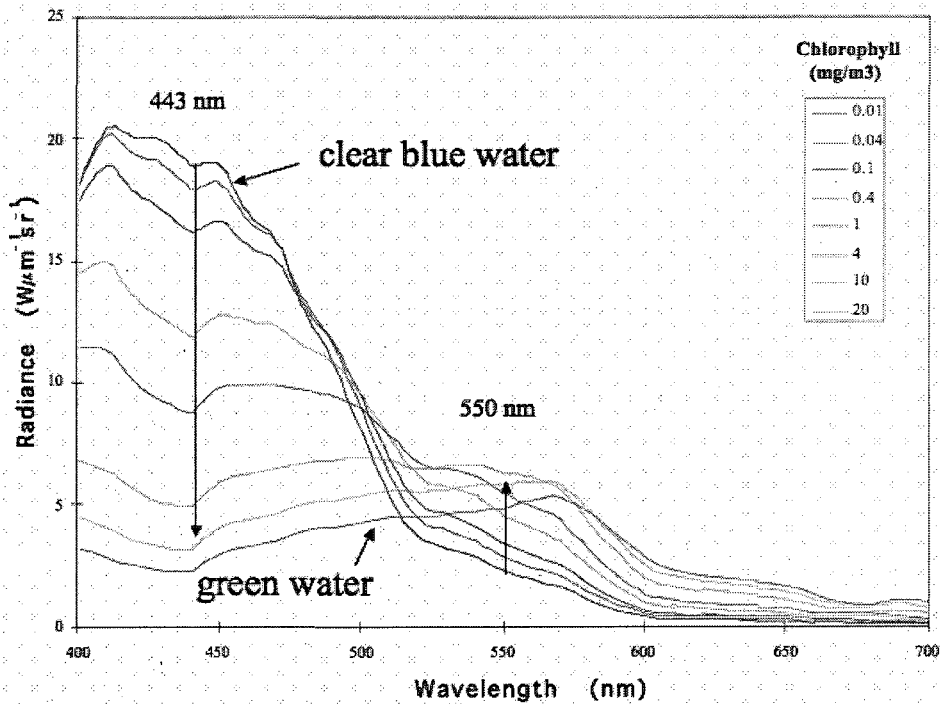
Figure 2-6: **The effect of chlorophyll on water-leaving radiance.** The radiance at 443 nm decreases and the radiance at 550 nm increases (but not as strongly) with increasing chlorophyll concentration. In this transition, the water's color changes from blue to green.

CHAPTER 3

OCEANIC BIASES IN THE EMPIRICAL
CHLOROPHYLL ALGORITHMS

3.1 NOMAD v.1 data

Oceanic biases were found in the empirical chlorophyll algorithms through an analysis of NOMADv.1, NASA's global dataset of bio-optical *in situ* measurements (Werdell and Bailey, 2005). NOMADv.1 contains simultaneous stations of *in situ* *Chl*, and *in situ* L_w and E_s at 20 wavelengths used for satellite sensors, made by numerous research institutions and consolidated into NASA's SeaBASS archive (SeaWiFS Bio-optical Archive and Storage System). Stations were taken at various locations between 1993 and 2003. See Figure 3-1 for the location of the stations at which measurements were collected. The *Chl* in NOMADv.1 ranges from 0.012 to 72.12 mg m^{-3}, and the geometric mean for *Chl* is 1.18 mg m^{-3}.

3.1.1 Trophic categories

In an attempt to organize the global data, the wavelength used to calculate the Maximum Band Ratio (MBR): oligotrophic for the 443 nm, mesotrophic for 490 nm, and eutrophic for 510 nm, was used to define three "trophic" categories. See Figure 3-3. Simultaneously, these categories also reflect different ranges in *Chl*. The oligotrophic category generally represents *Chl* between 0.01 and 0.31 mg m^{-3}, the mesotrophic category, between 0.31 and 3.1 mg m^{-3}, and the eutrophic category, above 3.1 mg m^{-3}. NOMAD was sorted by trophic and ocean category for analysis; the number of stations in each subset is shown in Table 3.1.

3.1.2 Consolidation of the dataset

Detailed descriptions of the various methods for producing Chl and R_{rs} measurements are provided in Werdell and Bailey (2005). Below are just some of the issues considered for compilation.

Fluorometric chlorophyll measurements vs HPLC chlorophyll measurements

The chlorophyll concentrations were predominantly made either using a High Pressure Liquid Chromotography (HPLC) instrument or a fluorometer (Werdell and Bailey, 2005). The HPLC utilizes the differences in polarity of the molecules in the sample to distinguish chlorophyll pigments, and the fluorometer exposes the sample to a light at a blue wavelength and measures the intensity of light emitted at 683 nm as chlorophyll fluorescence. The difference between the two is that the fluorometer measures fluorescence due to chlorophyll-a pigments along with fluorescence due to inorganic compounds and degradation products such as chlorophyllyde-a and pheophytin, while an HPLC yields different concentrations for the intact pigments and each of the degradation products, so that the sum of these concentrations would be approximately equivalent to a corresponding fluorometer measurement (Mueller et al., 2003a).

Fluorometer measurements are less accurate and influenced by regional and temporal biases, but they are cheaper than the HPLC method. Research groups are advised to account for such biases through a scaling factor specific to each cruise. The factor is determined by a comparison of fluorometric measurements with corresponding HPLC measurements for total Chl made for a subset of the observations on the cruise(Mueller et al., 2003a).

Above- vs. below-water radiometers

Radiometers for producing L_w and E_s come in two forms: above- and below-water. Above-water radiometers are placed on either a research ship or moored

station. Below-water radiometers descend from the sub-surface interface towards deeper depths. The upward-facing sensors generally measure E_d and the downward-facing sensors measure L_u (Morrison, personal communication). The E_d sensor is a flat cosine detector whereas the L_u sensor contains a rim around the signal-receiving aperture that designates the solid angle of the measurement (Mueller et al., 2003b). Measured values are translated to the above-surface measurements E_s and L_w according to the exponential attenuation with depth (Mueller et al., 2003b).

Stations with missing components

For NOMAD, several institutions submitted their data to SeaBASS as final above-water R_{rs} measurements and some included E_s. L_w was then calculated as the product of R_{rs} and E_s. E_s was estimated from a clear sky model if it was not available (Werdell and Bailey, 2005). For NOMAD v.1, roughly 40% of the above-water measurements were in this format.

Measurements from a flow-through system

A small portion of the *Chl* and radiance values was observed underway via a flow-through fluorometric system (Werdell and Bailey, 2005). These measurements were averaged over a 15-minute run. Exceptions to these measurement constraints are described in Werdell and Bailey (2005).

3.2   Algorithm uncertainty defined

The discrepancies between *in situ* and satellite-based estimates of *Chl* represent the algorithm uncertainty. Quantitatively, the term that will be used for analysis is the relative chlorophyll error (RCE), defined as the following. See Figure 3-2.

$$RCE = \frac{\text{algorithm } Chl}{\text{in situ } Chl} \qquad (3.1)$$

The RCE is essentially the algorithm's estimate of *Chl* expressed in relation to

the corresponding *in situ* observation from NOMAD based on the maximum R_{rs} band ratio (MBR). Hereafter, I designate RCE > 1, in which the algorithm *Chl* product is greater than the *in situ* measurement, as an overestimation by the algorithm. RCE < 1, in which the algorithm *Chl* is less than the *in situ* measurement, is denoted as an underestimation by the algorithm.

With the assumption that the distribution of RCE is log-normal in NOMAD (Campbell, 1995), statistics such as the mean and standard deviation are calculated on the base-10 logarithm of RCE, hereafter denoted as Δ.

3.3   Oceanic biases

An investigation of NOMAD v.1 revealed that the algorithms produced *Chl* estimates that systematically deviated from the corresponding *in situ* values when the data were sorted by ocean (Figure 3-4). Such systematic algorithm uncertainty is denoted hereafter as the oceanic biases. See Table 3.2 in which the oceanic biases are indicated by the mean of the Δ and the median RCE ratio within each ocean category and within each ocean-trophic category. The median ratio is equivalent to the mean of the Δ and is calculated as the following.

$$\text{median RCE ratio} = 10^{mean(log\,error)} \tag{3.2}$$

It is easier to interpret than the mean of the Δ. A median ratio x such that $x > 1$ indicates an algorithm overestimation by $x-1 * 100\%$. A median ratio x such that $x < 1$ indicates an algorithm underestimation by $x-1 * 100$ %.

The root mean squared error (RMSE), provided for the ocean categories, reflects a combination of the mean and standard deviation for Δ.

For the eutrophic category, the algorithm overestimated Atlantic Ocean stations by 34% at the median, and underestimated Pacific Ocean stations by 20% at the median. For the mesotrophic category, the algorithm overestimated Atlantic Ocean stations by 25 % at the median, and underestimated Pacific Ocean stations by 22 % at the median. For all trophic categories, the algorithm underestimated stations

from the Southern Ocean by about 50% at the median. Stations from the Indian Ocean were insufficient for analysis.

3.4 Possible artifacts

Four factors were considered as possible explanations for the apparent oceanic biases. These include the brand of the radiometer used to measure L_w and E_s, whether the radiometer was the above- or below-water type, whether the *Chl* measurements were made either using a fluorometer or an HPLC, and the project investigator for the observation. Based on an analysis of variance (ANOVA), effects from these features were found to be insignificant (P< 0.01).

Effects from the combination of methods used for each station was considered when sorting NOMAD by project investigator, and the analysis verified the oceanic biases (Figure 3-5). The data shown highlight the stations from investigators who contributed data from more than one ocean. The stations are sorted by ocean and by investigator. In the eutrophic and mesotrophic categories, the algorithm overestimates Robert Arnone's Atlantic points but underestimates his Pacific ones, indicating that the ocean biases exist for the same investigator. Greg Mitchell's stations span all three oceans, and the algorithm systematically over- or underestimates them according to ocean rather than investigator. In the Southern Ocean, Ray Smith and Greg Mitchell are the only investigators, and the algorithm underestimates both their data, indicating that the ocean bias exists regardless of the investigator.

3.5 Hypotheses about optical differences

I speculate that the oceans may in fact be optically different. Based on past research on regional differences in IOPs, I hypothesize that the oceanic biases can be explained by influences from CDM (CDOM and NAP) and the phytoplankton community structure. Using NOMAD v.2, which contains coincident absorption measurements for a subset of stations (Werdell, white paper 2005), I was able to

evaluate the validity of the oceanic biases and the supposed sources for the algorithm uncertainty. Results are reported in Chapter 4.

This topic of regional variation in bio-optical properties has been undertaken by oceanographers in the past using satellite products and models (Siegel et al., 2005a; Brown et al., 2008), and regional scale *in situ* stations (Darecki and Stramski, 2004; D'Ortenzio et al., 2002; Garcia et al., 2005; Gohin et al., 2002; Morel and Maritorena, 2001; Morel et al., 2007; Kahru and Mitchell, 1999; Mitchell and Holmhansen, 1991; Mitchell and Kiefer, 1988a; Dmitriev et al., 2009; Lutz et al., 2006; Pan et al., 2008; Ahn et al., 2008; Fenton et al., 1994; Werdell et al., 2009). This thesis reflects the first attempt to study the topic using *in situ* data on a global comprehensive scale. Results may allude to regional differences in biogeochemical processes, which shape the bio-optical properties over long time scales.

Past work based on empirical evidence has mainly associated the regional variation to differences in the the abundance of CDM (CDOM and NAP) and the phytoplankton community structure, and this has been indicated in AOP and IOP measurements. Specifically, the magnitude of pigment-specific particulate absorption a_p^* in various locales has been found to vary 10-fold as a result of variations in pigment packaging, species composition, and the abundance of detrital matter relative to phytoplankton biomass (Mitchell and Holmhansen, 1991; Maske and Haardt, 1987; Mitchell and Kiefer, 1988a,b; Bricaud et al., 1988; Morrow et al., 1989; Bricaud and Stramski, 1990). These factors were also suggested as the cause for lower signals of the pigment-specific $K_d(\lambda)$ in polar regions compared to those from temperate regions (Mitchell and Kiefer, 1988b; Dierssen and Smith, 2000; Mitchell, 1992). Another possible factor is regional variations in the pigment-specific backscattering coefficients, which alludes to taxonomical differences in the phytoplankton community (Morel, 1987; Dierssen and Smith, 2000).

Table 3.1: Number of stations within each ocean and trophic category for NOMAD v. 1.

NOMAD version 1				
Chl Category	Atlantic	Pacific	Southern	Total
Eutrophic	373	96	64	534
Mesotrophic	221	236	176	665
Oligotrophic	521	265	156	1009
Total	1113	598	396	2208

Table 3.2: **Statistics for NOMAD v.1.** TOP: The mean, standard deviation, and RMSE for Δ, and the median RCE ratio categorized by ocean. BOTTOM: Mean of Δ and the median RCE ratio categorized by ocean and maximum R_{rs} band (Eutrophic, Mesotrophic, and Oligotrophic).

Ocean	N	mean of Δ	median RCE ratio	st. dev. of Δ	RMSE of Δ
Atlantic	1113	0.06	1.14	0.22	0.23
Pacific	598	-0.07	0.85	0.21	0.22
Indian	101	-0.08	0.83	0.19	0.21
Southern	396	-0.30	0.50	0.21	0.37
Global	2208	-0.05	0.89	0.25	0.26

	Eutrophic			Mesotrophic			Oligotrophic		
Ocean	N	mean of Δ	median RCE ratio	N	mean of Δ	median RCE ratio	N	mean of Δ	median RCE ratio
Atlantic	373	0.13	1.34	221	0.10	1.25	521	0.00	1.00
Pacific	96	-0.10	0.80	236	-0.11	0.78	265	-0.03	0.93
Indian	2	0.48	3.05	32	0.01	1.03	67	-0.15	0.72
Southern	64	-0.27	0.53	176	-0.33	0.46	156	-0.27	0.54
Global	534	0.04	1.10	665	-0.09	0.80	1009	-0.06	0.87
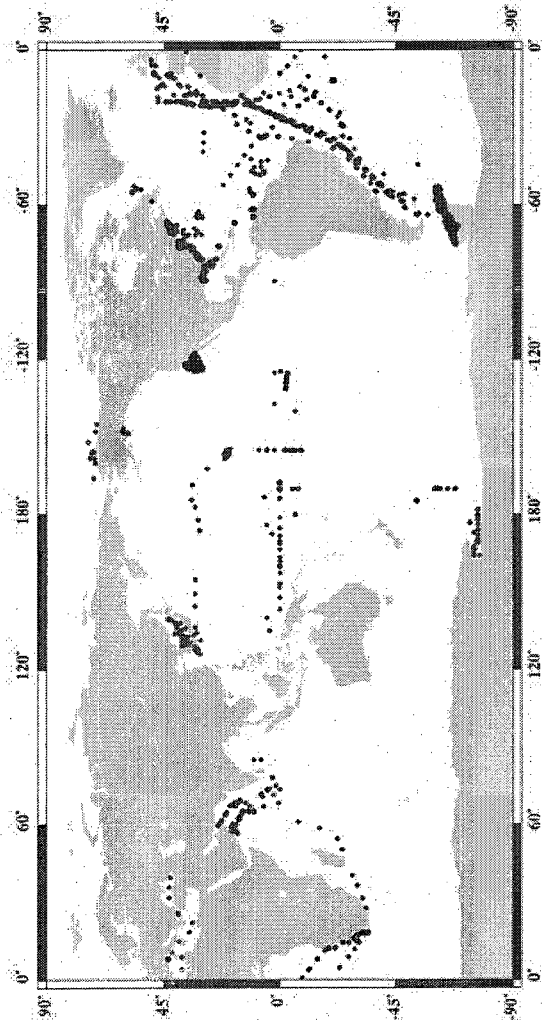
Fig. 7. The global distribution of the NOMAD data set.

Figure 3-1: **Locations of NOMAD v.1 stations** Figure 7 from Werdell and Bailey (2005).
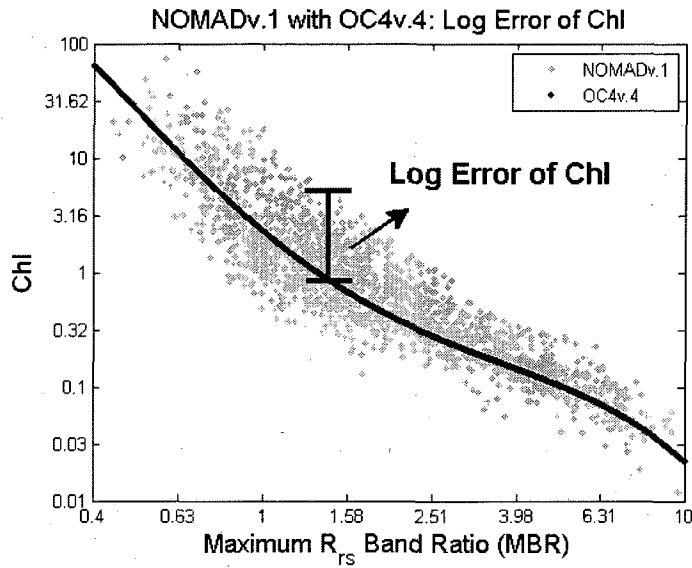
Figure 3-2: **NOMAD v.1 with OC4.v4: Log Error of *Chl* , (Δ). NOMADv.1** is displayed with the OC4 v.4 algorithm, and the log error of *Chl* is illustrated.
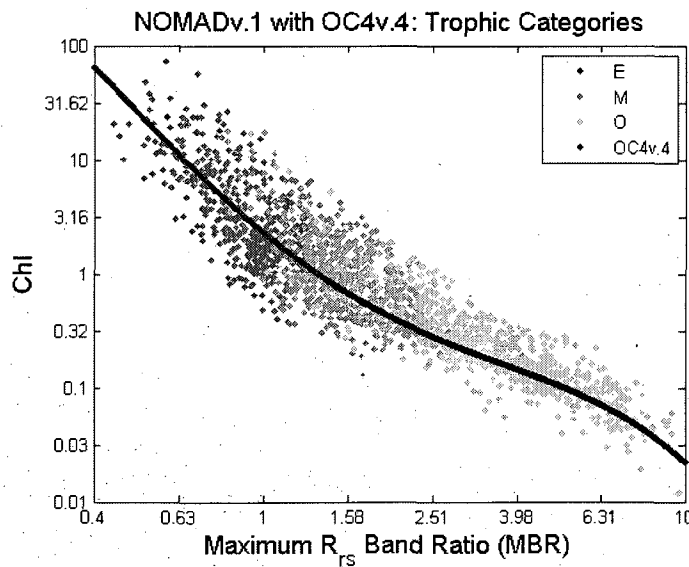
Figure 3-3: **NOMAD v.1 with OC4v.4: the trophic categories.** For the eutrophic stations, the maximum wavelength used for the MBR calculation is 510 nm. For the mesotrophic stations, it is 490 nm and for the oligotrophic stations, it is 443 nm.
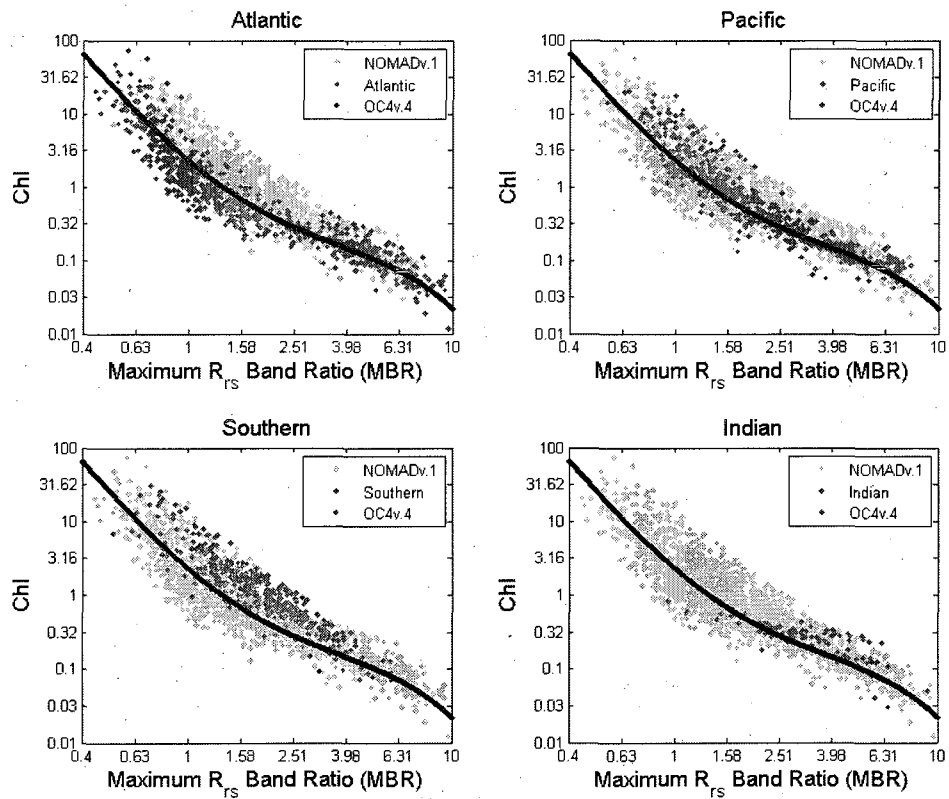
Figure 3-4: **NOMAD v.1 with OC4v.4: the oceanic biases.** The oceanic biases are illustrated in four panels. TOP LEFT: Atlantic. TOP RIGHT: Pacific. BOTTOM LEFT: Southern. BOTTOM RIGHT: Indian.
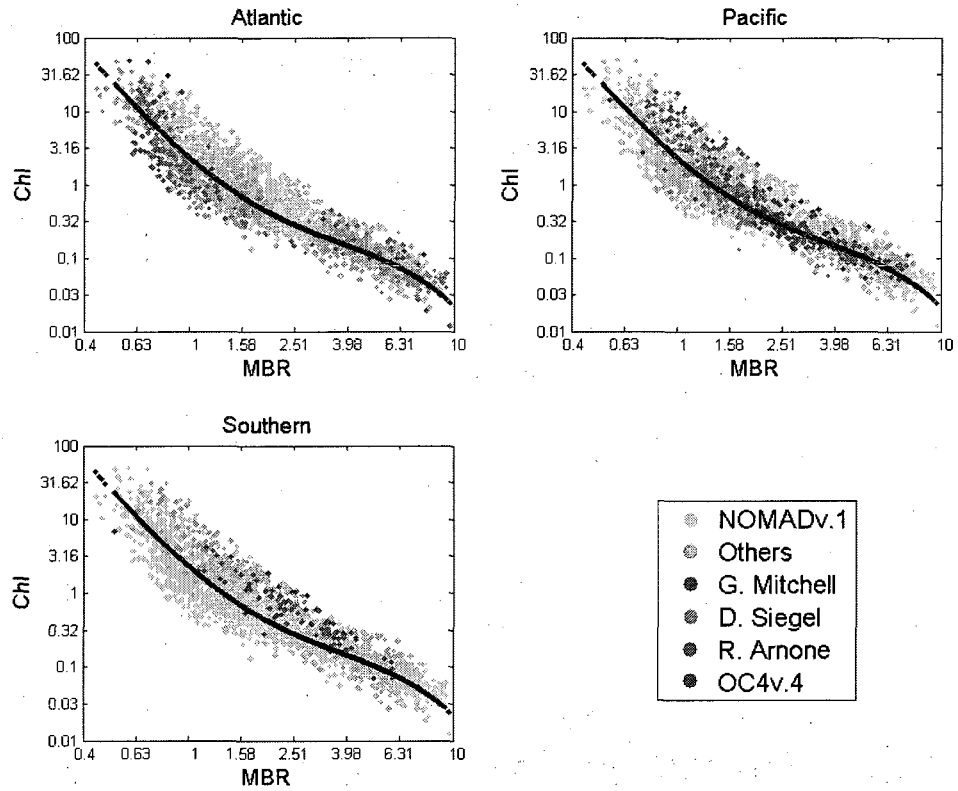
Figure 3-5: **The investigator analysis in support of the oceanic biases.** Investigators contributing data from more than one ocean are color coded. Biases are consistent with data from the same ocean.

CHAPTER 4

OCEANIC DIFFERENCES EXPLAINED BY INHERENT OPTICAL PROPERTIES

4.1   NOMAD v.2 data

NOMAD v.2 contains a subset of stations (n=696) for the Atlantic, Pacific, and Southern oceans with coincident absorption measurements including values for a_{tot}, a_ϕ, a_{cdom}, and a_{nap} at the 20 wavelengths used for satellite sensors (white paper, Werdell 2005). These measurements were made using lab spectroscopy as described in Pegau et al. (2002), and they were integrated over the first-optical depth (white paper, Werdell 2005). Figures 4-1 - 4-3 show the locations of these stations color-coded to represent NOMAD v.2 with and without absorption measurements. Table 4.1 displays the number of stations in each ocean-trophic category.

In this subset, only the meso- and oligotrophic categories contains a sufficient number of stations from the Southern Ocean. See Figure 4-4 and Table 4.2. Consequently, such categories, especially the mesotrophic, will be utilized to consider the effects on the oceanic biases, while all stations will be utilized to consider algorithm uncertainty in general. Figure 4-5 illustrates the algorithm's oceanic biases within the mesotrophic category, which contains the most stations from the Southern Ocean.

4.2   Oceanic biases in the total absorption properties

Further validation of the oceanic biases involved the following approximation of the MBR, which is based on Equation 2.5.

$$MBR = \frac{R_{rs}(\lambda)}{R_{rs}(555)} \sim \frac{a_{tot}(555)b_b(\lambda)}{a_{tot}(\lambda)b_b(555)} \sim \frac{a_{tot}(555)}{a_{tot}(\lambda)} \tag{4.1}$$

Here, λ represents the wavelength used to calculate the MBR: 443, 490, or 510, and a_{tot} is used to specify total absorption by all ocean water constituents (also used hereafter). The approximation reflects a way to represent the MBR in terms of the IOP variables available in NOMAD v.2. It is important to recognize here that the IOP measurements, made from laboratory spectroscopy methods, are completely independent from the radiometric measurements. Since the backscattering measurements in NOMAD v.2 were not sufficient for analysis, the resulting approximation only involves the total absorption properties.

Upon relating the total absorption ratio to *Chl*, several options were available because MBR was calculated differently for every observation, according to the maximum of $R_{rs}443$, $R_{rs}490$, and $R_{rs}510$. These options were $a_{tot}555/a_{tot}443$, $a_{tot}555/a_{tot}490$, $a_{tot}555/a_{tot}510$, and $a_{tot}555/a_{tot}\lambda$, for λ equal to the wavelength used to calculate MBR. See Figure 4-6.

Note that relating *Chl* to $a_{tot}555/a_{tot}\lambda$ resulted in the worst correlation. In fact, it appears that the correlation between *Chl* and $a_{tot}555/a_{tot}510$ for the eutrophic category is similar to that between *Chl* and $a_{tot}555/a_{tot}490$ for the mesotrophic, and both are better than the correlation between *Chl* and $a_{tot}555/a_{tot}443$ for the oligotrophic category. I speculate that this feature is due to strong variability in absorption by chlorophyll-a pigments at 443 nm, compared to the variability at 490 and 510 nm.

Since the mesotrophic category was a focus for the oceanic biases, the selected approximation was $a_{tot}555/a_{tot}490$, with $r^2 = 85\%$ for the correlation between *Chl* and $a_{tot}555/a_{tot}490$.

The fourth-order polynomial fit to the relationship between *Chl* and $a_{tot}555/a_{tot}490$ served in place of the standard algorithm to distinguish between under- and over-estimations. Similar oceanic biases about the polynomial fit were present (Figure 4-7). Statistics for the polynomial fit (designated as RCE_{atot} and Δ_{atot}), confirm these results (Figure 4-8 and Table 4.3). For the eutrophic category, the polynomial

fit overestimated Atlantic Ocean stations by 10% at the median, and underestimated Pacific Ocean stations by 40% at the median. For the mesotrophic category, the polynomial fit regression line overestimated Atlantic Ocean stations by 7% at the median, and underestimated Pacific Ocean stations by 26% at the median. For the mesotrophic and oligotrophic categories, the polynomial fit underestimated stations from the Southern Ocean by about 50% at the median.

Accordingly, the replacement of the MBR with the total-absorption approximation serves as an independent method to validate the existence of the oceanic biases related to true optical differences among the oceans.

4.3   Structure of analysis

In order to evaluate the effects of CDM and phytoplankton community structure on algorithm uncertainty, the parameters, $a_{cdm}443/Chl$, $a_\phi 443/Chl$, and a phytoplankton size model S_f from Ciotti et al. (2002), were determined to represent the different effects. Qualitative and quantitative analyses involved the relation of RCE to the parameters separately and combined. The qualitative analyses are visual (e.g. Figures 4-9) and self-explanatory. Additionally, the relation of RCE_{atot} to the parameters was qualitatively analyzed. See Sections 4.4.2 and 4.5.3. For the quantitative analyses of the separate parameters, NOMAD was sorted by trophic and ocean-trophic categories, and certain statistics were computed (hereafter denoted as "category statistics"). The distributions for $a_{cdm}443/Chl$ and $a_\phi 443/Chl$ were assumed to be log-normal, and so the category statistics included the mean and standard deviation of the base-10 logarithm of two parameters, and their median ratios. For S_f, the category statistics included the mean and standard deviation. The category statistics for the RCE (using the log error) were then analyzed in relation to the corresponding statistics for the respective parameter, such that RCE is expressed as a function of each effect parameter (e.g. Figure 4-10).

4.4 Effects of colored detrital matter (CDM)

The hypothesis that the oceanic biases can be explained by the effects of CDM is considered here. The presence of CDM was represented by the magnitude of the CDM absorption signal at 443 nm, assuming that the effects of backscattering due to CDM are negligible as commonly done for Case-1 waters (Morel and Prieur, 1977). The wavelength 443 nm is that at which a_{cdm} exhibits a substantial signal (since a_{cdm} is maximum at 400 nm in the visible spectrum and diminishes from there towards longer wavelengths), and that at which chlorophyll pigments predominantly absorb light.

An evaluation of the impact from CDM on algorithm uncertainty essentially involves the comparison between measurements of $a_{cdm}443$ and their corresponding algorithm-estimated Chl for each station. In order to indicate algorithm uncertainty, it is desired to utilize the RCE parameter. Consequently, the analysis involves a comparison between $a_{cdm}443/Chl$ and RCE. Here, both $a_{cdm}443$ and the algorithm Chl are normalized by the corresponding $in\ situ\ Chl$.

4.4.1 Effect of CDM with respect to chlorophyll concentration

Figure 4-9 displays the qualitative analysis performed to investigate the effect of CDM on algorithm uncertainty through the parameter $a_{cdm}443/Chl$. Table 4.4 and Figure 4-10 provide the quantitative results.

Algorithm uncertainty in general

With respect to Chl, the effect of CDM on algorithm uncertainty is clear for the eutrophic and mesotrophic stations and less so for the oligotrophic stations, as shown in the Global panel of the Figure 4-9. As $a_{cdm}443/Chl$ increases, the algorithm uncertainty changes from under- to overestimation.

The category statistics are presented in Table 4.4. Relating the category means for $a_{cdm}443/Chl$ to those for RCE in Figure 4-10 provides a confirmation of the qualitative analysis in the form of positive correlations for all three trophic cate-

gories. Furthermore, the rate of increase in $a_{cdm}443/Chl$ with RCE is relatively the same for all three oceans of the oligo- and mesotrophic stations.

Oceanic biases

Systematic differences in $a_{cdm}443/Chl$ are evident in the ocean-specific panels of Figure 4-9, and these are further validated in the statistics. The association of $a_{cdm}443/Chl$ to the oceanic biases, best represented through the mesotrophic Atlantic and Southern Ocean stations, is present in Figure 4-10. The Southern Ocean mesotrophic stations, which are, on average, most underestimated by the algorithm, have a median $a_{cdm}443/Chl$ value of 0.027, while the Atlantic Ocean mesotrophic stations, which are, on average, most overestimated by the algorithm, have a median $a_{cdm}443/Chl$ value of 0.108, which is significantly higher than its Southern Ocean counterpart. In the eutrophic category, the slightly underestimated Pacific Ocean stations have a median $a_{cdm}443/Chl$ value of 0.028, which is significantly less that the median $a_{cdm}443/Chl$ value of 0.079 for the overestimated Atlantic Ocean stations. For the oligotrophic category, the Southern Ocean stations, which are underestimated by the algorithm, have a median $a_{cdm}443/Chl$ value of 0.057. This value is compared to the median $a_{cdm}443/Chl$ value of 0.135 for the overestimated Atlantic Ocean stations.

4.4.2   Influence of the backscattering spectral shape

The analysis of the effect of CDM on RCE_{atot} was performed by approximating the MBR with $a_{tot}555/a_{tot}490$. See Figure 4-11, which shows the comparison of the analyses of CDM using MBR (left) and $a_{tot}555/a_{tot}490$ (right). For the oligotrophic category, systematic variation in $a_{cdm}443/Chl$ with respect to RCE_{atot} (right) is noticeably stronger than that in $a_{cdm}443/Chl$ with respect to RCE (left). Because the $a_{tot}555/a_{tot}490$ approximation essentially removes the influence of the backscattering spectral shape from MBR, this analysis suggests that the effect of CDM on algorithm uncertainty is confounded by the influence of the backscattering spectral shape in the oligotrophic category.

4.4.3 Effect of CDM with respect to phytoplankton absorption

Originally, the effect of CDM on algorithm uncertainty was analyzed with respect to phytoplankton absorption through the parameter $a_{cdm}443/a_\phi443$. The purpose was to convey a shift within the total absorption between CDM and phytoplankton such that *Chl*, is expected to be inversely related to $a_{cdm}443/a_\phi443$. Results, not shown, were different, and it was then realized that in normalizing by $a_\phi443$, the analysis of the effect would not account for variation in absorption per *Chl*, an indication of pigment packaging.

4.5 Effects of phytoplankton community structure

The hypothesis that the oceanic biases can be explained by the effects of the phytoplankton community structure is considered here. Community structure can vary according to pigment packaging and cell size. Such features are represented in terms of absorption measurements by $a_\phi443/Chl$, and the S_f size model from Ciotti et al. (2002), respectively.

For pigment packaging, chlorophyll pigments absorb strongly at 443 nm, and so the $a_\phi443$ signal relative to the amount of chlorophyll in the water sample likely indicates the intensity at which absorption is suppressed by the packaging. While a_ϕ at 443 nm can be attributed to accessory pigments as well, such a source is considered secondary (Bricaud et al., 1995, 2004). With the normalization by *in situ Chl*, the $a_\phi443/Chl$ parameter also has the advantage of behaving similarly to $a_{cdm}443/Chl$ in relation to RCE.

A size parameter, S_f, was derived based on the Ciotti et al. (2002) model, which represents absorption spectra from mixed populations as a linear combination of picoplankton and microplankton absorption spectra (Figure 4-17). The parameter ranges from $S_f = 1$ for 100% picoplankton (small cells) to $S_f = 0$ for 100% microplankton (large cells) (See Table 4 from Ciotti et al. (2002) shown in Figure 4-18). Details of the Ciotti et al. model and its implementation are given in Section 4.5.4.

4.5.1 Pigment packaging

The qualitative analyses for $a_\phi 443/Chl$ are presented in Figure 4-12. The quantitative analyses are presented in Table 4.5 and Figure 4-13.

Algorithm uncertainty in general

The visual analysis of $a_\phi 443/Chl$ in the Global panel of Figure 4-12 reveals that pigment packaging systematically varies with the shift in algorithm uncertainty for all trophic categories. The parameter $a_\phi 443/Chl$ generally increases with a change from under- to overestimation.

Category statistics for $a_\phi 443/Chl$ are presented in Table 4.5. The medians of RCE and their corresponding means for $\log_{10} a_\phi 443/Chl$ are positively correlated (Figure 4-13) for all trophic categories. The relationships are different for each trophic category, suggesting that the effect of pigment packaging is variable among the different trophic categories, and among the different oceans within each category.

Oceanic biases

The ocean-specific panels in Figure 4-12 show that systematic variation in $a_\phi 443/Chl$ is related to the oceanic biases as well. Such analyses are confirmed with statistics as shown in Figure 4-13. The Southern Ocean mesotrophic stations that are underestimated by the algorithm have a median $a_\phi 443/Chl$ value of 0.037. The Atlantic Ocean mesotrophic stations that are overestimated by the algorithm have a median $a_\phi 443/Chl$ value of 0.073, due to more absorption per Chl, and is indicative of less pigment packaging than the Southern Ocean counterparts. The Southern Ocean oligotrophic stations, which are more underestimated than that Atlantic Ocean oligotrophic stations, have a median $a_\phi 443/Chl$ value of 0.049. The Atlantic Ocean oligotrophic stations, which are only slightly underestimated by the algorithm, have a median $a_\phi 443/Chl$ value of 0.093.

4.5.2 Cell size

The qualitative analyses for the cell size parameter S_f are presented in Figure 4-14. The quantitative analyses are presented in Table 4.6 and Figure 4-15.

Algorithm uncertainty in general

In general, a visual analysis of the Global panel in Figure 4-14 shows that cell size systematically varies with a shift in algorithm uncertainty for stations from the mesotrophic category and those from the oligotrophic category. For such stations, the parameter S_f increases towards 1 with a change from under- to overestimation. No systematic order is evident in the eutrophic category (global panel, Figure 4-14).

Category statistics for S_f are presented in Table 4.6. The relationship between the corresponding median RCE and mean S_f have positive correlations for the mesotrophic and oligotrophic categories (Figure 4-15). The relationships are different for the two categories, indicating that on average, the effect of cell size is variable between and within the two categories. The negative correlation for the Atlantic- and Pacific-eutrophic category suggests a contradiction to expectations, in which a shift from under- to overestimation is associated with an increase in S_f towards 1 (where picoplankton dominate the phytoplankton community).

Oceanic biases

The oceanic biases best represented through the RCE values from the mesotrophic Atlantic and Southern Ocean stations show a significant corresponding deviation in the mean values of S_f. See Figures 4-14 and 4-15. The Southern Ocean mesotrophic mean S_f value is 0.51, suggesting that on average the community structure is composed of phytoplankton with moderate cell size, while the Atlantic Ocean mesotrophic mean S_f value is 0.77, suggesting that on average the community structure is dominated by picoplankton, which are small in size. The reference to size groups is provided in the table from Ciotti et al. (2002) shown in Figure 4-18.

The association of cell size to oceanic biases is also present in the oligotrophic

stations. The Southern Ocean stations, which are more underestimated than the Atlantic Ocean stations, have a mean S_f value of 0.60, which is associated with a community structure predominantly composed of moderately sized phytoplanton. The slightly underestimated Atlantic Ocean stations have a mean S_f value of 0.95, indicating community structure predominantly composed of picoplankton.

4.5.3   Influence of the backscattering spectral shape

Figure 4-16 presents the global analyses for both MBR (left) and $a_{tot}555/a_{tot}490$ (right). Little improvement in the systematic variation of $a_\phi443/Chl$ and S_f comes from the removal of the backscattering spectral shape. Apparently, the effect of the backscattering spectral shape, attributed to backscattering from both CDM and phytoplankton, is less significant than the effects of the phytoplankton community structure.

4.5.4   Calculating the picoplankton proportion parameter

The picoplankton proportion parameter, S_f, indicates the amount of picoplankton within a phytoplankton community structure. Adapted from Ciotti et al. (2002), the parameter is calculated from the following equation.

$$a_{\phi n} = [S_f \, a_{pico}(\lambda)] + [(1 - S_f) \, a_{micro}(\lambda)] \qquad (4.2)$$

The absorption spectra a_{pico} and a_{micro} were pre-determined from laboratory work to represent a community of picoplankton and one of microplankton, respectively. The term $a_{\phi n}$ is expressed as a linear combination of normalized absorption spectra for the picoplankton community (a_{pico}) and the microplankton community (a_{micro}), where spectra are normalized by the mean absorption across the 300 visible wavelengths. These pico- and microplankton $a_{\phi n}$ spectra were empirically developed and specified in Table 3 of Ciotti et al. (2002). The two spectra are weighted with S_f (ranging from 0 to 1).

Executing the model

To calculate S_f, one thousand possible values between 0 and 1 were used to compute modeled $a_{\phi n}$ spectra. Using least squares optimization, each NOMAD $a_{\phi n}$ was matched to a particular $a_{\phi n}$ model. See Figure 4-17. The S_f value corresponding to the selected model then indicated the fraction of picoplankton-sized cells in the NOMAD sample. Figure 4-18 shows Table 4, extracted from Ciotti et al. (2002). It shows the relation of the size parameter to the different size groups based on data from their research.

Issues with normalization

Ciotti et al. (2002) normalizes a_ϕ by the mean absorption across the 300 visible wavelengths. NOMAD, with only 20 wavelengths of data, is not hyper-spectral. Consequently, each value of phytoplankton absorption was normalized by its mean absorption across the 20 wavelengths available in NOMAD. This approach is chosen out of several, which were attempted on hyper-spectral absorption data from the Coastal Observing Center (COOA) at UNH. Selection was based on the minimum difference between the resulting $a_{\phi n}$ spectrum and the corresponding spectrum using the normalization method of Ciotti et al. (2002).

Using S_f as a indicator for cell size

Changes in spectral shape of phytoplankton absorption can be attributed to either cell size or photoacclimation. Because NOMAD absorption measurements are integrated over the first optical depth, they incorporate a broad reference of time that better reveals changes in cell size than photoacclimation (Bricaud et al., 2004).

4.6 Relative importance of CDM and community structure

An evaluation of the relative importance of CDM and phytoplankton community structure is presented here. Only the parameters $a_{cdm}443/Chl$ and $a_\phi443/Chl$ are used. The parameter S_f was left out because it is not scale invariant, meaning it does not have and cannot be simply transformed to have a normal distribution for linear regression analysis. Consequently, community structure is represented only through pigment packaging here.

4.6.1 Qualitative analysis

Figure 4-19 provides a qualitative analysis through the relationship between $a_{cdm}443/Chl$ and $a_\phi443/Chl$ for NOMAD when sorted by trophic categories with RCE color-coded on the top and the oceans color-coded on the bottom. The results are described in the following sections in terms of the abundance of stations below or above the one-to-one line, and a visual assessment of the trends in RCE relative to variation in $a_{cdm}443/Chl$ and $a_\phi443/Chl$.

Abundance of stations below or above the one-to-one line

CDM absorption is greater than phytoplankton absorption for stations above the one-to-one line, whereas phytoplankton absorption is greater than CDM absorption for stations below the one-to-one line. From the top panels of Figure 4-19, it is evident that the majority (77.2 %) of stations are above the line. In the eutrophic category, 85.3% of the stations are above the line. In the mesotrophic category, 67.2% of the stations are above the line, and in the oligotrophic category, 71.8 % of the stations are above the line. Furthermore, CDM absorption has a greater range of variability than phytoplankton absorption within each category, and similar ranges in the eutrophic and mesotrophic categories. Interestingly, the range of CDM absorption in the oligotrophic category was shifted upward, indicating that there was more CDM absorption relative to *Chl* there than elsewhere.

Results from the bottom panels of Figure 4-19 are presented in Table 5.1.

Trends in RCE relative to variation in $a_{cdm}443/Chl$ and $a_\phi 443/Chl$

A trend in RCE relative to (vertical) variation in $a_{cdm}443/Chl$ indicates the effect of CDM on algorithm uncertainty. A trend in RCE relative to (horizontal) variation in $a_\phi 443/Chl$ indicates the effect of pigment packaging on algorithm uncertainty. Considering the top panels of Figure 4-19, it is evident that nearly all stations in which Chl is overestimated (RCE > 1) are above the one-to-one line. However, trends in RCE with respect to variation in $a_{cdm}443/Chl$ and $a_\phi 443/Chl$ are difficult to differentiate because these two parameters are correlated to each other (See Table 4.7). To determine which parameter has the greatest effect requires a more quantitative analysis.

4.6.2 Quantitative analysis

Step-wise ordinary least-squares regression analyses were performed for all the stations, and for the stations when sorted by trophic and ocean-trophic categories. Matlab routine "stepwisefit" was used (2007a, The MathWorks, Natick, MA).

Methods

The log error (Δ) was predicted as a linear combination of the base-10 logarithms of $a_{cdm}443/Chl$ and $a_\phi 443/Chl$. The regression format is defined mathematically as the following:

$$\Delta = b_1 + b_2 \, log_{10}\left(\frac{a_\phi 443}{Chl}\right) + b_3 \, log_{10}\left(\frac{a_{cdm}443}{Chl}\right) \qquad (4.3)$$

which is equivalent to a power relationship:

$$RCE = 10^{b_1}\left(\frac{a_\phi 443}{Chl}\right)^{b_2}\left(\frac{a_{cdm}443}{Chl}\right)^{b_3} \qquad (4.4)$$

49

where b_1, b_2, and b_3 stand for resulting coefficients from each analysis. The correlation coefficients between all combinations of the three parameters Δ, $\log_{10} a_\phi 443/Chl$, and $\log_{10} a_{cdm}443/Chl$ were computed (Table 4.7).

In the step-wise regression, the parameter with the higher correlation with Δ is used to predict Δ in the first step. This parameter explains more of the variance of Δ than the other. Then, the second parameter is added if it significantly reduces the residuals. The significance is based on a comparison of the variance (F-test) with or without the potential parameter ($P < 0.05$).

Results of regression analyses

Table 4.8 presents the coefficients, standard deviations, the number of stations in the subset, and r^2 (the portion of variance in Δ explained by the regression) for each analysis. The parameter used in the initial model is labeled with an asterisk next to the respective coefficient.

The coefficients indicate the relative magnitudes of $a_{cdm}443/Chl$ and $a_\phi 443/Chl$, but are not necessarily an indication of the relative importance of the effects. Rather, the sequence of parameters used in the model indicates the relative importance. The parameter used to fit the initial model of every step-wise regression is the parameter with the stronger influence on algorithm uncertainty.

Overall, the results indicate that CDM is generally the stronger influence on algorithm uncertainty. This is the case for the eutrophic and mesotrophic categories but not the oligotrophic category. See Table 5.1 for the results of the analyses for the ocean-trophic categories.

The amount of variance explained by the regressions (r^2) was relatively low in all cases. It ranges from 22 % to 28 %. However, the regression analysis was not performed with the intention of reducing the algorithm uncertainty, since it is not feasible to estimate the IOPs needed with sufficient accuracy to make them useful. The step-wise regression was intended to reveal how much effect the IOP parameters had on the algorithm uncertainty.

Table 4.1: NOMAD v.2: number of stations within each ocean and trophic category

NOMAD version 2				
Chl Category	Atlantic	Pacific	Southern	Total
Eutrophic	626	94	64	784
Mesotrophic	317	242	178	737
Oligotrophic	306	259	158	723
Total	1249	595	400	2244

NOMAD version 2 subset with absorption measurements				
Chl Category	Atlantic	Pacific	Southern	Total
Eutrophic	296	38	0	334
Mesotrophic	81	75	18	174
Oligotrophic	101	66	21	188
Total	478	179	39	696

Table 4.2: **Statistics for NOMAD v.2.** TOP: The mean, standard deviation, and RMSE for Δ and the median RCE ratio categorized by ocean. BOTTOM: Mean of Δ and the median RCE ratio for ocean-trophic categories.

Ocean	N	mean of Δ	median RCE ratio	st. dev. of Δ	RMSE of Δ
Atlantic	478	0.10	1.26	0.25	0.27
Pacific	179	-0.07	0.85	0.16	0.17
Southern	39	-0.32	0.48	0.13	0.35
Global	696	0.03	1.07	0.25	0.26

		Eutrophic			Mesotrophic			Oligotrophic	
Ocean	N	mean of Δ	median RCE ratio	N	mean of Δ	median RCE ratio	N	mean of Δ	median RCE ratio
Atlantic	296	0.12	1.45	81	0.16	1.39	101	-0.01	0.97
Pacific	38	-0.03	0.89	75	-0.09	0.80	66	-0.07	0.87
Southern	1			18	-0.34	0.46	21	-0.31	0.47
Global	334	0.11	1.31	174	0.00	0.98	188	-0.06	0.92

Table 4.3: **Statistics for the Total Absorption Ratio analysis.** TOP: The mean, standard deviation, and RMSE for Δ_{atot} and the median RCE_{atot} ratio categorized by ocean. BOTTOM: The mean of Δ_{atot} and median RCE_{atot} ratio for the ocean-trophic categories.

Ocean	N	mean of Δ_{atot}	median RCE_{atot} ratio	st. dev. of Δ_{atot}	RMSE of Δ_{atot}
Atlantic	478	0.05	1.12	0.24	0.25
Pacific	179	-0.07	0.85	0.28	0.29
Southern	39	-0.25	0.56	0.17	0.30
Global	696	-0.00	1.00	0.26	0.26

	Eutrophic			Mesotrophic			Oligotrophic		
Ocean	N	mean of Δ_{atot}	median RCE_{atot} ratio	N	mean of Δ_{atot}	median RCE_{atot} ratio	N	mean of Δ_{atot}	median RCE_{atot} ratio
Atlantic	296	0.02	1.10	81	0.09	1.07	101	0.09	1.12
Pacific	38	-0.22	0.60	75	-0.13	0.74	66	0.07	1.04
Southern	1			18	-0.34	0.41	21	-0.17	0.59
Global	334	0.00	1.06	174	-0.05	0.91	188	0.05	1.04

Table 4.4: **The effects of CDM on the oceanic biases: Statistics for $\mathbf{a}_{cdm}\mathbf{443/Chl}$.** The mean and standard deviation for $\log_{10} a_{cdm}443/Chl$ the median of $a_{cdm}443/Chl$ are presented for the ocean-trophic categories.

Eutrophic				
Ocean	N	Mean, $\log_{10} \frac{a_{cdm}443}{Chl}$	St. Dev., $\log_{10} \frac{a_{cdm}443}{Chl}$	Median, $\frac{a_{cdm}443}{Chl}$
Atlantic	296	-1.1	0.26	0.079
Pacific	38	-1.59	0.28	0.028
Southern	1			
Global	334	-1.15	0.31	0.073
Mesotrophic				
Ocean	N	Mean, $\log_{10} \frac{a_{cdm}443}{Chl}$	St. Dev., $\log_{10} \frac{a_{cdm}443}{Chl}$	Median, $\frac{a_{cdm}443}{Chl}$
Atlantic	81	-0.93	0.27	0.108
Pacific	75	-1.19	0.33	0.061
Southern	18	-1.60	0.28	0.027
Global	174	-1.11	0.36	0.078
Oligotrophic				
Ocean	N	Mean, $\log_{10} \frac{a_{cdm}443}{Chl}$	St. Dev., $\log_{10} \frac{a_{cdm}443}{Chl}$	Median, $\frac{a_{cdm}443}{Chl}$
Atlantic	101	-0.85	0.31	0.135
Pacific	66	-0.91	0.39	0.118
Southern	21	-1.21	0.29	0.057
Global	188	-0.91	0.36	0.118

Table 4.5: **The effect of pigment packaging on the oceanic biases: Statistics for $a_\phi 443$/Chl.** The mean and standard deviation for $\log_{10} a_\phi 443/Chl$ the median of $a_\phi 443/Chl$ are presented for the ocean-trophic categories.

Eutrophic				
Ocean	N	Mean, $\log_{10} \frac{a_\phi 443}{Chl}$	St. Dev., $\log_{10} \frac{a_\phi 443}{Chl}$	Median, $\frac{a_\phi 443}{Chl}$
Atlantic	296	-1.38	0.19	0.042
Pacific	38	-1.43	0.20	0.037
Southern	1			
Global	334	-1.39	0.19	0.042
Mesotrophic				
Ocean	N	Mean, $\log_{10} \frac{a_\phi 443}{Chl}$	St. Dev., $\log_{10} \frac{a_\phi 443}{Chl}$	Median, $\frac{a_\phi 443}{Chl}$
Atlantic	81	-1.12	0.15	0.073
Pacific	75	-1.38	0.20	0.044
Southern	18	-1.41	0.13	0.037
Global	174	-1.26	0.22	0.058
Oligotrophic				
Ocean	N	Mean, $\log_{10} \frac{a_\phi 443}{Chl}$	St. Dev., $\log_{10} \frac{a_\phi 443}{Chl}$	Median, $\frac{a_\phi 443}{Chl}$
Atlantic	101	-1.04	0.12	0.093
Pacific	66	-1.15	0.13	0.076
Southern	21	-1.31	0.13	0.049
Global	188	-1.11	0.15	0.082

Table 4.6: **The effects of cell size on the oceanic biases: Statistics for** $\mathbf{S}_f$. The mean and standard deviation of S_f are presented for the ocean-trophic categories.

Eutrophic			
Ocean	N	mean, S_f	St. Dev., S_f
Atlantic	296	0.37	0.19
Pacific	38	0.47	0.20
Southern	1		
Global	334	0.39	0.19
Mesotrophic			
Ocean	N	Mean, S_f	St. Dev., S_f
Atlantic	81	0.77	0.15
Pacific	75	0.50	0.18
Southern	18	0.51	0.12
Global	174	0.62	0.21
Oligotrophic			
Ocean	N	Mean, S_f	St. Dev., S_f
Atlantic	101	0.95	0.12
Pacific	66	0.78	0.17
Southern	21	0.60	0.08
Global	188	0.85	0.18

Table 4.7: **The relative importance of CDM and community structure: correlation of parameters.** The correlation coefficients for comparisons of all combinations of the three parameters $\log_{10} a_\phi 443/Chl$, $\log_{10} a_{cdm} 443/Chl$, and Δ are presented.

	Δ	$\log_{10} \frac{a_\phi 443}{Chl}$	$\log_{10} \frac{a_{cdm} 443}{Chl}$
Δ	1	0.375	0.524
$\log_{10} \frac{a_\phi 443}{Chl}$		1	0.600
$\log_{10} \frac{a_{cdm} 443}{Chl}$			1

Table 4.8: **The relative importance of CDM and community structure: regression statistics.** The results for the (step-wise) multi-linear regression analyses are displayed here. They include coefficients, standard deviations (SD), the number of stations, and r^2, which is the fraction of the variance of Δ that is explained by the regression. The term that is more influential to changes in Δ is labeled with an asterisk. When no coefficient is given, the term was considered to be insignificant in the regression. TOP: All stations. MIDDLE: NOMAD sorted by the trophic categories. BOTTOM: NOMAD sorted by ocean and trophic categories.

All Stations			
	b_1	b_2	b_3
Coeffs	0.527	0.107	0.332*
SD		0.045	0.029
n		696	
r^2		0.28	

Trophic Categories									
	Eutrophic			Mesotrophic			Oligotrophic		
	b_1	b_2	b_3	b_1	b_2	b_3	b_1	b_2	b_3
Coeffs	1.298	0.553	0.371*	0.890	0.326	0.433*	0.622	0.494*	0.152
SD		0.065	0.041		0.061	0.036		0.062	0.026
n	334			174			188		
r^2	0.25			0.27			0.22		

Ocean	Stats	Eutrophic			Mesotrophic			Oligotrophic		
		b_1	b_2	b_3	b_1	b_2	b_3	b_1	b_2	b_3
Atlantic	Coeffs	1.394	0.577	0.433*	0.667	—	0.550	0.502	0.390*	0.127
	SD		0.075	0.055		—	0.057		0.088	0.033
	n	296			81			101		
	r^2	0.26			0.27			0.22		
Pacific	Coeffs	0.450	—	0.307	0.616	0.248	0.307*	0.108	—	0.193
	SD		—	0.102		0.083	0.050		—	0.036
	n	38			75			66		
	r^2	0.27			0.27			0.26		
Southern	Coeffs	—	—	—	0.334	0.215	0.235*	0.767	0.508	0.335*
	SD	—	—	—		0.092	0.044		0.140	0.063
	n	0			18			22		
	r^2	—			0.27			0.25		
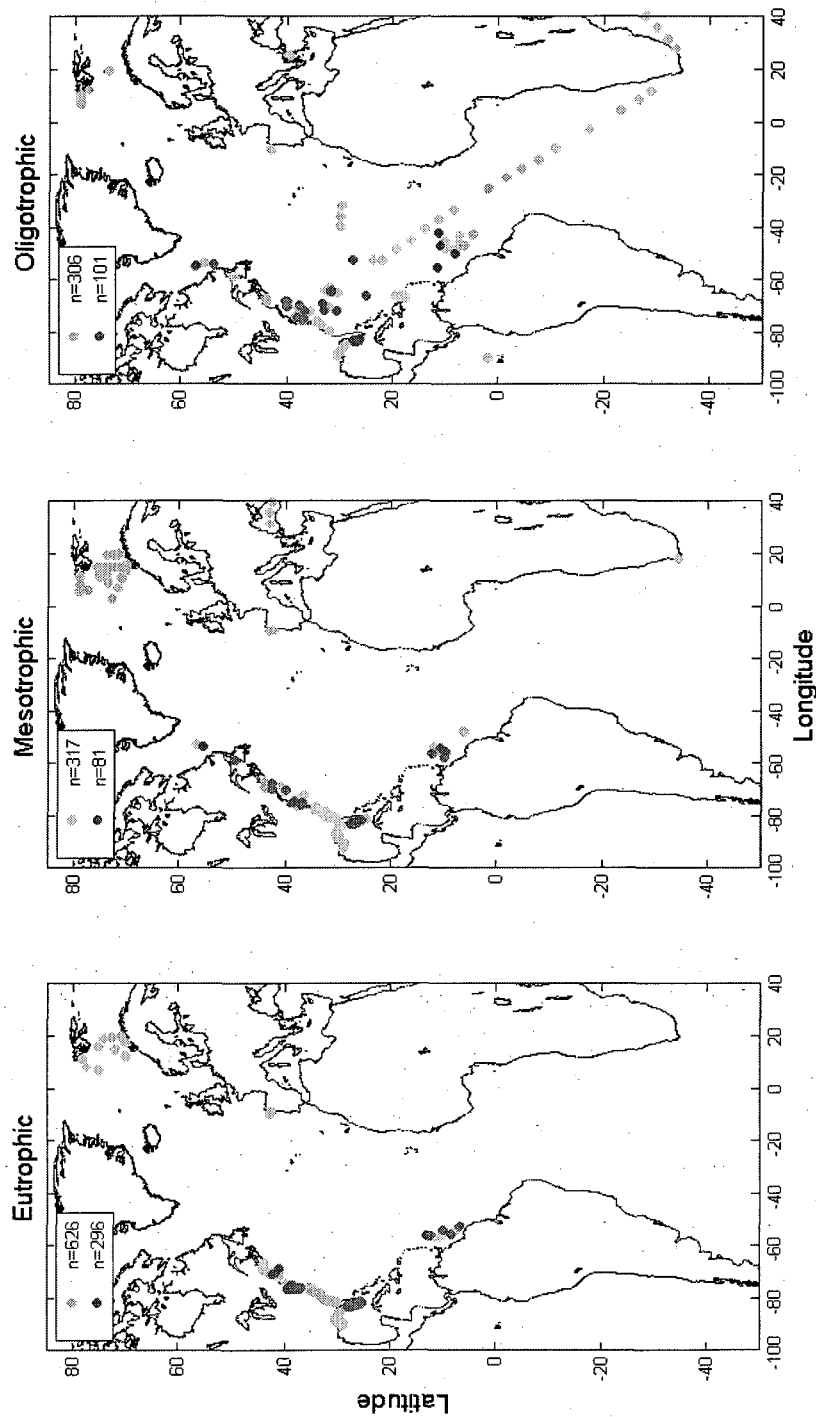
Figure 4-1: **Map of Atlantic stations from NOMADv.2 sorted by trophic category.** Light Grey = all stations (n=1249). Dark grey = stations with absorption spectra (n = 478).
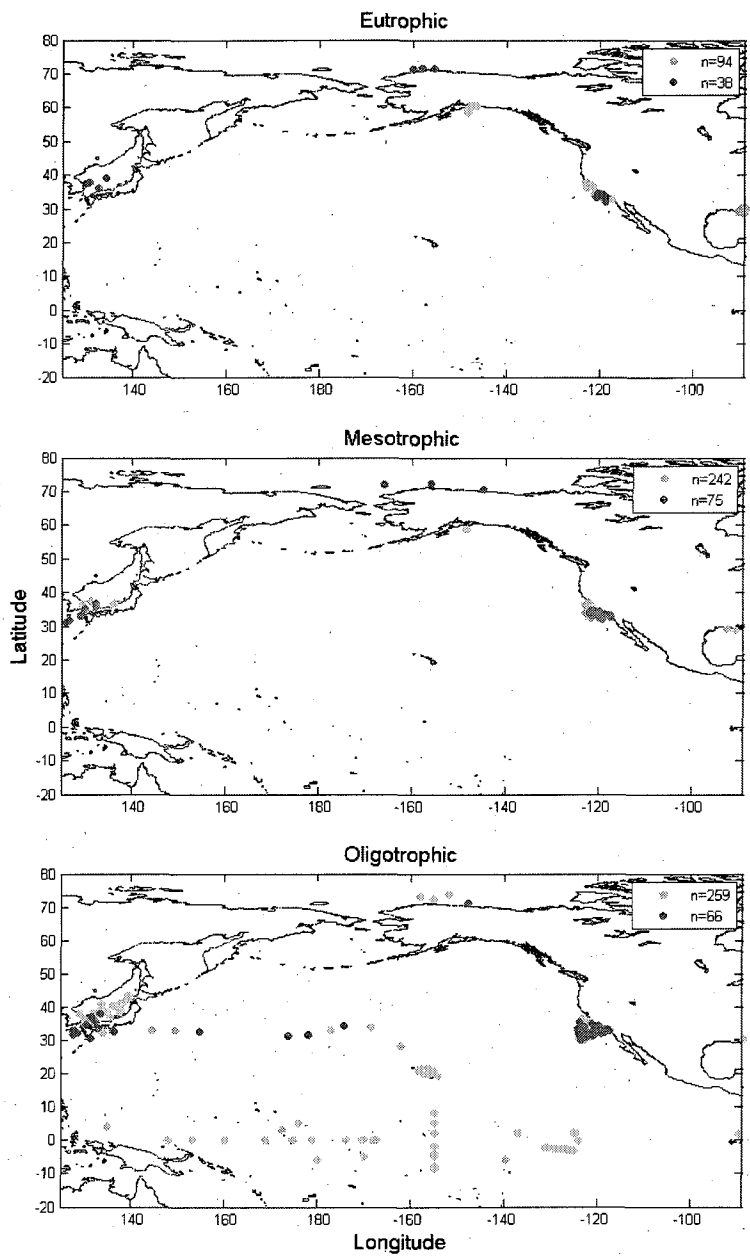
Figure 4-2: **Map of Pacific stations from NOMADv.2 sorted by trophic category.** Light Grey = all stations (n=595). Dark grey = stations with absorption spectra (n = 179).
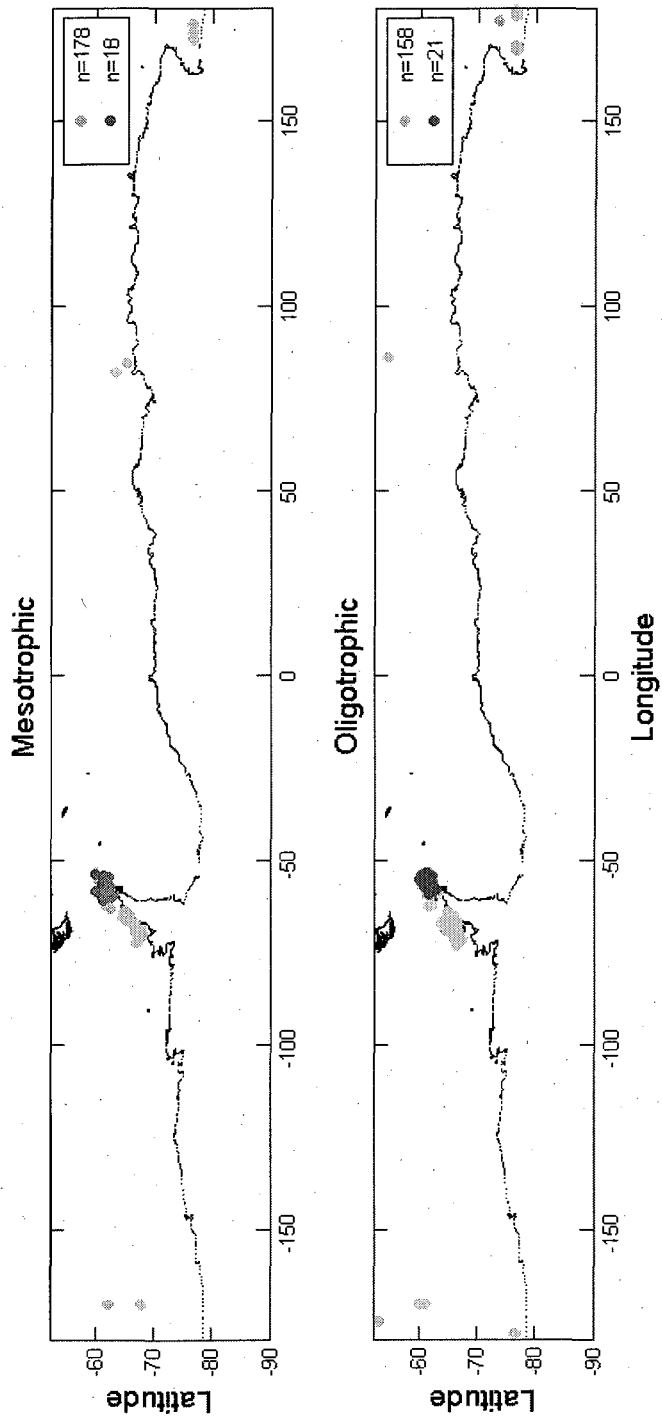
Figure 4-3: **Map of Southern stations from NOMADv.2 sorted by trophic category.** Light Grey = all stations (n=400). Dark grey = stations with absorption spectra (n = 39).
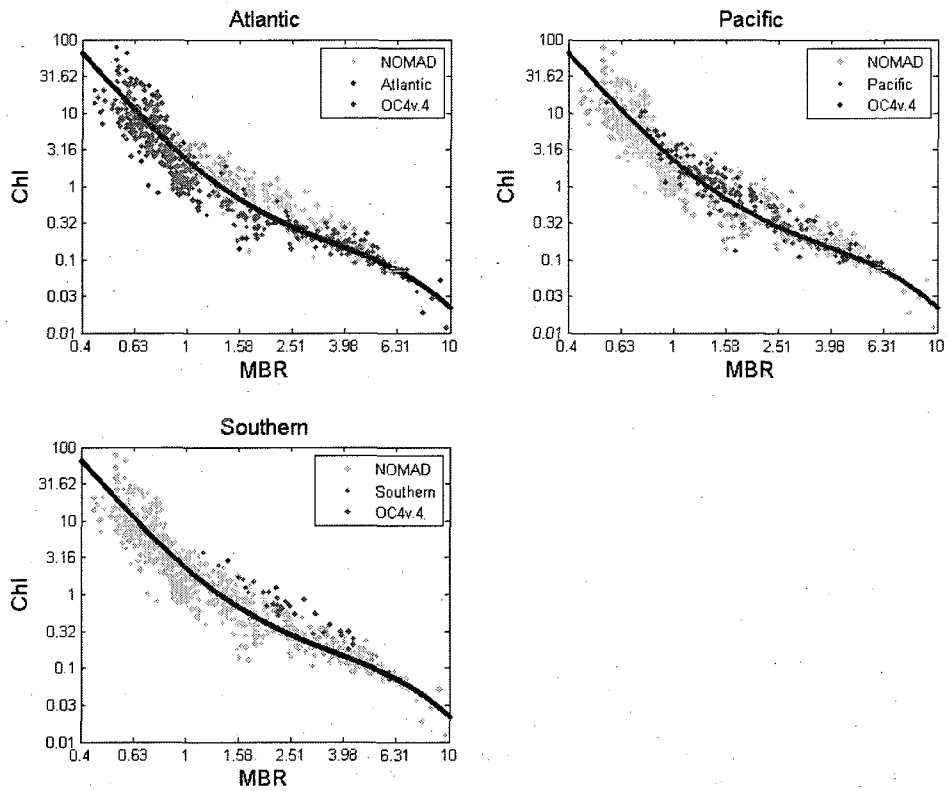
Figure 4-4: **NOMAD v.2 subset (n=696) with OC4v.4, separated by ocean.**
The grey points represent all the data, and the dark points represent the data from
the specified ocean. The thick black line represents the OC4v.4 algorithm.
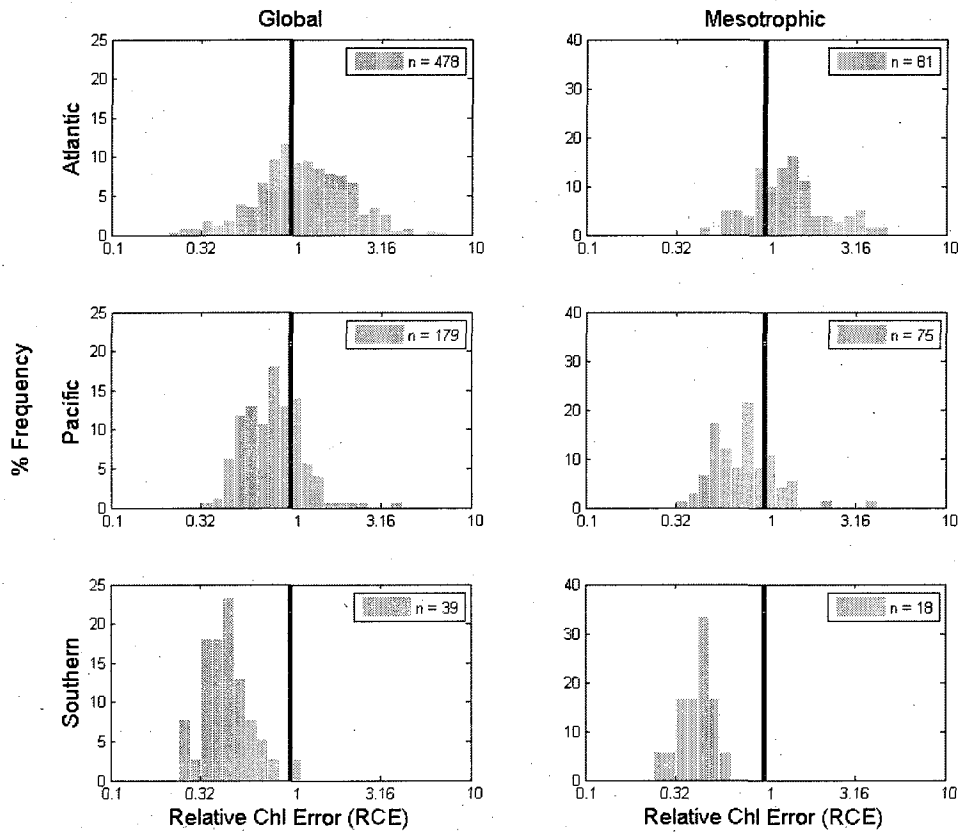
Figure 4-5: **Histograms for the % Frequency of the Relative Chlorophyll Error (RCE): Global vs Mesotrophic** TOP LEFT: Global Atlantic. MIDDLE LEFT: Global Pacific. BOTTOM LEFT: Global Southern. TOP RIGHT: Mesotrophic Atlantic. MIDDLE RIGHT: Mesotrophic Pacific. BOTTOM RIGHT: Mesotrophic Southern. The Black line represents zero algorithm uncertainty.
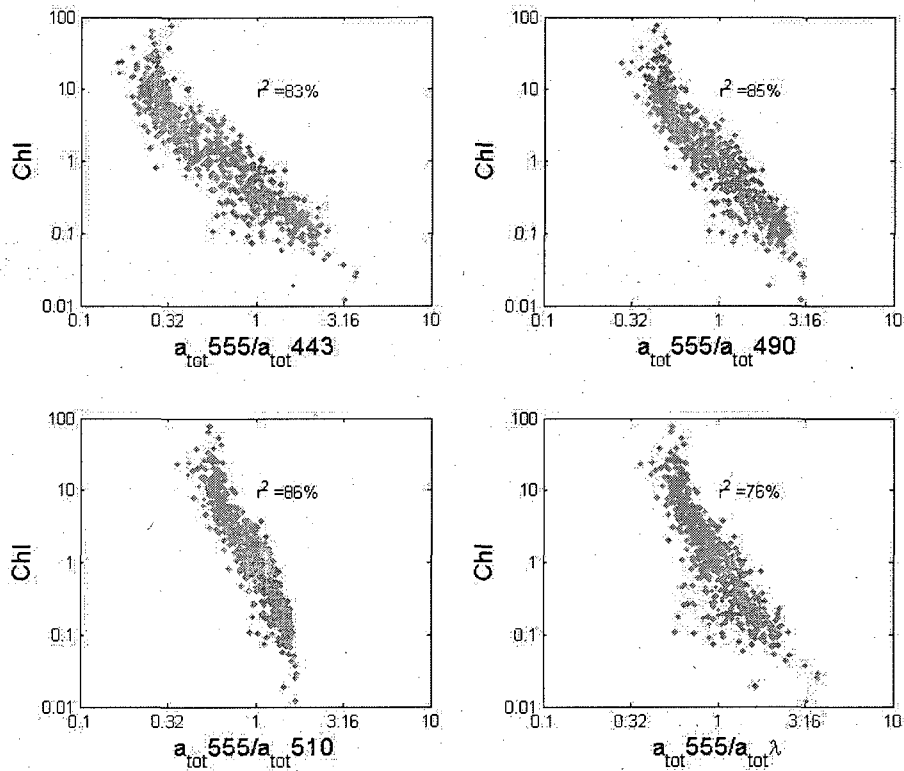
Figure 4-6: **Selecting the total absorption approximation for MBR.** TOP LEFT: $a_{tot}555/a_{tot}443$ vs. Chl. TOP RIGHT: $a_{tot}555/a_{tot}490$ vs. Chl. BOTTOM LEFT: $a_{tot}555/a_{tot}510$ vs. Chl. BOTTOM RIGHT: $a_{tot}555/a_{tot}\lambda$ vs. Chl.
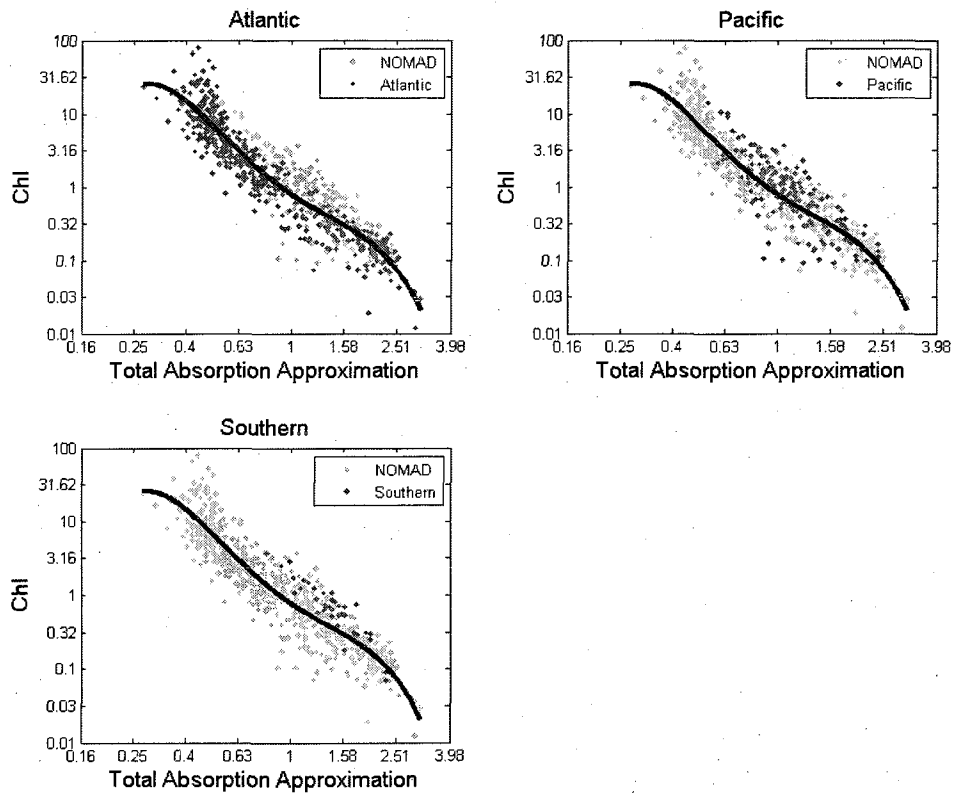
Figure 4-7: **NOMAD v.2 subset (n=696) with RCE$_{atot}$ fit, separated by ocean.** The grey points represent all the data, and the dark points represent the data from the specified ocean. The thick black line represents the RCE$_{atot}$ fourth-order polynomial fit to the data.
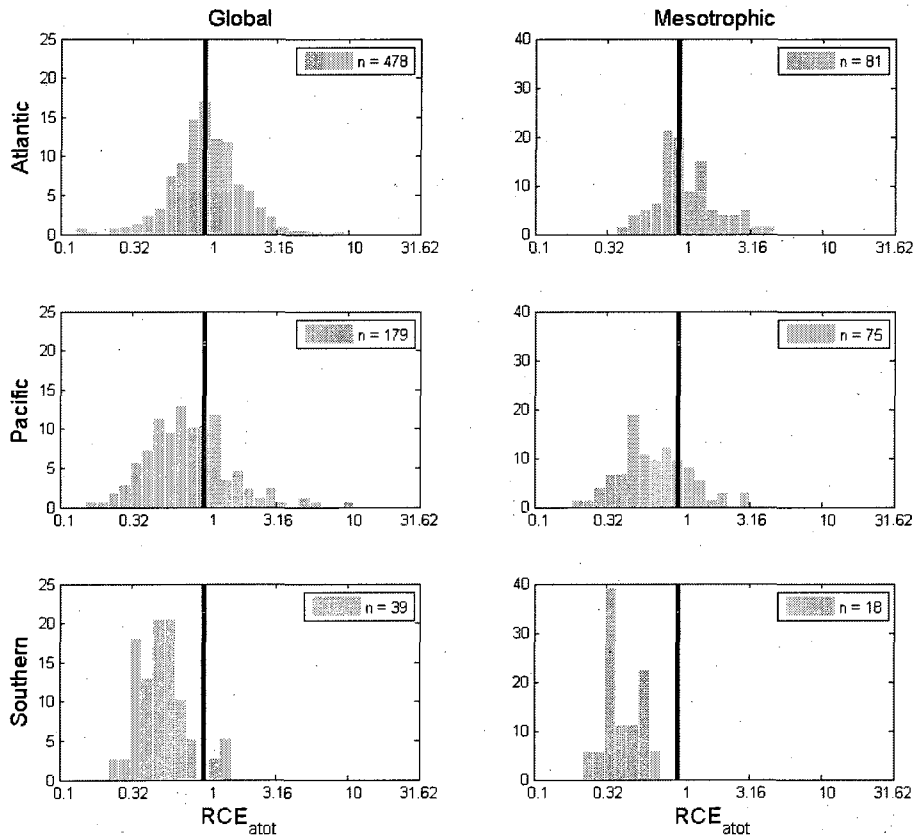
Figure 4-8: **Histograms for the % Frequency of RCE_{atot}: Global vs Mesotrophic** TOP LEFT: Global Atlantic. MIDDLE LEFT: Global Pacific. BOTTOM LEFT: Global Southern. TOP RIGHT: Mesotrophic Atlantic. MIDDLE RIGHT: Mesotrophic Pacific. BOTTOM RIGHT: Mesotrophic Southern. The Black line represents zero uncertainty.
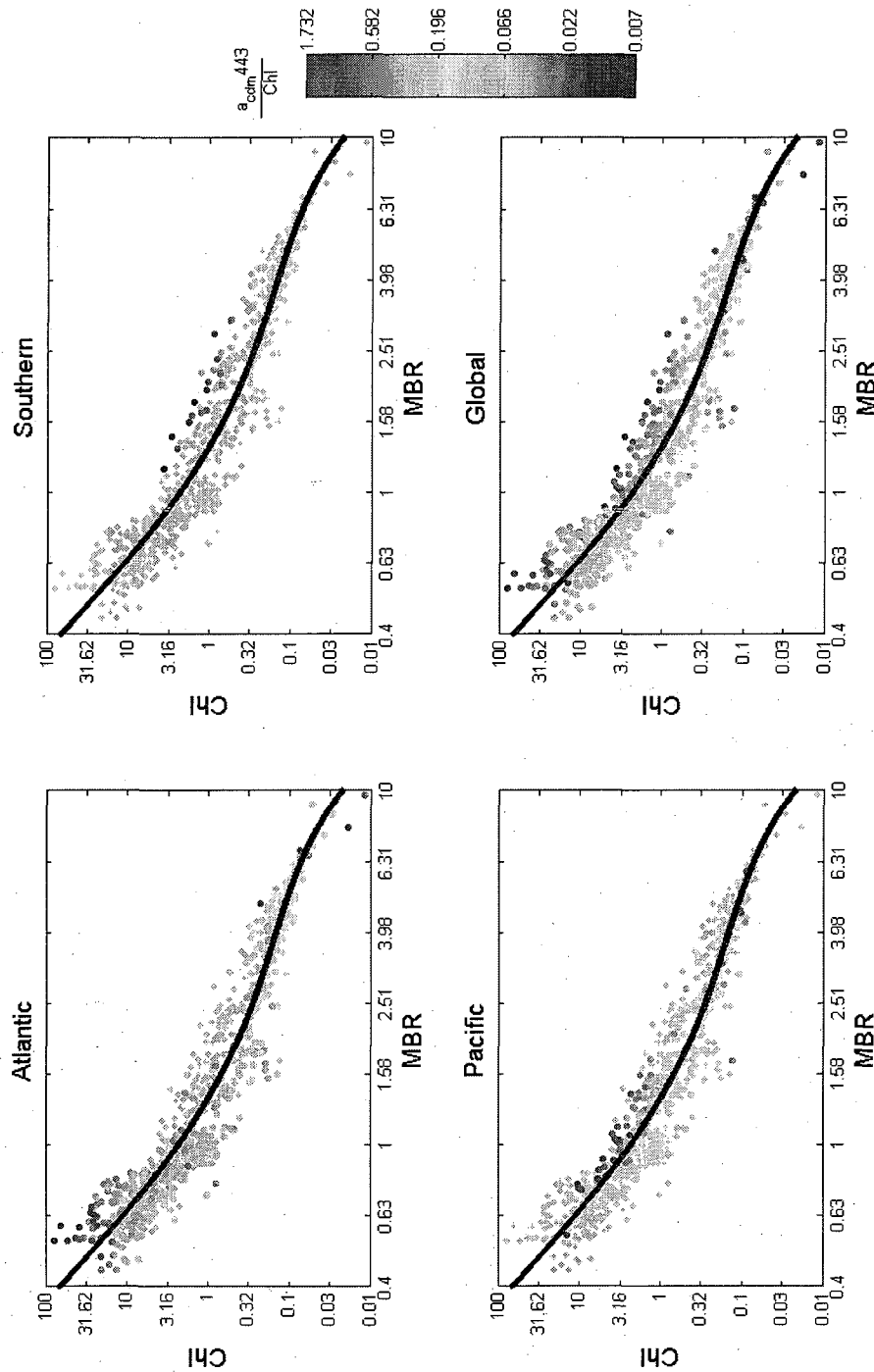
Figure 4-9: **The effects of CDM on the oceanic biases:** $a_{cdm}443/$Chl. The values for $a_{cdm}443/$Chl are color-coded according to the scale shown. The ratio $a_{cdm}443/$Chl is analyzed with respect to the algorithm biases when the data are sorted by ocean and viewed as a whole (bottom right).
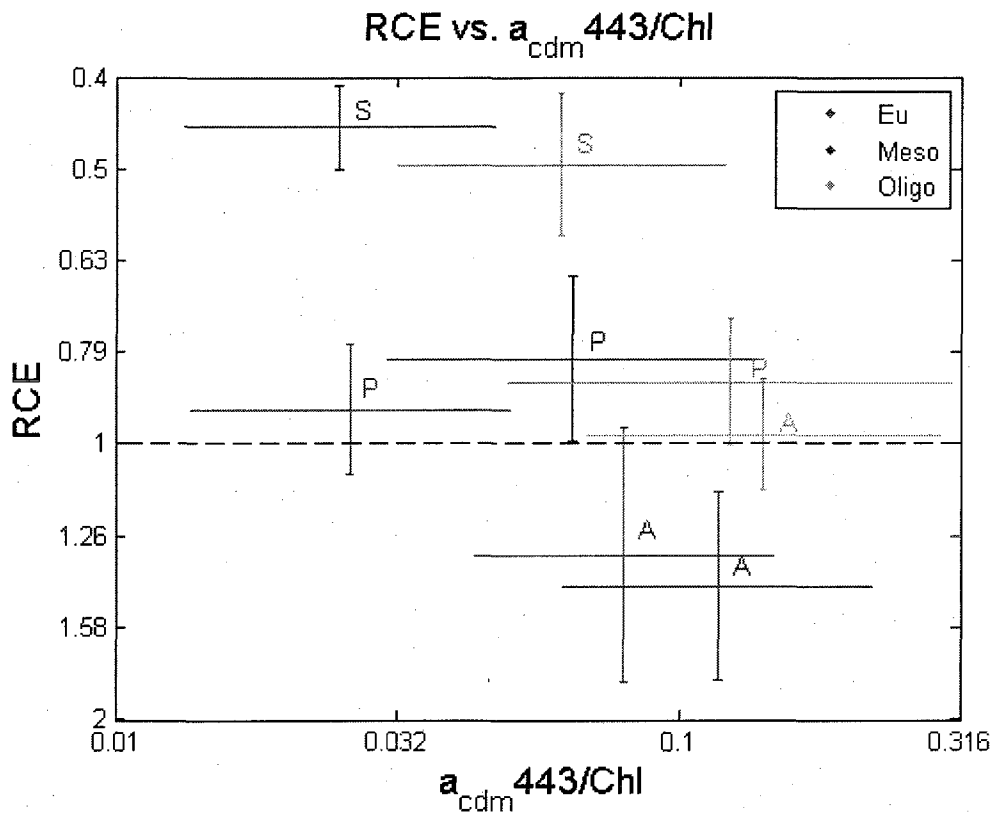
Figure 4-10: **The Category Statistics: RCE vs.** $a_{cdm}443/Chl$. The relationship between the median RCE ratio and the median $a_{cdm}443/Chl$ is presented for all ocean-trophic categories. The oceans are indicated by the letters, 'A', 'P', and 'S' and the trophic category by the colors. Each category's statistics are represented by a vertical and horizontal line. The lines represent the standard deviation about the median, which is located at the intersection. Note the vertical increase in RCE; RCE > 1 indicates overestimations and RCE < 1 indicates underestimations.
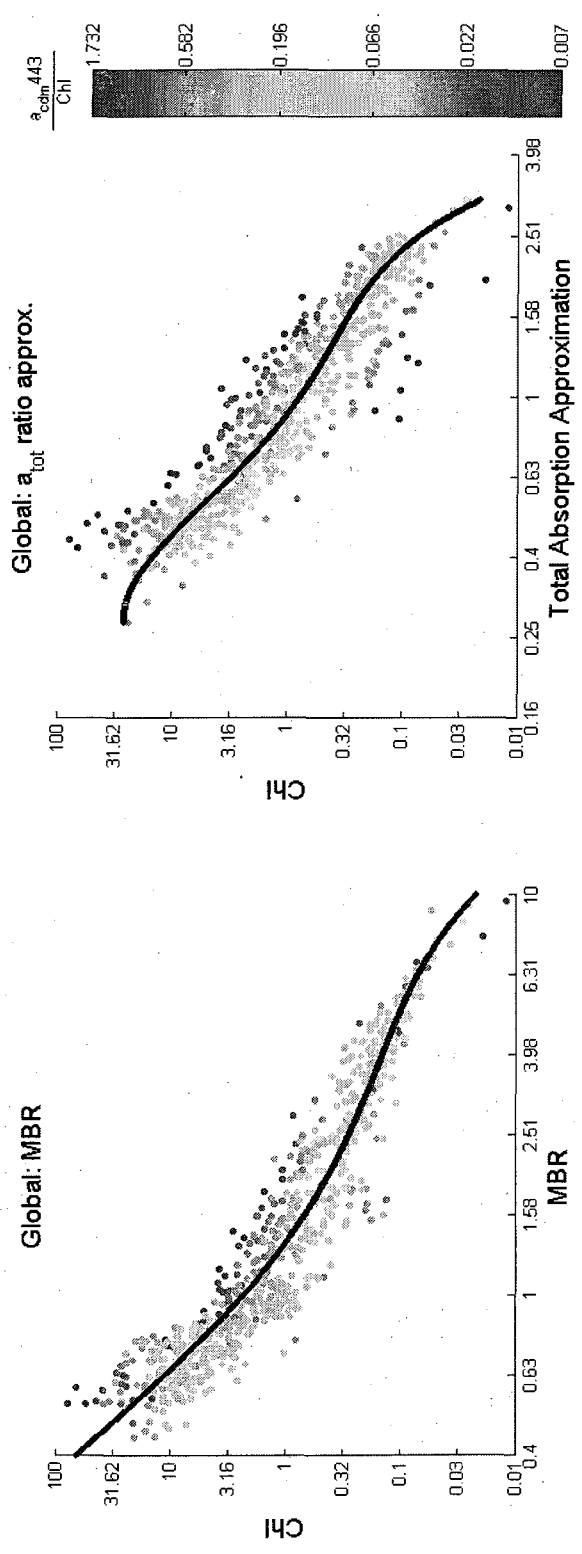
Figure 4-11: The effects of CDM on the oceanic biases: MBR vs Total Absorption Approximation. The ratio $a_{cdm}443/Chl$ (color-coded) is analyzed with respect to the algorithm biases when the data are viewed as a whole. Left= the original analysis. Right= the analysis with the $a_{tot}555/a_{tot}490$ approximation of MBR.
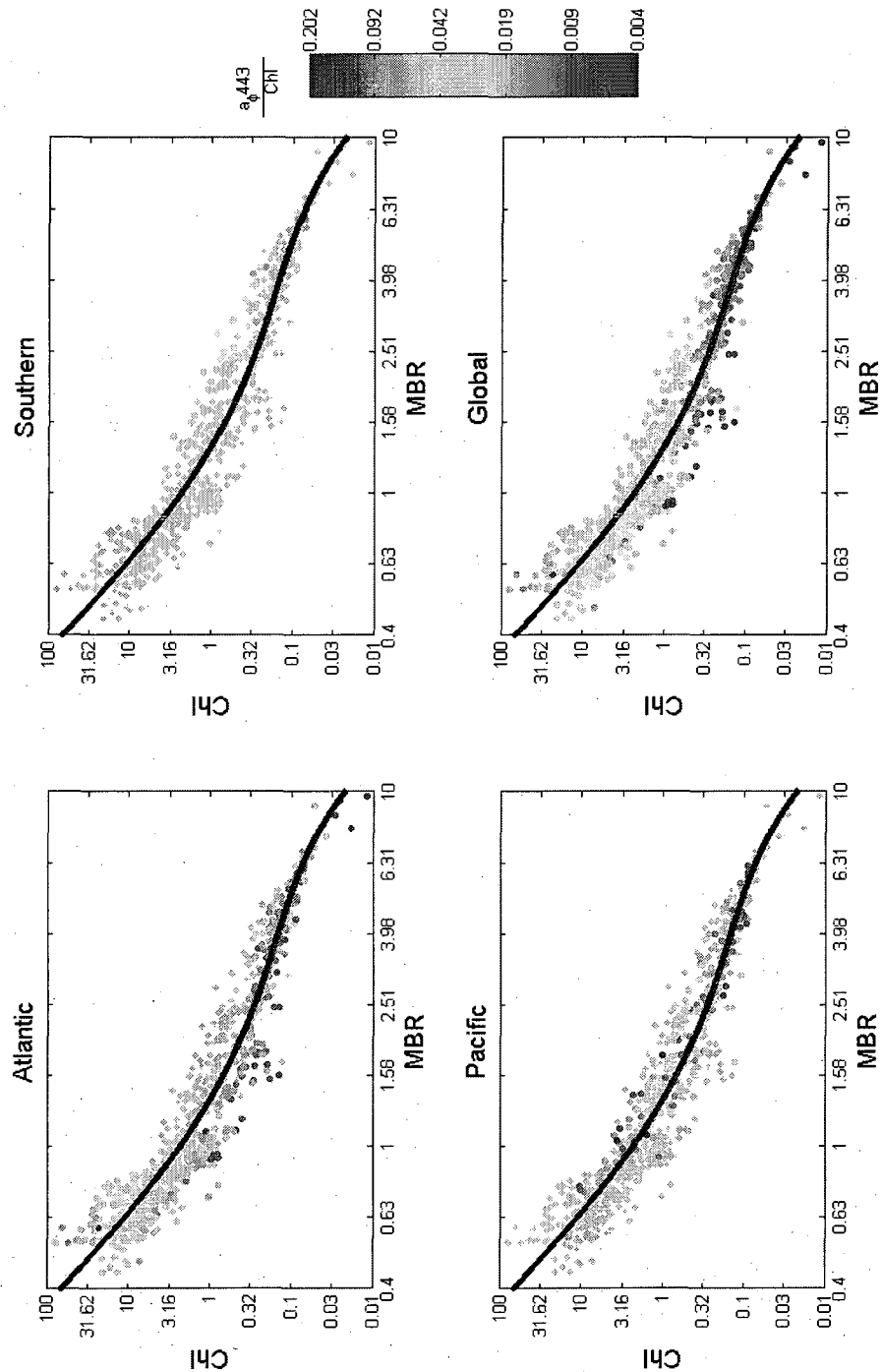
Figure 4-12: **The effects of pigment packaging on the oceanic biases:** $a_\phi 443/Chl$. The values for $a_\phi 443/Chl$ are color-coded according to the scale shown. $a_\phi 443/Chl$ is analyzed with respect to the algorithm biases when the data are sorted by ocean and viewed as a whole (bottom right).
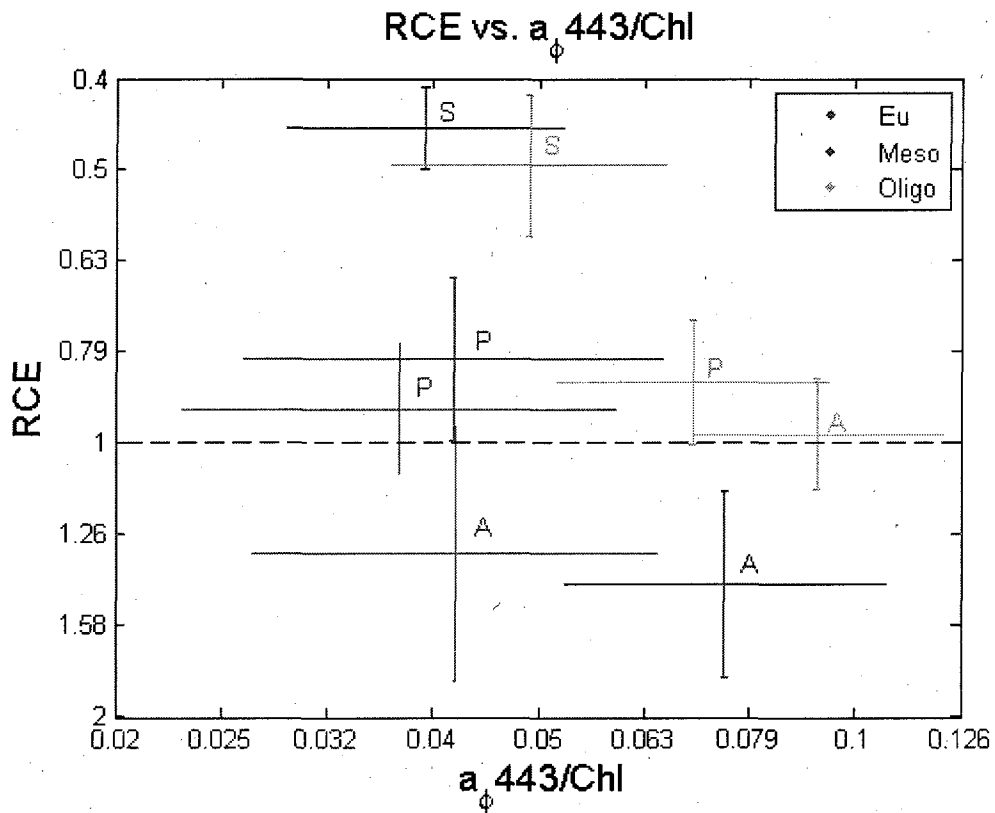
Figure 4-13: **The Category Statistics: RCE vs. $a_\phi 443/Chl$.** The relationship between the median RCE ratio and the median $a_\phi 443/Chl$ is presented for all ocean-trophic categories. The oceans are indicated by the letters, 'A', 'P', and 'S' and the trophic category by the colors. Each category's statistics are represented by a vertical and horizontal line. The lines represent the standard deviation about the median, which is located at the intersection. Note the vertical increase in RCE; RCE > 1 indicates overestimations and RCE<1 indicates underestimations.
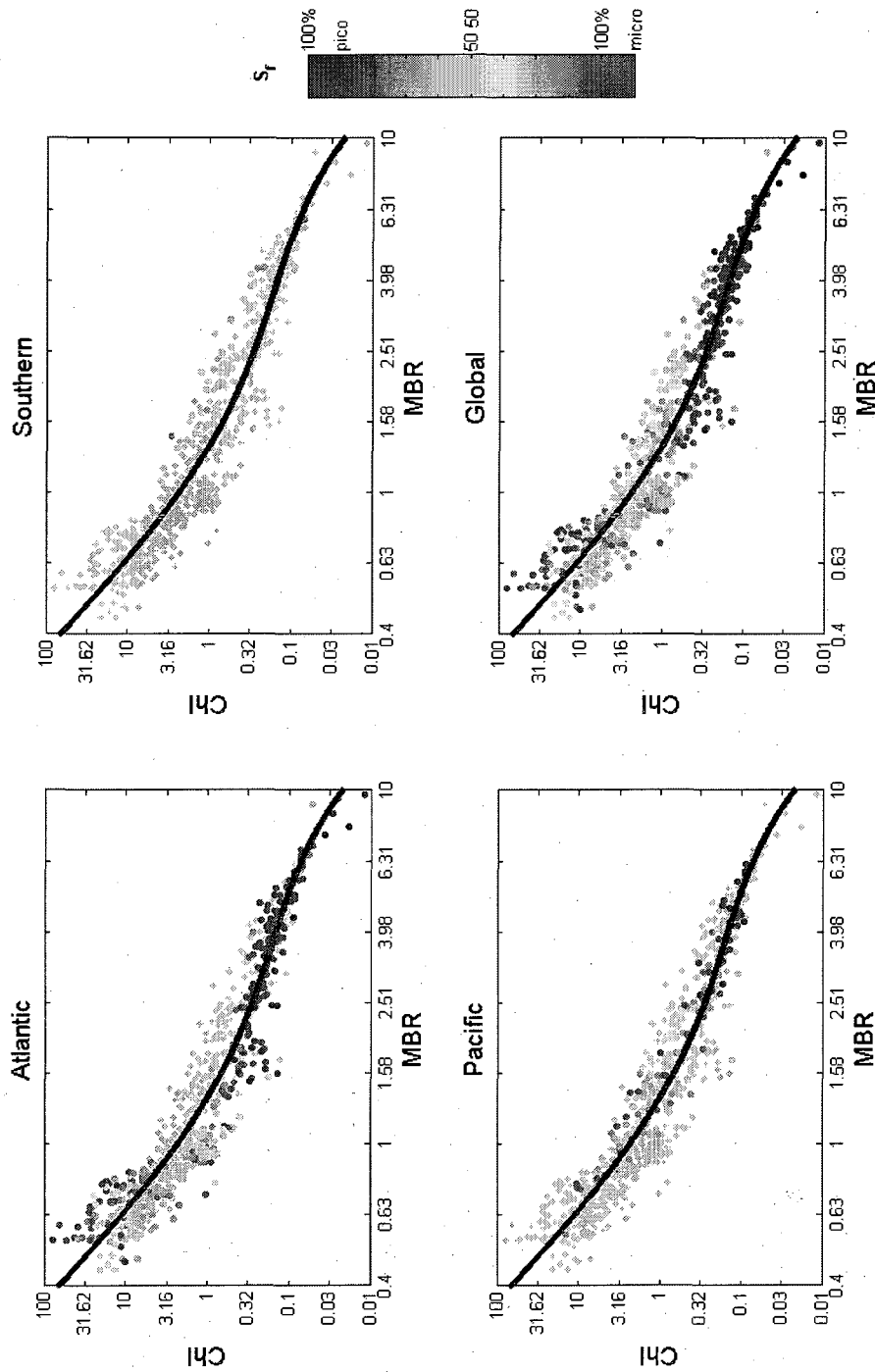
Figure 4-14: **The effects of cell size on the oceanic biases:** S_f. The values for S_f are color-coded according to the scale shown. S_f is analyzed with respect to the algorithm biases when the data are sorted by ocean and viewed as a whole (bottom right).
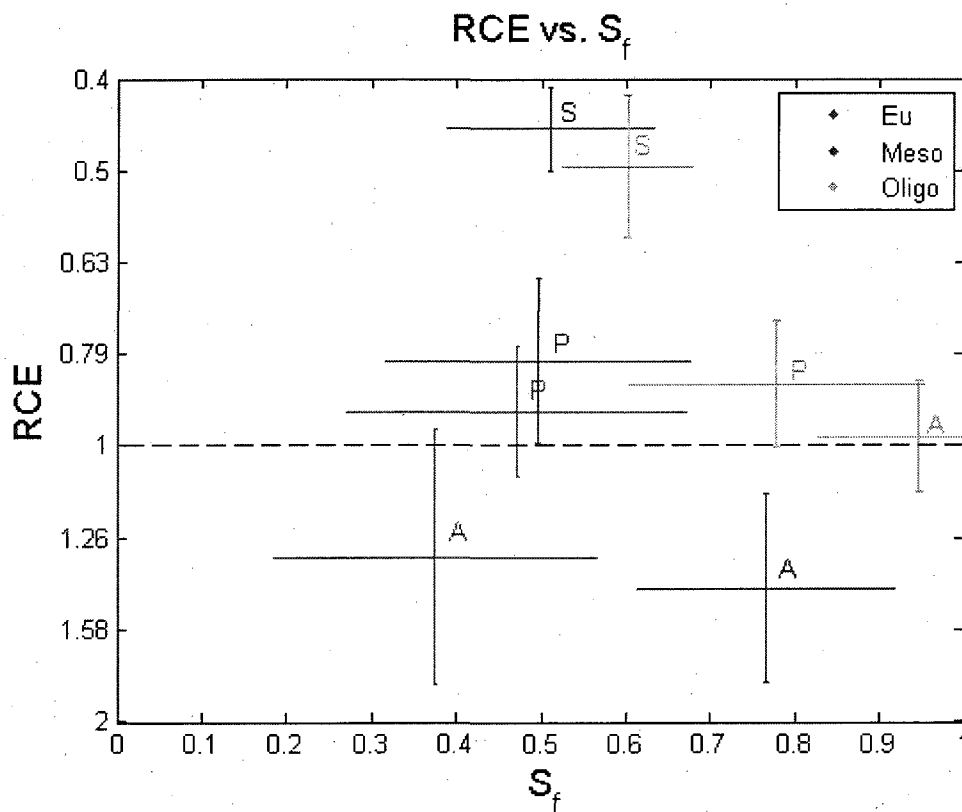
Figure 4-15: **The Category Statistics: RCE vs. S_f.** The relationship between the median RCE ratio and the mean S_f is presented for all ocean-trophic categories. The oceans are indicated by the letters, 'A', 'P', and 'S' and the trophic category by the colors. Each category's statistics are represented by a vertical and horizontal line. The lines represent the standard deviation about the mean, which is located at the intersection. Note the vertical increase in RCE; RCE > 1 indicates overestimations and RCE<1 indicates underestimations.
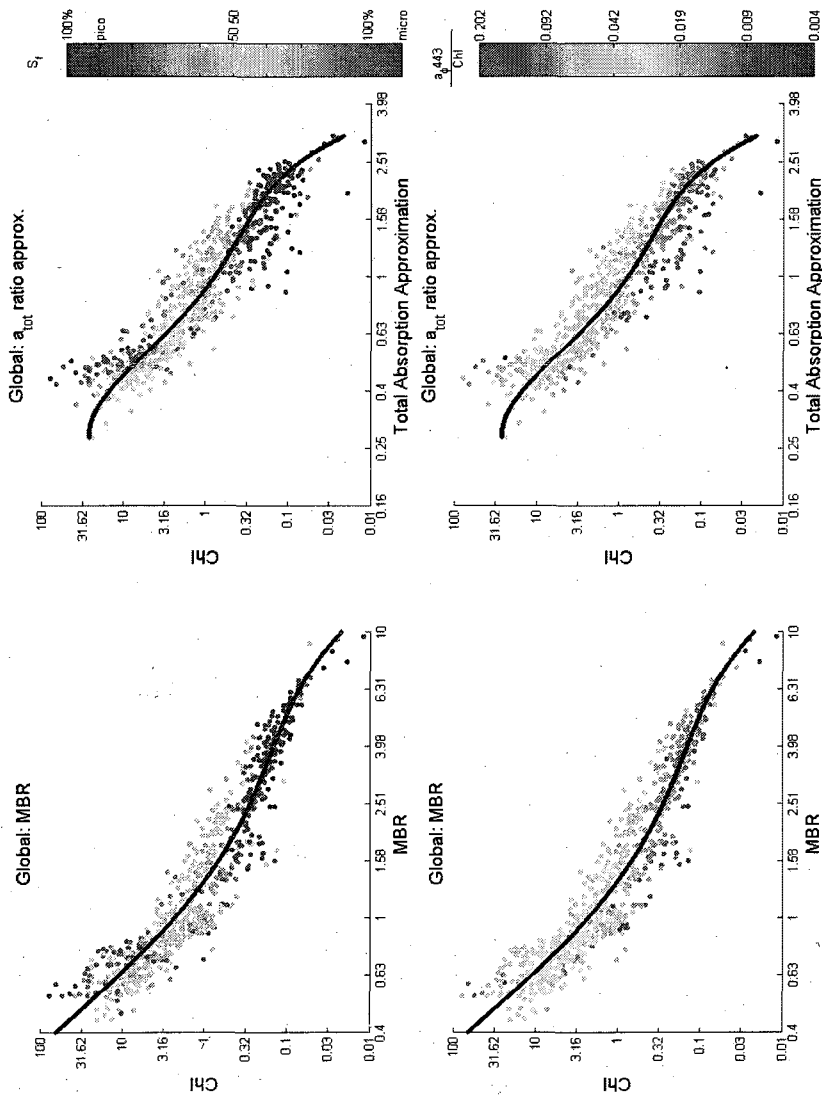
Figure 4-16: **The effects of phytoplankton community structure on the oceanic biases: MBR vs Total Absorption Approximation (S_f and $a_\phi 443/$Chl).** The parameters S_f and $a_\phi 443/$Chl are analyzed with respect to the algorithm biases when the data are viewed as a whole. TOP LEFT= S_f with MBR, TOP RIGHT = S_f with Total Absorption Approximation. BOTTOM LEFT= $a_\phi 443/$Chl with MBR, TOP RIGHT = $a_\phi 443/$Chl with Total Absorption Approximation.
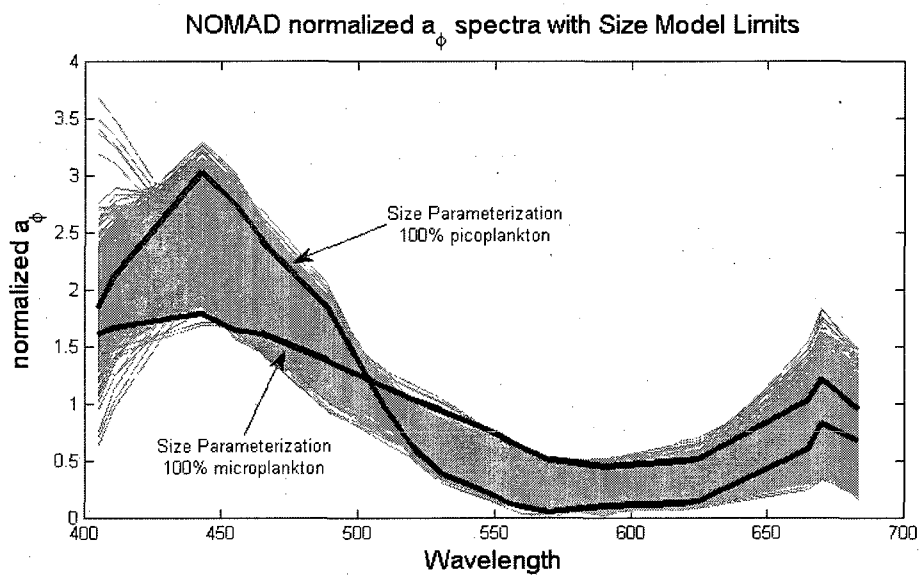
Figure 4-17: **Normalized a_ϕ spectra from NOMAD.** NOMAD's $a_{\phi n}$ spectra (grey lines) and the $a_{\phi n}$ spectra associated with picoplankton (larger peak near 450) and microplankton based on Eqn. 3 from Ciotti et al. (2002) (black lines).

Table 4. Results from a linear decomposition of the phytoplankton absorption spectra for the different communities (*see Table 2*) using a linear regression subjected to constraints (Eq. 3). The size factor S_{f} is estimated and varies from 1.0 to zero for small and large cell sizes, respectively; r^2 is the coefficient of determination between observed and estimated spectra for 301 wavelengths from 400 to 700 nm. nr, not relevant. The linear regression uses two basis vectors representing the minimum and maximum cell size found in our data set (Table 3). For reference, $\langle a_{ph}^* \rangle$, the average $a_{ph}^*(\lambda)$ for each community (400–700 nm) is presented. Spectra of $a_{ph}^*(\lambda)$ can be reconstructed for each community by substituting S_{f} into Eq. 3 and multiplying the result by $\langle a_{ph}^* \rangle$.

Community	S_{f}	r^2	No. of samples	$\langle a_{ph}^* \rangle$ (m^2 mg^{-1})
P-Pro	1.000	nr	7	0.0259
P-Syn	0.663	0.993	9	0.0195
U-flag1	0.598	0.979	20	0.0160
U-flag2	0.369	0.992	4	0.0180
U-flag3	0.558	0.995	14	0.0181
U-unkw	0.491	0.992	9	0.0170
U-Phae	0.664	0.982	12	0.0175
N-din	0.287	0.987	7	0.0111
N-cfd1	0.370	0.981	8	0.0126
N-cfd2	0.266	0.963	5	0.0169
N-cfd3	0.151	0.954	3	0.0138
N-flag	0.442	0.995	11	0.0136
M-cfd1	0.002	0.989	8	0.0067
M-cfd2	0.014	0.993	15	0.0076
M-din1	0.025	0.987	2	0.0059
M-din2	0.000	0.990	2	0.0072

Figure 4-18: **Table 4 from Ciotti et al. (2002): the cell size parameter.** This table shows the categorization of the S_{f} parameter into the different sizes of phytoplankton: pico-, ultra-, nano-, and micro.
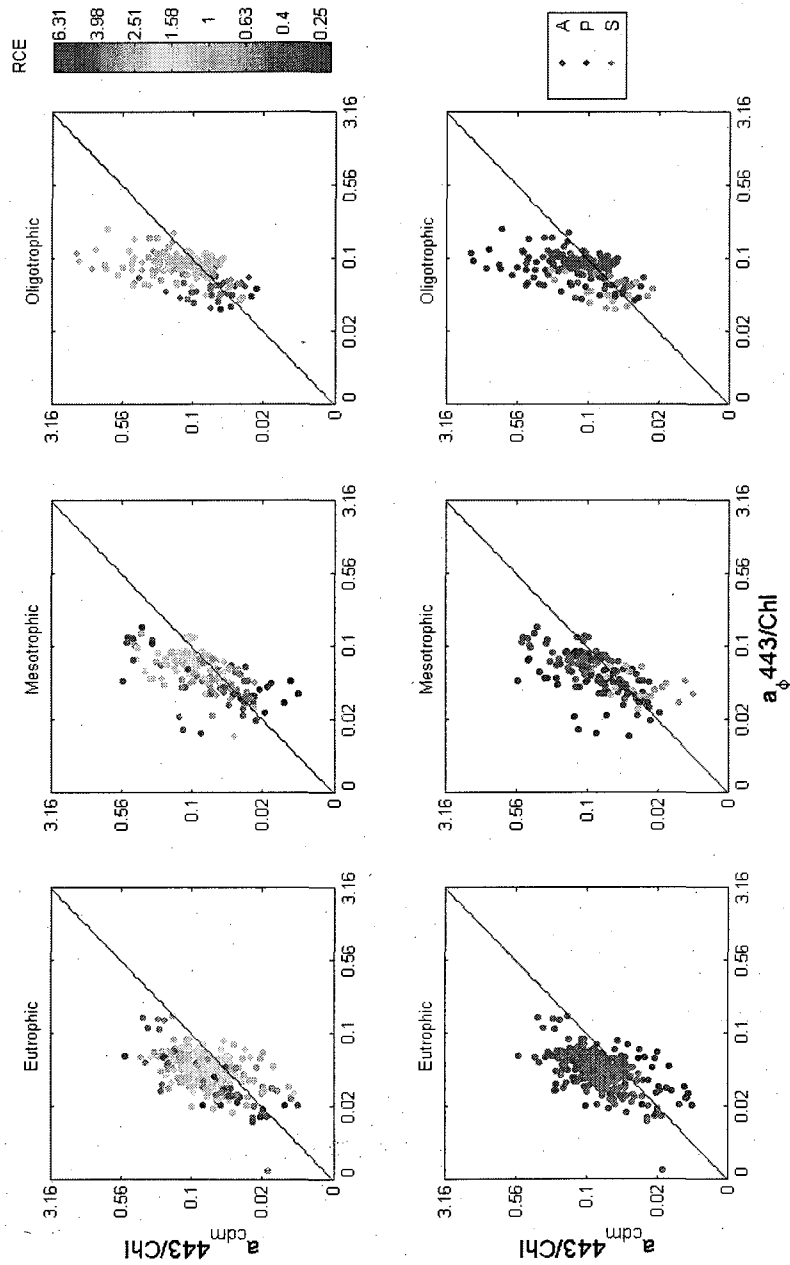
Figure 4-19: **The dependence of RCE on the parameters** $a_{cdm}443/Chl$ **and** $a_\phi 443/Chl$ **for NOMAD sorted by trophic category.** Note: Axes and color scales are logarithmic. TOP: RCE is color-coded over the relationship between $a_{cdm}443/Chl$ and $a_\phi 443/Chl$ for NOMAD when sorted by trophic category (LEFT=Eutrophic, MIDDLE=Mesotrophic, RIGHT=Oligotrophic). BOTTOM: Data are color-coded for the oceans (Red = Atlantic, Blue = Pacific, and Green = Southern).

CHAPTER 5

DISCUSSION AND CONCLUSIONS

5.1 Validation and explanation of the algorithm uncertainty through inherent optical properties

Upon utilizing the absorption measurements of NOMAD, the analyses of this work provide evidence that confirms the existence of the oceanic biases and the hypotheses that such biases depend on the relative presence of CDM and the phytoplankton community structure. The validation of the oceanic biases was accomplished using the total absorption approximation of MBR. By exhibiting similar oceanic biases with the approximation, a measurement produced independently from MBR, it is evident that the oceans are in fact, optically different. Possible artifacts were analyzed, and no algorithm biases were found for such factors.

This work corroborates the predicted effects of CDM and phytoplankton community structure on the algorithm uncertainty, as hypothesized from past literature. When evaluating the effects separately, the parameters $a_{cdm}443/Chl$, S_f, and $a_\phi443/Chl$, clearly exhibited systematic variation with algorithm uncertainty, which was denoted by RCE. Increases in $a_{cdm}443/Chl$ followed a general shift from under- to overestimation for the eutrophic and mesotrophic stations. Likewise, increases in $a_\phi443/Chl$ followed a general shift from under- to overestimation for all the stations excluding a few oligotrophic ones (where MBR ~ 6.31), and an increase in S_f followed a shift from under- to overstimation for mainly the mesotrophic stations. Evidently, such parameters indicated the effects of the two features on the oceanic biases themselves.

From these analyses, global predictions of the parameters $a_{cdm}443/Chl$, S_f, and

$a_\phi 443/Chl$ can be made, thereby introducing new satellite-derived products. Additionally, quantitatively comparing the global estimates of these respective parameters to corresponding observed measurements from NOMAD could be used to account for the oceanic biases of the empirical ocean color algorithms.

In actuality, the general effect of the three factors are not novel to the ocean optics community, as they are consistent with theoretical expectations. MBR represents the shape of the R_{rs} spectra, which is inversely related to total absorption, the sum of a_w, a_{cdm}, and a_ϕ. Waters can have similar MBR values, but different compositions of total absorption, which can be associated to different levels of Chl. The different distributions of total absorption can stem from different levels of CDM abundance as seen in the CDM effect analysis, and different cell sizes and levels of pigment packaging as seen in the phytoplankton community structure analysis. Ultimately, the world's oceans have different inherent optical properties corresponding to similar apparent optical properties.

Furthermore, the separate analyses using the total absorption approximation suggest that the spectral shape of backscattering, an indication of particle size and composition, confounds the effects of CDM on the algorithm uncertainty for oligotrophic waters. This conclusion is also consistent with theoretical expectations. In oligotrophic waters with low levels of Chl, changes in the backscattering spectral shape could exhibit a similar strength to changes in total absorption spectral shape due to the presence of CDM. In such a case, the assumption that the backscattering spectral shape is considered negligible in Eqn. 2.5 may not hold.

Removing the backscattering spectral shape did not significantly improve the systematic variation of $a_\phi 443/Chl$ with Chl in oligotrophic waters, and this can be attributed to two reasons. Either the change in backscattering spectral shape is not as strong as the change in total absorption spectral shape due to phytoplankton, or the backscattering spectral shape in oligotrophic waters is due predominantly to CDM (*i.e.*, NAP) rather than to phytoplankton. Actually, a significant negative correlation has been found for the backscattering spectral shape and Chl in the open ocean (Huot et al., 2008). Still, it is difficult to know the relative plausibility of each one.

5.2 The relative significance of CDM and phytoplankton community structure on algorithm uncertainty

Having gone through the fundamental mechanisms that drive the algorithm uncertainty, it is then compelling to consider the relative significance of these mechanisms. This assessment was performed both qualitatively and quantitatively. The results are summarized in Table 5.1.

The qualitative analysis (Figure 4-19) shows that CDM is generally the stronger component in total absorption. In fact, this is the case for all the overestimated stations, and about half of the underestimated stations. Such statements speak for the relative magnitudes of the two parameters, but do not suggest the relative importance of their effects on algorithm uncertainty. Trends in RCE relative to variations in $a_{cdm}443/Chl$ and $a_\phi 443/Chl$ were hypothesized, and quantitative results were obtained through the regression analyses.

The regression models explained about 22 to 28 % of the algorithm uncertainty, as indicated by the values for r^2 of each regression. Results revealed that CDM in fact, had the stronger influence on algorithm uncertainty than pigment packaging for all categories except for the Oligotrophic category and the Atlantic-Oligotrophic category, which makes up most of the Oligotrophic category. In the Atlantic-Mesotrophic, and the Pacific-Eutrophic and -Oligotrophic categories, the pigment packaging parameter did not effectively reduce the residuals, and thus did not appear in the final model. In the Eutrophic, the Atlantic-Eutrophic (representing 88 % of the Eutrophic stations), and the Southern-Oligotrophic categories, the parameter with the stronger influence corresponded to the smaller coefficient (b_1 aside), proving that the relative magnitudes of the coefficients are not a sufficient indicator of the relative importance of the two effects.

The regression results on the relative importance are consistent with qualitative results, and this is best observed by a comparison of the variation in $a_{cdm}443/Chl$ and $a_\phi 443/Chl$ relative to RCE in Figures 4-9 and 4-12. For instance, in the Atlantic-Eutrophic category, CDM has the stronger influence, and in the figures, the variation of $a_{cdm}443/Chl$ is more systematic than that of $a_\phi 443/Chl$ (relative

to RCE).

Perhaps, the greater effect of CDM on oceanic biases can be explained by the fact that pigment packaging is influenced more by biological influences than the presence of CDM, and biological influences in general (though may be arguable) can be more complex than chemical or physical influences. Pigment packaging may possibly vary by region depending on the type of nutrients available, grazing activity, and community structure. In fact, the ambiguity of pigment packaging levels for different species within the same size range is evident in the overlapping size classifications for the S_f parameter from Ciotti et al. (2002). See Figure 4-18. Phytoplankton may also have distinct survival features that allow them some control of the community structure. For instance, certain large-sized phytoplankton have flagella with which to move vertically to avoid certain dangers or to find nutrients. On the other hand, the constituents of CDM would change mainly due to mixing and chemical reactions in the waters.

The result that pigment packaging has a stronger influence than CDM on algorithm uncertainty in the oligotrophic category can be explained by the results that suggest the confounding of the CDM effect by the backscattering spectral shape. Such a suggestion is supported by the theoretical understanding of bio-optics. In the Southern oligotrophic category, CDM actually has a stronger influence than pigment packaging, based on the regression results. This is possibly attributed to the limited number of stations (n=22), and also the chance that the stations in this category were composed of similar phytoplankton communities, such that the pigment packaging reflected a limited number of phytoplankton species.

In relating the oceans' inherent optical properties to differences in CDM concentration and phytoplankton community structure, this work suggests that differences in the oceans' optical properties are due to differences in the biogeochemical processes, which are ultimately attributed to differences in the oceans' deep-water chemistry. Reflected in profiles of nutrient concentrations among the oceans, deep-water chemistry is determined by the thermohaline circulation (Segar, 2007). North-Atlantic-Deep-Water formation at the poles establishes an eastward path for deep water from the Atlantic Ocean to the Pacific Ocean, and deep-water is upwelled

along the way in certain locations (Segar, 2007). Based on the work of this thesis, one would suggest that the optical properties of surface waters would reflect the chemical nature of the waters from which they were upwelled.

The conclusions of this thesis are ultimately contingent on the capability of the NOMAD subset (n=696) in representing the world's oceans. While the oceanic biases were observed in both the entire dataset and its subset, there are two concerns. One is the geographic distribution of the subset. The other is the existence of ambiguities in the RCE-IOP relationship such that different IOP combinations can give rise to the same biases.

5.3   Considering the geographic distribution of NOMAD data

In considering the overall representation of locations covered in NOMAD, un-observed bio-optical relationships indeed appear likely. A majority of NOMAD's stations with absorption measurements stem from regions less than 100 miles off the coast. The Pacific Ocean stations are mainly from the Southern California coast, the East China Sea, the Sea of Japan, and the coast of Northern Alaska. In the Southern Ocean, the stations are all from the Drake Passage and Bransfield Strait off the tip of the Western Antarctic Peninsula. In the Atlantic Ocean, 70% of the mesotrophic samples are from the Western Florida Shelf. Consequently, it is likely that regions and subsets with a lack of stations, such as the Southern-Ocean mesotrophic category, do not yield representative results.

The question of the extent of regional coverage from NOMAD was addressed by Moore et al. (2009), and their results support the caveat. Moore and colleagues classify reflectance spectra into eight categories using a clustering technique on the NOMAD dataset. They present the frequency at which the reflectance classes have been observed by satellite (Moore et al., 2009). Figure 5-1 shows the eight classes. Class 4 is considered to be the only mesotrophic category based on my definition (See Section 3.1.1). In assessing the frequency of this class from global satellite observations, the work of Moore et al. (2009) suggests that mesotrophic waters are

prevalent in several areas not covered in NOMAD including the Malvinas current off the southeast coast of South America, the Benguela current off the southwest coast of Africa, and the northern section of the entire North Atlantic Ocean in which the spring bloom occurs annually (Figure 5-2). Based solely on the limited spatial coverage, it appears risky to extrapolate the relationships observed in NOMAD to other locations.

5.4   Ambiguities in RCE-IOP relationships

Based on the explanation of the algorithm uncertainty through IOPs, it is reasonable to believe that similar levels of RCE are associated to different combinations of the level of pigment packaging and the abundance of CDM. The mesotrophic Pacific Ocean outliers, seen in Figure 4-19, serve as examples. These outliers exhibit a strong pigment packaging effect and a moderate CDM effect, while stations with corresponding RCE values exhibit a lower pigment packaging and lower levels of the CDM effect. Such outliers cast doubt on the generality of the relationships already observed in NOMAD.

An assessment of the ambiguities was made based on an evaluation of the literature (Fiorani et al., 2006; Clementson et al., 2001; Dierssen and Smith, 2000; Arrigo et al., 1998; Mitchell and Holmhansen, 1991; Barbini et al., 2003; Garcia et al., 2005; Nelson et al., 2007; Tarran et al., 2006; Siegel et al., 2005b,a; Bricaud et al., 1981). Unfortunately, there are rarely reported simultaneous measurements of a_ϕ, a_{cdm}, (or a_{cdom}), Chl, reflectance, and phytoplankton species.

Here, the discussion of these ambiguities will be focused on the ocean-trophic categories that best portrayed the oceanic biases: the mesotrophic Southern and Atlantic Oceans. The possible ambiguities for the Southern Ocean and Atlantic Ocean are considered separately. It is assumed that the mesotrophic CDM is predominantly autochthonous CDOM in the Southern Ocean, and both autochthonous and terrigenous CDOM in the Atlantic Ocean. The variability within $a_{nap}443/a_{cdom}443$ (Figure 5-3) and the spectral shape of a_{cdom}, S, (Figure 5-4) show that the current data convey such characteristics.

I hypothesize that the conditions not present in NOMAD for the mesotrophic Southern Ocean are likely to exhibit weaker pigment packaging levels and stronger CDM influence compared to the conditions reported in NOMAD. For the mesotrophic Atlantic Ocean, I speculate that the conditions not present in NOMAD are likely to exhibit stronger pigment packaging levels and weaker CDM influence compared to the conditions reported in NOMAD. The following sections present the explanations for my hypotheses.

5.4.1 Southern Ocean

The mesotrophic NOMAD stations of the Southern Ocean were underestimated by the algorithm, and they corresponded to low levels of $a_{cdm}443/Chl$ and relatively low levels of $a_\phi 443/Chl$. Other combinations of these properties that can lead to levels of underestimation (low RCE) include higher levels of $a_{cdm}443/Chl$ associated to lower $a_\phi 443/Chl$ (larger cell size), or lower levels of $a_{cdm}443/Chl$ associated to higher levels of $a_\phi 443/Chl$ (smaller cell size). Since the values for $a_{cdm}443/Chl$ reported for such regions represent the lowest levels observed from the entire mesotrophic category, it is more likely that unreported scenarios will have higher values for $a_{cdm}443/Chl$ and lower values for $a_\phi 443/Chl$.

Evidence from the literature search generally supported the levels of influence from CDOM, pigment packaging, and cell size reported in NOMAD. One work (Fiorani et al., 2006) reports the existence of CDOM levels higher than those observed in NOMAD supposedly in the mesotrophic Southern Ocean, but differences can actually be attributed to the oceanic bias of the algorithm. Therefore, this work ultimately supports the Southern Ocean conditions reported in NOMAD. While no evidence of the unreported scenario (higher $a_{cdm}443/Chl$ with lower $a_\phi 443/Chl$) was found in the literature, possible conditions to create this scenario were considered.

Support for results from NOMAD on community structure and CDM fraction

Phytoplankton that adapt well to low light levels, like those found in the Southern Ocean (Mitchell, 1992), will produce more chlorophyll pigments per cell and hence, enhance pigment packaging and reduce absorption per *Chl* (Mitchell and Kiefer, 1988b; Mitchell and Holmhansen, 1991). Such inferences support the NOMAD results of Southern Ocean stations having relatively strong pigment packaging. While no exact cases were found in the literature, the review did suggest that a strong presence of CDM is unlikely in this high latitude region, thus, supporting the conditions for the Southern Ocean reported in NOMAD.

Fiorani et al. (2006): an example of an effect of the algorithm oceanic bias

Fiorani et al. (2006) presented ratios of $a_{cdom}440/Chl$ for the Ross Sea that are higher than those in NOMAD for *Chl* associated to the mesotrophic category (*Chl* ranging from 0.316 to 3.16 mg m^{-3}). This work involved the estimate of $a_{cdom}440/Chl$ using a unique LIDAR calibration of the SeaWiFS algorithm. For mesotrophic conditions, average estimates of $a_{cdom}440/Chl$ derived from several 8-day composites of SeaWiFS reflectance images between 2001 and 2003 consistently fall within the range 0.05 and 0.06 m^{-1}/mg m^{-3}. In comparison, the corresponding $a_{cdom}440/Chl$ values for the few Southern Ocean stations in NOMAD are approximately 0.03 m^{-1}/mg m^{-3}. This difference of 0.02 units can be attributed to the Southern Ocean bias of the SeaWiFS algorithm from which the *Chl* was calculated. If the estimates of *Chl* were higher as they are for the NOMAD observations, then the values for $a_{cdom}440/Chl$ would be consistent with those found in NOMAD.

Speculation on the conditions that could yield stronger CDM and weaker pigment packaging levels in the mesotrophic Southern Ocean

One possible way to reach conditions of stronger CDM and weaker pigment packaging levels is through selective grazing by different sizes of zooplankton. This

is based on the finding that large phytoplankton are generally grazed by large zooplankton and small phytoplankton by small microzooplankton (Froneman and Perissinoto, 1996). In the case where large phytoplankton are grazed by large zooplankton, heavy excretion from heterotrophic organisms could establish a strong presence of CDM while large-sized phytoplankton are removed by selective grazing. In the case where small phytoplankton are grazed by small microzooplankton, the conditions to develop small-sized phytoplankton communities would not likely be optimal to develop large-sized phytoplankton, and so these conditions would yield weak pigment packaging (small cell size), and grazing may establish a substantial presence of CDM. While such grazing would likely be less intense than that from large zooplankton, the degradation products have been found to stay suspended for a longer period of time than those of larger-sized organisms (Froneman and Perissinoto, 1996), thereby allowing for more time to create the desired conditions.

These two scenarios seem likely to occur at the decay of phytoplankton blooms. While seemingly plausible, they have not been reported in the current literature to my knowledge. Only low production of CDOM has been reported for Southern Ocean waters. Accordingly, I discuss in the order listed, CDOM produced by grazing activity, bacteria and viruses, and terrestrial inputs (Nelson and Siegel, 2002).

On the sources of CDOM production   Research on correlations between grazing activity and phytoplankton community structure show mixed results for these high latitude waters. Overall, the literature does suggest that heavy grazing activity (and consequently, a strong presence of CDM) would not occur in small-sized phytoplankton communities (Tagliabue and Arrigo, 2003; Shields and Smith, 2009; Tang et al., 2008; Froneman and Perissinoto, 1996). In the Subtropical Convergence and a warm-core eddy in the Atlantic sector of the Southern Ocean, large phytoplankton were grazed by large zooplankton and small phytoplankton by small microzooplankton (Froneman and Perissinoto, 1996), suggesting that microzooplankton are less capable than larger zooplankton of heavy grazing. Tagliabue and Arrigo (2003) and Tang et al. (2008) found that some nanoflagellates, such as Phaeocystis *Antarctica*, which are widely distributed in the Southern Ocean and the dominant

prymnesiophyte in the Ross Sea (Shields and Smith, 2009), can form colonies to deter grazing from microzooplankton. However, Shields and Smith (2009) reported findings of colonial cells inside the food vacuoles of ciliates, a microzooplankton.

A large concentration of CDOM produced from bacteria and viral lysing also appears unlikely from relatively low *Chl*, and this is supported in the literature. Nearly all Southern Ocean marine ecosystems have been found to contain low bacterial biomass (Cota et al., 1990; Zdanowski and Donachie, 1993). For the western Antarctic Peninsula region, it was found that bacterial biomass in the Antarctic Peninsula region only represented < 1-2 % of the phytoplankton biomass (Karl and Tien, 1991), and that phytoplankton performed the bulk of heterotrophic respiration although the abundance of bacteria was found to vary independently of chlorophyll biomass (Karl and Tien, 1991). Additionally, a model has shown that bacterial growth efficiency increases with chlorophyll biomass (Polimene et al., 2006). Hence low *Chl* would not yield high bacterial growth efficiency as needed to produce the strong CDOM signal.

Ultimately, terrestrial input from sea ice melting in the Southern Ocean appears most plausible as a source of strong CDOM concentrations in a small-sized phytoplankton community. Such a case has actually been observed during the XV (1999/2000) campaign of the Italian Research Programme for Antarctica, in which relatively high CDOM concentrations corresponded to ice-melting in the Terranova Bay, a region known to host P. *Antarctica* (Barbini et al., 2003). Unfortunately, apparent optical properties were not measured. Additionally, it has been suggested that river discharge and water from sea ice were the source of abundant dissolved carbon in the Artic Ocean waters of the Holocene (Belanger et al., 2007; Macdonald et al., 2006; Mcclelland et al., 2006), and this could possibly occur in the Southern Ocean. Still, the CDOM signatures of the Atlantic Ocean, known to be strong due to frequent river discharge of anthropogenic chemicals, would rarely occur in the barren ice-covered terrain of Antarctica, and empirical evidence has been found, in which only 10% of the organic matter was dissolved in the Ross Sea (Carlson et al., 2000).

Evidently, more work must be done to quantify and compare the rate of CDOM

production from these sources in order to assess their relative contribution to producing the contradicting scenario. Ideally, a deeper understanding of particulate backscattering (Stramski et al., 2004) and generally more stations of the optical properties would best resolve the remaining issues in this work.

5.4.2 Atlantic Ocean

The mesotrophic NOMAD stations of the Atlantic Ocean were overestimated by the algorithm, and they corresponded to high levels of $a_{cdm}443/Chl$ and high levels of $a_\phi 443/Chl$. Other combinations of these properties that can lead to similar levels of overestimation (high RCE) in the mesotrophic Atlantic include lower levels of $a_{cdm}443/Chl$ associated to higher levels of $a_\phi 443/Chl$, or higher levels of $a_{cdm}443/Chl$ associated to lower levels of $a_\phi 443/Chl$. Since the values for $a_\phi 443/Chl$ reported for such regions represent the highest levels observed from the entire mesotrophic category, it is more likely that unreported scenarios will have a higher influence from CDM associated to a stronger influence from pigment packaging (lower $a_\phi 443/Chl$).

First, the assessment of work by Moore et al. (2009) explained previously indicates the areas in which possible unreported scenarios can occur (Figure 5-2). Such regions include the Malvinas current off the southeast coast of South America, the Benguela current off the southwest coast of Africa, and the northern section of the entire North Atlantic Ocean in which the spring bloom occurs annually (Figure 5-2).

NOMAD data from the mesotrophic Atlantic category are consistent with the empirical evidence that CDOM decreases with distance from shore (Kowalczuk et al., 2009; Mannino et al., 2008; Pan et al., 2008; Del Vecchio and Subramaniam, 2004; Branco and Kremer, 2005; Vodacek et al., 1997). Terrestrial input of CDOM has been found to dominate the absorption signal only in estuaries and river mouths, inferring that such areas are eutrophic. The signal diminishes abruptly off-shore due to photo-oxidation, and so CDOM abundance is distinctively lower in off-shore mesotrophic waters, and even lower in open-ocean oligotrophic waters as the CDOM has more time to diminish.

Exceptions to this rule include the Amazon and Orinoco River outflows, which

significantly affect the absorption signals from the North Equatorial Countercurrent (Siegel et al., 2002). Actually, such off-shore regions affected by the strong outflows may actually host a contradicting scenario upon bleaching of the surface CDOM (Vodacek et al., 1997). Costa et al. (2009) supports the possible occurrence of the scenario, with empirical evidence showing that strong river flows support nanoplankton blooms.

CDOM in most off-shore waters is then predominantly the result of biological activity over a long period of time (Bricaud et al., 1981), and so variability in CDOM levels would occur gradually. Such conditions have been observed in the Mauritanian upwelling, in which CDOM levels were low and consistent while *Chl* varied over two orders of magnitude (Bricaud et al., 1981). Although it was not stated in this work whether the waters were mesotrophic or if their phytoplankton distributions were dominated by nanoplankton (Bricaud et al., 1981), the analysis of work of Moore et al. (2009) does suggest that the Canary Current, which coincides with this region, can be mesotrophic. Simultaneously, AMT cruises reveal that such waters were dominated by nanoplankton in 1996 and 1997 from April through May and from September through October (Gibb et al., 2000). Thus, such conditions yield an unreported scenario pertaining to both CDM and community structure.

Several mesotrophic stations in NOMADv.2 (n=2365) in the North Atlantic subpolar gyre may have different scenarios, and studies in the literature suggest this may be true (Gibb et al., 2000; Nelson et al., 2007; Siegel et al., 2005b). In particular, such works speculate that the region may encounter moderate CDM levels with nanoplankton-dominated communities. This region is poorly covered in NOMAD v.2 (n=696), and the nanoplankton-dominated communities would contradict the predominance of picoplankton reported for Atlantic mesotrophic waters. Gibb et al. (2000) presented a summary of pigment distributions from AMT cruises 2-5 with conclusions that the North Atlantic temperate waters, including the North Atlantic subpolar gyre, were found to host nanoplankton blooms, especially after the decline of the spring bloom. Bricaud et al. (2004), Bresnan et al. (2009), and Tarran et al. (2006) provide similar results.

The presence of CDM has been speculated to be fairly substantial for this area

in a satellite-based evaluation of global distributions of CDOM based on GSM products, (Siegel et al., 2005b), and the hypothesis was confirmed by *in situ* measurements in Nelson et al. (2007). The increased CDOM levels are most likely attributed to the weaker intensity of solar radiation, which enables deeper mixing, reduces photo-oxidation, and enhances biological activity (Nelson et al., 2007). Additionally, Cleveland (1995) claims that her findings from the North Atlantic subpolar gyres were comparable to the results for the Southern Ocean from Mitchell and Holmhansen (1991), a representation of the scenario that contradicts the observed trends in the Atlantic Ocean.

Some caution was taken when citing the literature for properties of stations with missing absorption data in NOMADv.2 (n=2365). In particular, reported absorption measurements, CDOM concentrations, and *Chl* may be sampled and measured differently, and particularly, not integrated over the first optical depth. For example, Cleveland (1995) claims that photoacclimation could yield similar MBR associated to different pigment compositions but similar cell size, particularly in the North Atlantic subpolar gyres. However, the NOMAD absorption measurements reflect changes in cell size more than changes due to photoadaptation because they are integrated over the first optical depth (Bricaud et al., 2004).

5.5 Final words

In understanding the sources of algorithm uncertainty through oceanic differences in the inherent optical properties, the significance of environmental factors becomes apparent. Regions that have consistently experienced certain physical conditions will be affected by those conditions over time, and this is true not only for the ocean's optical properties.

The evidence of such a phenomenon has been observed in NOMAD, suggesting that differences in the biogeochemical processes, which shape the inherent optical properties, fundamentally drive the regional differences in algorithm uncertainty. Additionally, it has been found that the effects of CDM on algorithm uncertainty are more clear than those of pigment packaging, possibly due to the complexity of

the biological factors that govern the pigment packaging, compared to the chemical and physical factors that govern the presense of CDM.

The investigation has also alluded to the scarcity of data in NOMAD. In order to observe the biogeochemical systems on regional scales, it would be ideal to collect observations of the entire range of phenomena that exist within a local region. In fact, the existing NOMAD stations with IOPs likely represent a low percent of the population of possibilities that could arise for each region covered, especially in the eutrophic and mesotrophic categories.

The conclusions of this thesis suggest that the regional approach to the development of ocean color algorithms is, in fact, a fruitful approach to reduce uncertainty in the global products. With the advancement of new technology such as ARGO floats, the goal to understand bio-optics on smaller scales appears more tenable.

Recommendations are made based on the work from each trophic category. The transient nature of water masses close to the coast strongly motivates the development of local-scale algorithms that ideally account for the characteristics unique to a specific region, especially for eutrophic waters. Results from the mesotrophic category motivate further efforts in producing bio-optical measurements from off-shore mesotrophic waters, especially in the regions mentioned, as well as mesotrophic waters from the Southern Ocean during the development and decay of the summer bloom. Results from the oligotrophic category suggest the need for further developments in measuring backscattering, and more studies on the nature of CDM in such waters.

Ultimately, this work highlights the significance in the coupling among the IOP- and AOP-based features, and the importance of consolidating regional datasets for facilitating global *in situ* analyses.

Table 5.1: **Results for the analyses of the relative influence of $a_{cdm}443/Chl$ and $a_\phi443/Chl$ on algorithm uncertainty.**

Atlantic Ocean	**Eutrophic Category (n=296)**
	OC4v.4 overestimates *Chl* (RCE > 1) by 45 % at the median. CDM absorption is greater than phytoplankton absorption for 93 % of the stations. Based on the regression, the effect of CDM ($a_{cdm}443/Chl$) on RCE is greater than that of pigment packaging ($a_\phi443/Chl$). 26 % of the variance in Δ was explained by the regression.
	Mesotrophic Category (n=81)
	OC4v.4 overestimates *Chl* (RCE > 1) by 39 % at the median. CDM absorption is greater than phytoplankton absorption for 73 % of the stations. Based on the regression, only the effect of CDM ($a_{cdm}443/Chl$) was used in the regression. The effect of pigment packaging ($a_\phi443/Chl$) was determined to be insignificant. 27 % of the variance in Δ was explained by the regression.
	Oligotrophic Category (n=14)
	OC4v.4 underestimates *Chl* (RCE < 1) by 3 % at the median. CDM absorption is greater than phytoplankton absorption for 72 % of the stations. Based on the regression, the effect of pigment packaging ($a_\phi443/Chl$) on RCE is greater than that of CDM ($a_{cdm}443/Chl$). 22 % of the variance in Δ was explained by the regression.
Pacific Ocean	**Eutrophic Category (n=38)**
	OC4v.4 underestimates *Chl* (RCE < 1) by 11 % at the median. Phytoplankton absorption is greater than CDM absorption for 74 % of the stations. Based on the regression, only the effect of CDM ($a_{cdm}443/Chl$) was used in the regression. The effect of pigment packaging ($a_\phi443/Chl$) was determined to be insignificant. 27 % of the variance in Δ was explained by the regression.
	Mesotrophic Category (n=75)
	OC4v.4 underestimates *Chl* (RCE < 1) by 20 % at the median. CDM absorption is greater than phytoplankton absorption for 72 % of the stations. Based on the regression, the effect of CDM ($a_{cdm}443/Chl$) on RCE is greater than that of pigment packaging ($a_\phi443/Chl$). 27 % of the variance in Δ was explained by the regression.
	Oligotrophic Category (n=66)
	OC4v.4 underestimates *Chl* by (RCE< 1) 13 % at the median. CDM absorption is greater than phytoplankton absorption for 76 % of the stations. Based on the regression, only the effect of CDM ($a_{cdm}443/Chl$) was used in the regression. The effect of pigment packaging ($a_\phi443/Chl$) was determined to be insignificant. 26 % of the variance in Δ was explained by the regression.
Southern Ocean	**Mesotrophic Category (n=18)**
	OC4v.4 underestimates *Chl* (RCE < 1) by 54 % at the median. Phytoplankton absorption is greater than CDM absorption for 78 % of the stations. Based on the regression, the effect of CDM ($a_{cdm}443/Chl$) on RCE is greater than that of pigment packaging ($a_\phi443/Chl$). 27 % of the variance in Δ was explained by the regression.
	Oligotrophic Category (n=21)
	OC4v.4 underestimates *Chl* (RCE < 1) by 53 % at the median. CDM absorption is greater than phytoplankton absorption for 57 % of the stations. Based on the regression, the effect of CDM ($a_{cdm}443/Chl$) on RCE is greater than that of pigment packaging ($a_\phi443/Chl$). 25 % of the variance in Δ was explained by the regression.
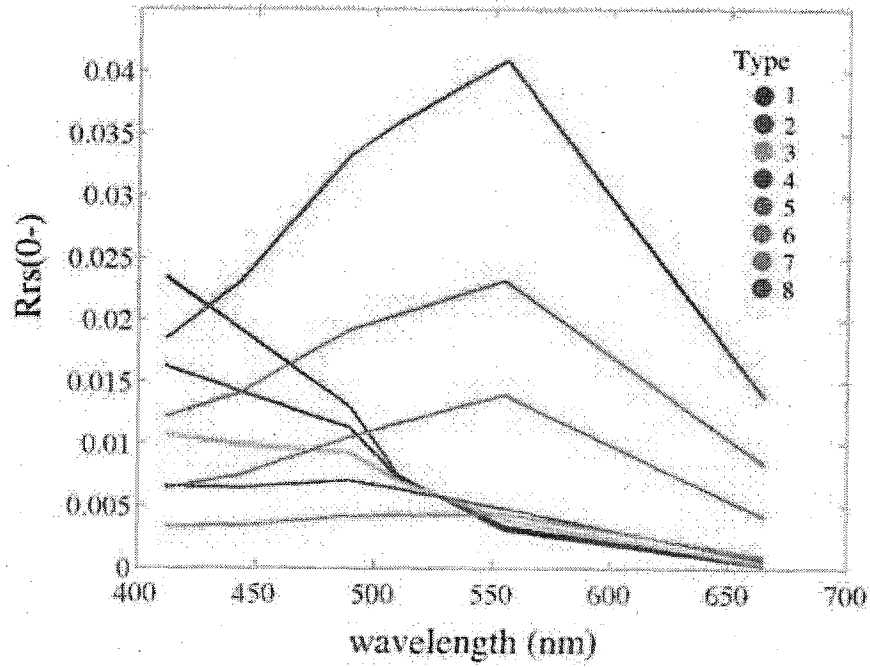
Figure 5-1: $R_{rs}(0-)$ spectra for the eight classes from Moore et al. (2009) $R_{rs}490$ is greater than $R_{rs}443$ and $R_{rs}510$ for only class 4. This work is from Moore et al. (2009).
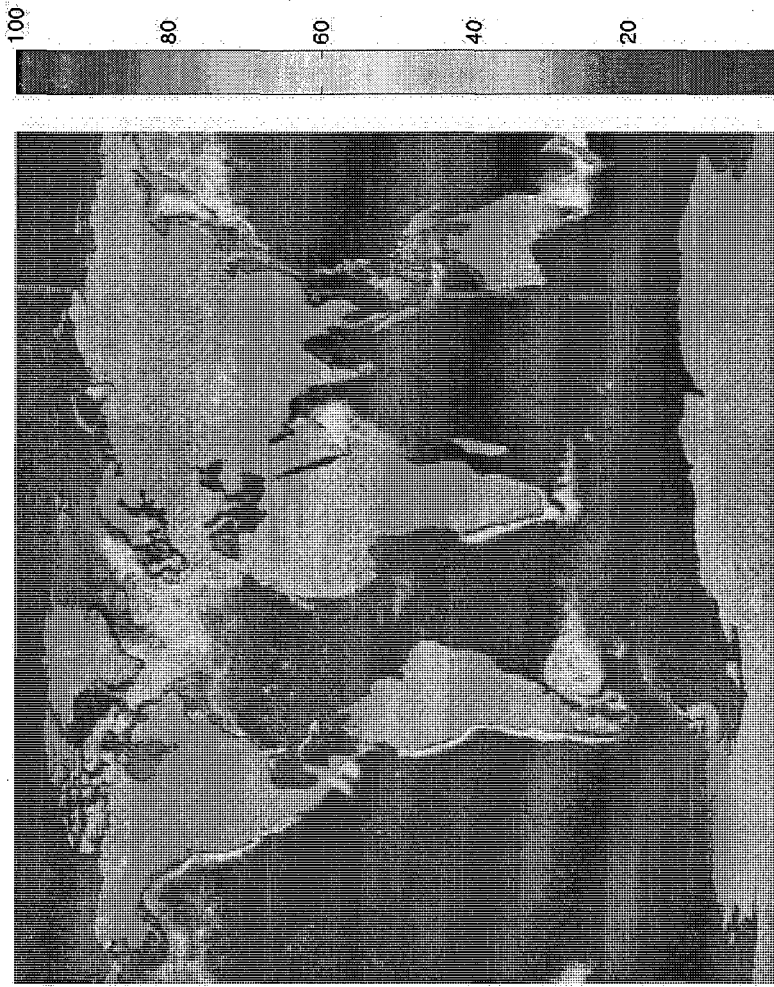
Figure 5-2: **The frequency map for mesotrophic waters in the world's oceans.** The map was derived from the application of class # 4 to global time series of 8-day composites of MODIS Aqua satellite data from 2005-2007 at 4-km resolution obtained from the NASA Ocean Color data archive (oceancolor.gsfc.nasa.gov). This work is from Moore et al. (2009)
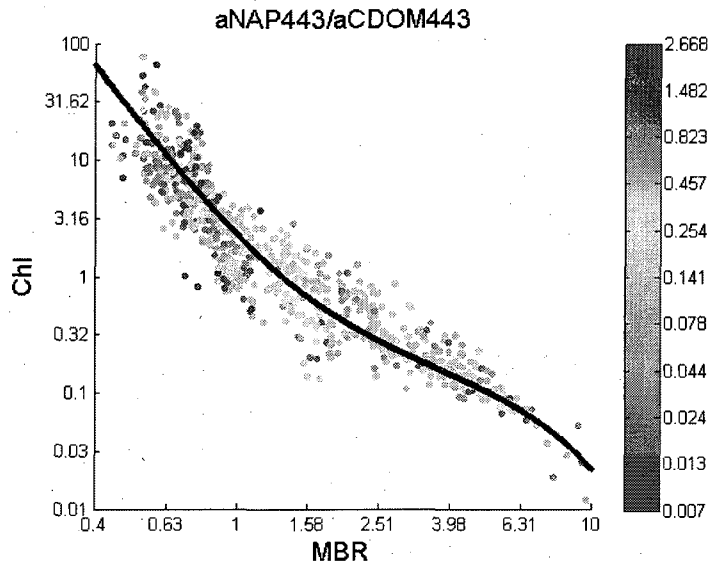
Figure 5-3: **The relative effect of NAP and CDOM on algorithm uncertainty:** $a_{nap}443/a_{cdom}443.$ The values for $a_{nap}443/a_{cdom}443$ are color-coded according to the scale shown. The ratio $a_{nap}443/a_{cdom}443$ is analyzed with respect to the *Chl*-MBR relationship for the NOMAD subset (n=696).
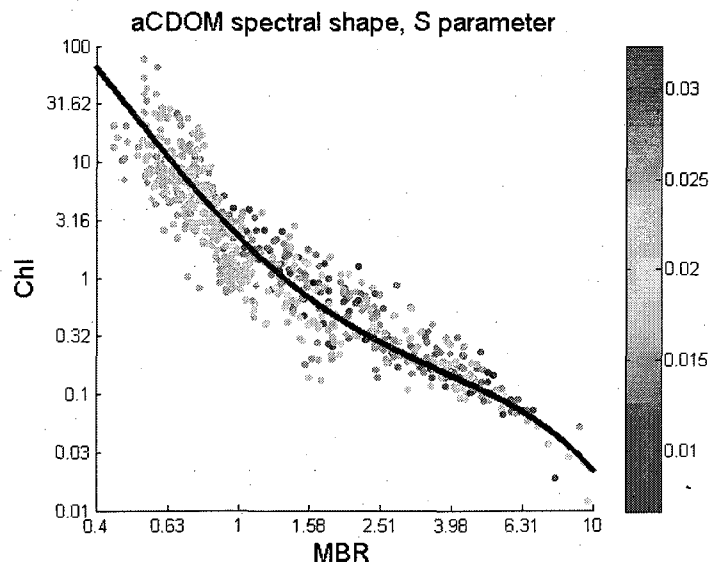
Figure 5-4: **The relative effect of the spectral shape of** a_{cdom} **on algorithm uncertainty: S from Equation 2.6.** The values for the spectral shape of a_{cdom}, S, are color-coded according to the scale shown. The S parameter is analyzed with respect to the *Chl*-MBR relationship for the NOMAD subset (n=696).

Bibliography

Ahn, Y. H., Shanmugam, P., Moon, J. E., and Ryu, J. H. (2008). Satellite Remote Sensing Of A Low-Salinity Water Plume In The East China Sea. *Annales Geophysicae*, 26(7):2019–2035.

Albert, A. and Mobley, C. (2003). An Analytical Model For Subsurface Irradiance And Remote Sensing Reflectance In Deep And Shallow Case-2 Waters. *Optics Express*, 11(22):2873–2890.

Antoine, D., Andre, J., and Morel, A. (1996). Oceanic Primary Production .2. Estimation At Global Scale From Satellite (Coastal Zone Color Scanner) Chlorophyll. *Global Biogeochemical Cycles*, 10(1):57–69.

Arrigo, K. and Brown, C. (1996). Impact Of Chromophoric Dissolved Organic Matter On Uv Inhibition Of Primary Productivity In The Sea. *Marine Ecology-Progress Series*, 140(1-3):207–216.

Arrigo, K., Robinson, D., Worthen, D., Schieber, B., and Lizotte, M. (1998). Bio-Optical Properties Of The Southwestern Ross Sea. *Journal Of Geophysical Research-Oceans*, 103(C10):21683–21695.

Austin, R. (1974). The Remote Sensing Of Spectral Radiance From Below The Ocean Surface. In Jerlov, N.G. And Nielson, E.S., editor, *Optical Aspects Of Oceanography*, pages 317–344. Academic Press, London.

Bailey, S. and Werdell, P. (2006). A Multi-Sensor Approach For The On-Orbit Validation Of Ocean Color Satellite Data Products. *Remote Sensing Of Environment*, 102(1-2):12–23.

Barbini, R., Fantoni, R., Palucci, A., Colao, F., Sandrini, S., Ceradini, S., Tositti, L., Tubertini, O., and Ferrari, G. (2003). Simultaneous Measurements Of Remote Lidar Chlorophyll And Surface Co2 Distributions In The Ross Sea. *International Journal Of Remote Sensing*, 24(19):3807–3819.

Behrenfeld, M. and Falkowski, P. (1997a). A Consumer'S Guide To Phytoplankton Primary Productivity Models. *Limnology And Oceanography*, 42(7):1479–1491.

Behrenfeld, M. and Falkowski, P. (1997b). Photosynthetic Rates Derived From Satellite-Based Chlorophyll Concentration. *Limnology And Oceanography*, 42(1):1–20.

Belanger, S., Ehn, J. K., and Babin, M. (2007). Impact Of Sea Ice On The Retrieval Of Water-Leaving Reflectance, Chlorophyll A Concentration And Inherent Optical Properties From Satellite Ocean Color Data. *Remote Sensing Of Environment*, 111(1):51–68.

Boynton, G. and Gordon, H. (2002). Irradiance Inversion Algorithm For Absorption And Backscattering Profiles In Natural Waters: Improvement For Clear Waters. *Applied Optics*, 41(12):2224–2227.

Branco, A. and Kremer, J. (2005). The Relative Importance Of Chlorophyll And Colored Dissolved Organic Matter (Cdom) To The Prediction Of The Diffuse Attenuation Coefficient In Shallow Estuaries. *Estuaries*, 28(5):643–652.

Bresnan, E., Hay, S., Hughes, S. L., Fraser, S., Rasmussen, J., Webster, L., Slesser, G., Dunn, J., and Heath, M. R. (2009). Seasonal And Interannual Variation In The Phytoplankton Community In The North East Of Scotland. *Journal Of Sea Research*, 61(1-2):17–25.

Bricaud, A., Babin, M., Morel, A., and Claustre, H. (1995). Variability In The Chlorophyll-Specific Absorption-Coefficients Of Natural Phytoplankton - Analysis And Parameterization. *Journal Of Geophysical Research-Oceans*, 100(C7):13321–13332.

Bricaud, A., Bedhomme, A., and Morel, A. (1988). Optical-Properties Of Diverse Phytoplanktonic Species - Experimental Results And Theoretical Interpretation. *Journal Of Plankton Research*, 10(5):851–873.

Bricaud, A., Claustre, H., Ras, J., and Oubelkheir, K. (2004). Natural Variability Of Phytoplanktonic Absorption In Oceanic Waters: Influence Of The Size Structure Of Algal Populations. *Journal Of Geophysical Research-Oceans*, 109(C11).

Bricaud, A., Morel, A., and Prieur, L. (1981). Absorption By Dissolved Organic-Matter Of The Sea (Yellow Substance) In The Uv And Visible Domains. *Limnology And Oceanography*, 26(1):43–53.

Bricaud, A. and Stramski, D. (1990). Spectral Absorption-Coefficients Of Living Phytoplankton And Nonalgal Biogenous Matter - A Comparison Between The Peru Upwelling Area And The Sargasso Sea. *Limnology And Oceanography*, 35(3):562–582.

Brown, C. A., Huot, Y., Werdell, P. J., Gentili, B., and Claustre, H. (2008). The Origin And Global Distribution Of Second Order Variability In Satellite Ocean Color And Its Potential Applications To Algorithm Development. *Remote Sensing Of Environment*, 112(12):4186–4203.

Bushaw, K., Zepp, R., Tarr, M., Schulzjander, D., Bourbonniere, R., Hodson, R., Miller, W., Bronk, D., and Moran, M. (1996). Photochemical Release Of Biologically Available Nitrogen From Aquatic Dissolved Organic Matter. *Nature*, 381(6581):404–407.

Bushaw-Newton, K. and Moran, M. (1999). Photochemical Formation Of Biologically Available Nitrogen From Dissolved Humic Substances In Coastal Marine Systems. *Aquatic Microbial Ecology*, 18(3):285–292.

Campbell, J. (1995). The lognormal distribution as a model for bio-optical variability in the sea. *Journal Of Geophysical Research-Oceans*, 100(C7):13,237–13,254.

Carder, K., Chen, F., Lee, Z., Hawes, S., and Kamykowski, D. (1999). Semianalytic Moderate-Resolution Imaging Spectrometer Algorithms For Chlorophyll A And Absorption With Bio-Optical Domains Based On Nitrate-Depletion Temperatures. *Journal Of Geophysical Research-Oceans*, 104(C3):5403–5421.

Carlson, C., Hansell, D., Peltzer, E., and Smith, W. (2000). Stocks And Dynamics Of Dissolved And Particulate Organic Matter In The Southern Ross Sea, Antarctica. *Deep-Sea Research Part Ii-Topical Studies In Oceanography*, 47(15-16):3201–3225.

Chami, M. and Robilliard, D. (2002). Inversion Of Oceanic Constituents In

Case I And Ii Waters With Genetic Programming Algorithms. *Applied Optics*, 41(30):6260–6275.

Ciotti, A., Lewis, M., and Cullen, J. (2002). Assessment Of The Relationships Between Dominant Cell Size In Natural Phytoplankton Communities And The Spectral Shape Of The Absorption Coefficient. *Limnology And Oceanography*, 47(2):404–417.

Clark, C., Hiscock, W., Millero, F., Hitchcock, G., Brand, L., Miller, W., Ziolkowski, L., Chen, R., and Zika, R. (2002). Cdom distribution and co2 production on the southwest florida shelf. In *Ocean Sciences Meeting 2002*, volume 89.

Clementson, L., Parslow, J., Turnbull, A., Mckenzie, D., and Rathbone, C. (2001). Optical Properties Of Waters In The Australasian Sector Of The Southern Ocean. *Journal Of Geophysical Research-Oceans*, 106(C12):31611–31625.

Cleveland, J. (1995). Regional Models For Phytoplankton Absorption As A Function Of Chlorophyll-A Concentration. *Journal Of Geophysical Research-Oceans*, 100(C7):13333–13344.

Costa, L. S., Huszar, V. L. M., and Ovalle, A. R. (2009). Phytoplankton Functional Groups In A Tropical Estuary: Hydrological Control And Nutrient Limitation. *Estuaries And Coasts*, 32(3):508–521.

Cota, G., Kottmeier, S., Robinson, D., Smith, W., and Sullivan, C. (1990). Bacterioplankton In The Marginal Ice-Zone Of The Weddell Sea - Biomass, Production And Metabolic-Activities During Austral Autumn. *Deep-Sea Research Part A-Oceanographic Research Papers*, 37(7):1145–1167.

Darecki, M. and Stramski, D. (2004). An Evaluation Of Modis And Seawifs Bio-Optical Algorithms In The Baltic Sea. *Remote Sensing Of Environment*, 89(3):326–350.

Del Vecchio, R. and Subramaniam, A. (2004). Influence Of The Amazon River On The Surface Optical Properties Of The Western Tropical North Atlantic Ocean. *Journal Of Geophysical Research-Oceans*, 109(C11).

Dierssen, H. and Smith, R. (2000). Bio-Optical Properties And Remote Sensing Ocean Color Algorithms For Antarctic Peninsula Waters. *Journal Of Geophysical Research-Oceans*, 105(C11):26301–26312.

Dister, B. and Zafiriou, O. (1993). Photochemical Free-Radical Production-Rates In The Eastern Caribbean. *Journal Of Geophysical Research-Oceans*, 98(C2):2341–2352.

Dmitriev, E. V., Khomenko, G., Chami, M., Sokolov, A. A., Churilova, T. Y., and Korotaev, G. K. (2009). Parameterization Of Light Absorption By Components Of Seawater In Optically Complex Coastal Waters Of The Crimea Peninsula (Black Sea). *Applied Optics*, 48(7):1249–1261.

Doerffer, R. and Schiller, H. (2000). Neural network for retrieval of concentrations of water constituents with the possibility of detecting exceptional out of scope spectra. In *International Geoscience And Remote Sensing Symposium*, pages 714–717.

Doerffer, R. and Schiller, H. (2007). The Meris Case 2 Water Algorithm. *International Journal Of Remote Sensing*, 28(3-4):517–535.

D'Ortenzio, F., Marullo, S., Ragni, M., D'Alcala, M., and Santoleri, R. (2002). Validation Of Empirical Seawifs Algorithms For Chlorophyll-Alpha Retrieval In The Mediterranean Sea - A Case Study For Oligotrophic Seas. *Remote Sensing Of Environment*, 82(1):79–94.

Eppley, R., Stewart, E., Abbott, M., and Heyman, U. (1985). Estimating Ocean Primary Production From Satellite Chlorophyll - Introduction To Regional Differences And Statistics For The Southern-California Bight. *Journal Of Plankton Research*, 7(1):57–70.

Evans, R. and Gordon, H. (1994). Coastal zone color scanner system calibration - a retrospective examination. *Journal Of Geophysical Research-Oceans*, 99(C4):7293–7307.

Falkowski, P. and Raven, J. (2007). *Aquatic Photosynthesis: Second Edition*. Princeton University Press.

Fenton, N., Priddle, J., and Tett, P. (1994). Regional Variations In Biooptical Properties Of The Surface Waters In The Southern-Ocean. *Antarctic Science*, 6(4):443–448.

Fiorani, L., Fantoni, R., Lazzara, L., Nardello, I., Okladnikov, I., and Palucci, A. (2006). Lidar calibration of satellite sensed cdom in the southern ocean. In *Earsel Eproceedings*, pages 89–99.

Froneman, P. and Perissinoto, R. (1996). Microzooplankton Grazing In The Southern Ocean: Implications For The Carbon Cycle. *Marine Ecology-Pubblicazioni Della Stazione Zoologica Di Napoli I*, 17(1-3):99–115.

Gao, H. and Zepp, R. (1998). Factors Influencing Photoreactions Of Dissolved Organic Matter In A Coastal River Of The Southeastern United States. *Environmental Science & Technology*, 32(19):2940–2946.

Garcia, C., Garcia, V., and Mcclain, C. (2005). Evaluation Of Seawifs Chlorophyll Algorithms In The Southwestern Atlantic And Southern Oceans. *Remote Sensing Of Environment*, 95(1):125–137.

Garver, S. and Siegel, D. (1997). Inherent Optical Property Inversion Of Ocean Color Spectra And Its Biogeochemical Interpretation .1. Time Series From The Sargasso Sea. *Journal Of Geophysical Research-Oceans*, 102(C8):18607–18625.

Gibb, S., Barlow, R., Cummings, D., Rees, N., Trees, C., Holligan, P., and Suggett, D. (2000). Surface Phytoplankton Pigment Distributions In The Atlantic Ocean: An Assessment Of Basin Scale Variability Between 50 Degrees N And 50 Degrees S. *Progress In Oceanography*, 45(3-4):339–368.

Gohin, F., Druon, J., and Lampert, L. (2002). A Five Channel Chlorophyll Concentration Algorithm Applied To Seawifs Data Processed By Seadas In Coastal Waters. *International Journal Of Remote Sensing*, 23(8):1639–1661.

Gordon, H. (1989). Can The Lambert-Beer Law Be Applied To The Diffuse Attenuation Coefficient Of Ocean Water. *Limnology And Oceanography*, 34(8):1389–1409.

Gordon, H. (1991). Absorption And Scattering Estimates From Irradiance Measurements - Monte-Carlo Simulations. *Limnology And Oceanography*, 36(4):769–777.

Gordon, H., Brown, J., Brown, O., Evans, R., and Clark, D. (1983). Nimbus-7 Czcs - Reduction Of Its Radiometric Sensitivity With Time. *Applied Optics*, 22(24):3929–3931.

Gordon, H., Brown, O., Evans, R., Brown, J., Smith, R., Baker, K., and Clark, D. (1988). A Semianalytic Radiance Model Of Ocean Color. *Journal Of Geophysical Research-Atmospheres*, 93(D9):10909–10924.

Gordon, H., Brown, O., and Jacobs, M. (1975). Computed Relationships Between Inherent And Apparent Optical-Properties Of A Flat Homogeneous Ocean. *Applied Optics*, 14(2):417–427.

Gordon, H. and Clark, D. (1981). Clear water radiances for atmospheric correction of coastal zone color scanner imagery. *Applied Optics*, 20(24):4175–4180.

Gordon, H. and Mccluney, W. (1975). Estimation Of Depth Of Sunlight Penetration In Sea For Remote-Sensing. *Applied Optics*, 14(2):413–416.

Gordon, H. and Morel, A. (1983). *Remote Assessment Of Ocean Color For Interpretation Of Satellite Visible Imagery: A Review.* Springer-Verlag, New York.

Hoepffner, N. and Sathyendranath, S. (1993). Determination Of The Major Groups Of Phytoplankton Pigments From The Absorption-Spectra Of Total Particulate Matter. *Journal Of Geophysical Research-Oceans*, 98(C12):22789–22803.

Hoge, F. and Lyon, P. (1996). Satellite Retrieval Of Inherent Optical Properties By Linear Matrix Inversion Of Oceanic Radiance Models: An Analysis Of Model And Radiance Measurement Errors. *Journal Of Geophysical Research-Oceans*, 101(C7):16631–16648.

Hooker, S., Esaias, W., Feldman, W., Gregg, W., and Mcclain, C. (1992). An Overview Of Seawifs And Ocean Color. *Nasa Tech. Memo*, 104566.

Hovis, W., Clark, D., Anderson, F., Austin, R., Wilson, W., Baker, E., Ball, D., Gordon, H., Mueller, J., Elsayed, S., Sturm, B., Wrigley, R., and Yentsch, C. (1980). Nimbus-7 Coastal Zone Color Scanner - System Description And Initial Imagery. *Science*, 210(4465):60–63.

Huot, Y., Morel, A., Twardowski, M., Stramski, D., and Reynolds, R. (2008). Particle optical backscattering along a chlorophyll gradient in the upper layer of the eastern South Pacific Ocean. *Biogeosciences*, 5:495–507.

Jerlov, N. (1976). *Optical Oceanography*. Elsevier, New York.

Kahru, M. and Mitchell, B. (1999). Empirical Chlorophyll Algorithm And Preliminary Seawifs Validation For The California Current. *International Journal Of Remote Sensing*, 20(17):3423–3429.

Karl, D. and Tien, G. (1991). Bacterial Abundances During The 1989-90 Austral Summer Phytoplankton Bloom In Teh Gerlache Straite. *Antarctic Journal Of The United States*, 26:147–149.

Kieber, D., Mcdaniel, J., and Mopper, K. (1989). Photochemical Source Of Biological Substrates In Sea-Water - Implications For Carbon Cycling. *Nature*, 341(6243):637–639.

Kieber, R., Li, A., and Seaton, P. (1999). Production Of Nitrite From The Photodegradation Of Dissolved Organic Matter In Natural Waters. *Environmental Science & Technology*, 33(7):993–998.

Kirk, J. (1981). Estimation Of The Scattering Coefficient Of Natural Waters Using Underwater Irradiance Measurements. *Australian Journal Of Marine Freshwater Research*, 32:533–539.

Kirk, J. (1994a). Estimation Of The Absorption And Scattering Coefficient Of Natural Waters By Use Of Underwater Irradiance Measurements. *Applied Optics*, 33:3276–3278.

Kirk, J. (1994b). *Light And Photosynthesis In Aquatic Ecosystems, Second Edition*. Cambridge University Press.

Kitchen, J. and Zaneveld, J. (1992). A 3-Layered Sphere Model Of The Optical-Properties Of Phytoplankton. *Limnology And Oceanography*, 37(8):1680–1690.

Kitidis, V., Stubbins, A. P., Uher, G., Goddard, R. C. U., Law, C. S., and Woodward, E. M. S. (2006). Variability Of Chromophoric Organic Matter In Surface

Waters Of The Atlantic Ocean. *Deep-Sea Research Part Ii-Topical Studies In Oceanography*, 53(14-16):1666–1684.

Kowalczuk, P., Durako, M. J., Young, H., Kahn, A. E., Cooper, W. J., and Gonsior, M. (2009). Characterization Of Dissolved Organic Matter Fluorescence In The South Atlantic Bight With Use Of Parafac Model: Interannual Variability. *Marine Chemistry*, 113(3-4):182–196.

Lee, Z. and Carder, K. (2002). Effect Of Spectral Band Numbers On The Retrieval Of Water Column And Bottom Properties From Ocean Color Data. *Applied Optics*, 41(12):2191–2201.

Lee, Z., Carder, K., and Arnone, R. (2002). Deriving Inherent Optical Properties From Water Color: A Multiband Quasi-Analytical Algorithm For Optically Deep Waters. *Applied Optics*, 41(27):5755–5772.

Loisel, H., Meriaux, X., Berthon, J.-F., and Poteau, A. (2007). Investigation Of The Optical Backscattering To Scattering Ratio Of Marine Particles In Relation To Their Biogeochemical Composition In The Eastern English Channel And Southern North Sea. *Limnology And Oceanography*, 52(2):739–752.

Loisel, H. and Stramski, D. (2000). Estimation Of The Inherent Optical Properties Of Natural Waters From The Irradiance Attenuation Coefficient And Reflectance In The Presence Of Raman Scattering. *Applied Optics*, 39(18):3001–3011.

Longhurst, A., Sathyendranath, S., Platt, T., and Caverhill, C. (1995). An Estimate Of Global Primary Production In The Ocean From Satellite Radiometer Data. *Journal Of Plankton Research*, 17(6):1245–1271.

Lutz, V. A., Subramaniam, A., Negri, R. M., Silva, R. I., and Carreto, J. I. (2006). Annual Variations In Bio-Optical Properties At The 'Estacion Permanente De Estudios Ambientales (Epea)' Coastal Station, Argentina. *Continental Shelf Research*, 26(10):1093–1112.

Macdonald, G. M., Beilman, D. W., Kremenetski, K. V., Sheng, Y., Smith, L. C., and Velichko, A. A. (2006). Rapid Early Development Of Circumarctic Peatlands And Atmospheric Ch4 And Co2 Variations. *Science*, 314(5797):285–288.

Mannino, A., Russ, M. E., and Hooker, S. B. (2008). Algorithm Development And Validation For Satellite-Derived Distributions Of Doc And Cdom In The Us Middle Atlantic Bight. *Journal Of Geophysical Research-Oceans*, 113(C7).

Maritorena, S., Siegel, D., and Peterson, A. (2002). Optimization Of A Semi-analytical Ocean Color Model For Global-Scale Applications. *Applied Optics*, 41(15):2705–2714.

Martin, S. (2004). *Ocean Remote Sensing*, page 134. Cambridge University Press, Cambridge, UK.

Maske, H. and Haardt, H. (1987). Quantitative Invivo Absorption-Spectra Of Phytoplankton - Detrital Absorption And Comparison With Fluorescence Excitation-Spectra. *Limnology And Oceanography*, 32(3):620–633.

Mcclain, C., Feldman, G., Hooker, S., and Bontempi, P. (2006). Satellite Data For Ocean Biology, Biogeochemistry, And Climate Research. *Eos Transactions*, 87(34):337–343.

Mcclelland, J., Dery, S., Peterson, B., Holmes, R., and Wood, E. (2006). A Pan-Arctic Evaluation Of Changes In River Discharge During The Latter Half Of The 20th Century. *Geophysical Research Letters*, 33(6).

Menesguen, A. and Gohin, F. (2006). Observation And Modelling Of Natural Retention Structures In The English Channel. *Journal Of Marine Systems*, 63(3-4):244–256.

Miller, W. and Zepp, R. (1995). Photochemical Production Of Dissolved Inorganic Carbon From Terrestrial Organic-Matter - Significance To The Oceanic Organic-Carbon Cycle. *Geophysical Research Letters*, 22(4):417–420.

Mitchell, B. (1992). Predictive Biooptical Relationships For Polar Oceans And Marginal Ice Zones. *Journal Of Marine Systems*, 3(1-2):91–105.

Mitchell, B. and Holmhansen, O. (1991). Observations And Modeling Of The Antarctic Phytoplankton Crop In Relation To Mixing Depth. *Deep-Sea Research Part A-Oceanographic Research Papers*, 38(8-9):981–1007.

Mitchell, B. and Kiefer, D. (1988a). Chlorophyll-Alpha Specific Absorption And Fluorescence Excitation-Spectra For Light-Limited Phytoplankton. *Deep-Sea Research Part A-Oceanographic Research Papers*, 35(5):639–663.

Mitchell, B. and Kiefer, D. (1988b). Variability In Pigment Specific Particulate Fluorescence And Absorption-Spectra In The Northeastern Pacific-Ocean. *Deep-Sea Research Part A-Oceanographic Research Papers*, 35(5):665–689.

Mobley (1994). *Light And Water: Radiative Transfer In Natural Waters*. Academic Press, San Diego, Ca.

Moore, T., Campell, J., and Dowell, M. (2009). A Class-Based Approach For Characterizing The Uncertainty Of The Modis Chlorophyll Product. *Remote Sensing Of The Environment*, 113:2424–2430.

Mopper, K. and Zhou, X. (1990). Hydroxyl Radical Photoproduction In The Sea And Its Potential Impact On Marine Processes. *Science*, 250(4981):661–664.

Moran, M. and Zepp, R. (1997). Role Of Photoreactions In The Formation Of Biologically Labile Compounds From Dissolved Organic Matter. *Limnology And Oceanography*, 42(6):1307–1316.

Morel, A. (1974). Optical properties of pure water and pure seawater. In Jerlov, N. and Nielsen, E., editors, *Optical Aspects Of Oceanography*, pages 1–24. Academic Press.

Morel, A. (1987). Chlorophyll-Specific Scattering Coefficient Of Phytoplankton - A Simplified Theoretical Approach. *Deep-Sea Research Part A-Oceanographic Research Papers*, 34(7):1093–1105.

Morel, A. (1988). Optical Modeling Of The Upper Ocean In Relation To Its Biogenous Matter Content (Case-I Waters). *Journal Of Geophysical Research-Oceans*, 93(C9):10749–10768.

Morel, A. and Ahn, Y. (1991). Optics Of Heterotrophic Nanoflagellates And Ciliates - A Tentative Assessment Of Their Scattering Role In Oceanic Waters Compared To Those Of Bacterial And Algal Cells. *Journal Of Marine Research*, 49(1):177–202.

Morel, A., Antoine, D., and Gentili, B. (2002). Bidirectional Reflectance Of Oceanic Waters: Accounting For Raman Emission And Varying Particle Scattering Phase Function. *Applied Optics*, 41(30):6289–6306.

Morel, A. and Berthon, J. (1989). Surface Pigments, Algal Biomass Profiles, And Potential Production Of The Euphotic Layer - Relationships Reinvestigated In View Of Remote-Sensing Applications. *Limnology And Oceanography*, 34(8):1545–1562.

Morel, A. and Bricaud, A. (1981). Theoretical Results Concerning Light-Absorption In A Discrete Medium, And Application To Specific Absorption Of Phytoplankton. *Deep-Sea Research Part A-Oceanographic Research Papers*, 28(11):1375–1393.

Morel, A., Claustre, H., Antoine, D., and Gentili, B. (2007). Natural Variability Of Bio-Optical Properties In Case 1 Waters: Attenuation And Reflectance Within The Visible And Near-Uv Spectral Domains, As Observed In South Pacific And Mediterranean Waters. *Biogeosciences*, 4(5):913–925.

Morel, A. and Gentili, B. (1991). Diffuse Reflectance Of Oceanic Waters - Its Dependence On Sun Angle As Influenced By The Molecular-Scattering Contribution. *Applied Optics*, 30(30):4427–4438.

Morel, A. and Gentili, B. (1993). Diffuse-Reflectance Of Oceanic Waters .2. Bidirectional Aspects. *Applied Optics*, 32(33):6864–6879.

Morel, A. and Gentili, B. (1996). Diffuse Reflectance Of Oceanic Waters .3. Implication Of Bidirectionality For The Remote-Sensing Problem. *Applied Optics*, 35(24):4850–4862.

Morel, A. and Gordon, H. (1980). Report Of The Working Group On Water Color. *Boundary Layer Meteorology*, 18:343–355.

Morel, A. and Maritorena, S. (2001). Bio-Optical Properties Of Oceanic Waters: A Reappraisal. *Journal Of Geophysical Research-Oceans*, 106(C4):7163–7180.

Morel, A. and Prieur, L. (1977). Analysis Of Variations In Ocean Color. *Limnology And Oceanography*, 22(4):709–722.

Morrow, J., Chamberlin, W., and Kiefer, D. (1989). A 2-Component Description Of Spectral Absorption By Marine Particles. *Limnology And Oceanography*, 34(8):1500–1509.

Mueller, J., Bidigare, R., Trees, C., Balch, W., Dore, J., Drapeau, D., Karl, D., Van Heukelem, L., and Perl, J. (2003a). *Ocean Optics Protocols For Satellite Ocean Color Sensor Validation, Revision 5*. Nasa Tech. Memo, Greenbelt:Nasa Goddard Space Flight Center, Rev5-Vol.V edition.

Mueller, J., Morel, A., Frouin, R., Davis, C., Arnone, R., Carder, K., Lee, Z., Steward, R., Hooker, S., Mobley, C., McLean, S., Holben, B., Miller, M., Pietras, C., Knobelspiesse, K., Fargion, G., Porter, J., and Voss, K. (2003b). *Ocean Optics Protocols For Satellite Ocean Color Sensor Validation, Revision 4*. Nasa Tech. Memo, Greenbelt:Nasa Goddard Space Flight Center, Rev4-Vol.III edition.

Nelson, N. and Siegel, D. (2002). Chromophoric dom in the open ocean. In Hansell, D. and Carlson, C., editors, *Biogeochemistry Of Marine Dissolved Organic Matter*, pages 545–578. Academic Press, San Diego, Ca.

Nelson, N. B., Siegel, D. A., Carlson, C. A., Swan, C., Smethie, Jr., W. M., and Khatiwala, S. (2007). Hydrography Of Chromophoric Dissolved Organic Matter In The North Atlantic. *Deep-Sea Research Part I-Oceanographic Research Papers*, 54(5):710–731.

O'Reilly, J., Maritorena, S., Siegel, D., O'Brien, M., Toole, D., Mitchell, G., Kahru, M., Chavez, F., Strutton, P., Cota, G., Hooker, S., McClain, C., Carder, K., F., M.-K., Harding, L., Magnuson, A., Phinney, D., Moore, G., Aiken, J., Arrigo, K., Letelier, R., and Culver, M. (2002). Ocean color chlorophyll a algorithms for seawifs, oc2, and oc4: Version 4 in: O'reilly, j.e., and 24 coauthors, 2000: Seawifs postlaunch calibration and validation analyses, part 3. Technical memo, NASA, Goddard Space Flight Center.

Palmer, J. and Totterdell, I. (2001). Production And Export In A Global Ocean Ecosystem Model. *Deep-Sea Research Part I-Oceanographic Research Papers*, 48(5):1169–1198.

Pan, X., Mannino, A., Russ, M. E., and Hooker, S. B. (2008). Remote Sensing Of The Absorption Coefficients And Chlorophyll A Concentration In The United States Southern Middle Atlantic Bight From Seawifs And Modis-Aqua. *Journal Of Geophysical Research-Oceans*, 113(C11).

Pegau, S., Zaneveld, R., Mitchell, G., Mueller, J., Kahru, M., Wieland, J., and Stramska, M. (2002). Ocean optics protocols for satellite ocean color sensor validation, revision 4. Technical memo, NASA, Goddard Space Flight Center.

Polimene, L., Allen, J. I., and Zavatarelli, M. (2006). Model Of Interactions Between Dissolved Organic Carbon And Bacteria In Marine Systems. *Aquatic Microbial Ecology*, 43(2):127–138.

Pope, R. and Fry, E. (1997). Absorption Spectrum (380-700 Nm) Of Pure Water .2. Integrating Cavity Measurements. *Applied Optics*, 36(33):8710–8723.

Preisendorfer, R. (1960). Application Of Radiative Transfer Energy To Light Measurements In The Sea. In *Symposium On Radiant Energy In The Sea*, pages 11–30.

Prieur, L. and Sathyendranath, S. (1981). An Optical Classification Of Coastal And Oceanic Waters Based On The Specific Spectral Absorption Curves Of Phytoplankton Pigments, Dissolved Organic-Matter, And Other Particulate Materials. *Limnology And Oceanography*, 26(4):671–689.

Riemer, D., Milne, P., Zika, R., and Pos, W. (2000). Photoproduction Of Nonmethane Hydrocarbons (Nmhcs) In Seawater. *Marine Chemistry*, 71(3-4):177–198.

Roesler, C. and Perry, M. (1995). In-Situ Phytoplankton Absorption, Fluorescence Emission, And Particulate Backscattering Spectra Determined From Reflectance. *Journal Of Geophysical Research-Oceans*, 100(C7):13279–13294.

Roesler, C., Perry, M., and Carder, K. (1989). Modeling Insitu Phytoplankton Absorption From Total Absorption-Spectra In Productive Inland Marine Waters. *Limnology And Oceanography*, 34(8):1510–1523.

Sathyendranath, S., Longhurst, A., Caverhill, C., and Platt, T. (1995). Regionally And Seasonally Differentiated Primary Production In The North Atlantic. *Deep-Sea Research Part I-Oceanographic Research Papers*, 42(10):1773–1802.

Sathyendranath, S., Prieur, L., and Morel, A. (1989). A 3-Component Model Of Ocean Color And Its Application To Remote-Sensing Of Phytoplankton Pigments In Coastal Waters. *International Journal Of Remote Sensing*, 10(8):1373–1394.

Schiller, H. and Doerffer, R. (2005). Improved Determination Of Coastal Water Constituent Concentrations From Meris Data. *Ieee Transactions On Geoscience And Remote Sensing*, 43(7):1585–1591.

Segar, D. (2007). *Introduction to Ocean Sciences*. W.W. Norton & Company, New York & London.

Shields, A. R. and Smith, W. O. (2009). Size-Fractionated Photosynthesis/Irradiance Relationships During Phaeocystis Antarctica-Dominated Blooms In The Ross Sea, Antarctica. *Journal Of Plankton Research*, 31(7):701–712.

Siegel, D., Maritorena, S., Nelson, N., and Behrenfeld, M. (2005a). Independence And Interdependencies Among Global Ocean Color Properties: Reassessing The Bio-Optical Assumption. *Journal Of Geophysical Research-Oceans*, 110(C7).

Siegel, D., Maritorena, S., Nelson, N., Behrenfeld, M., and Mcclain, C. (2005b). Colored Dissolved Organic Matter And Its Influence On The Satellite-Based Characterization Of The Ocean Biosphere. *Geophysical Research Letters*, 32(20).

Siegel, D., Maritorena, S., Nelson, N., Hansell, D., and Lorenzi-Kayser, M. (2002). Global Distribution And Dynamics Of Colored Dissolved And Detrital Organic Materials. *Journal Of Geophysical Research-Oceans*, 107(C12).

Smith, R. and Baker, K. (1981). Optical-Properties Of The Clearest Natural-Waters (200-800 Nm). *Applied Optics*, 20(2):177–184.

Sogandares, F. and Fry, E. (1997). Absorption Spectrum (340-640 Nm) Of Pure Water .1. Photothermal Measurements. *Applied Optics*, 36(33):8699–8709.

Stedmon, C. and Markager, S. (2001). The Optics Of Chromophoric Dissolved Organic Matter (Cdom) In The Greenland Sea: An Algorithm For Differentiation Between Marine And Terrestrially Derived Organic Matter. *Limnology And Oceanography*, 46(8):2087–2093.

Steinberg, D., Nelson, N., Carlson, C., and Prusak, A. (2004). Production Of Chromophoric Dissolved Organic Matter (Cdom) In The Open Ocean By Zooplankton And The Colonial Cyanobacterium Trichodesmium Spp. *Marine Ecology-Progress Series*, 267:45–56.

Stramski, D., Boss, E., Bogucki, D., and Voss, K. (2004). The Role Of Seawater Constituents In Light Backscattering In The Ocean. *Progress In Oceanography*, 61(1):27–56.

Stramski, D. and Kiefer, D. (1991). Light-Scattering By Microorganisms In The Open Ocean. *Progress In Oceanography*, 28(4):343–383.

Sverdrup, H. (1953). On Conditions For The Vernal Blooming Of Phytoplankton. *J. Du Conseil*, pages 287–295.

Szeto, M., Campbell, J., and Moore, T. (2006). Reducing the Uncertainty in the MODIS and SeaWiFS Chlorophyll Algorithms. Research & Discover Internship at UNH.

Tagliabue, A. and Arrigo, K. (2003). Anomalously Low Zooplankton Abundance In The Ross Sea: An Alternative Explanation. *Limnology And Oceanography*, 48(2):686–699.

Tang, K. W., Smith, Jr., W. O., Elliott, D. T., and Shields, A. R. (2008). Colony Size Of Phaeocystis Antarctica (Prymnesiophyceae) As Influenced By Zooplankton Grazers. *Journal Of Phycology*, 44(6):1372–1378.

Tarran, G. A., Heywood, J. L., and Zubkov, M. V. (2006). Latitudinal Changes In The Standing Stocks Of Nano- And Picoeukaryotic Phytoplankton In The Atlantic Ocean. *Deep-Sea Research Part Ii-Topical Studies In Oceanography*, 53(14–16):1516–1529.

Twardowski, M., Boss, E., Sullivan, J., and Donaghay, P. (2004). Modeling The Spectral Shape Of Absorption By Chromophoric Dissolved Organic Matter. *Marine Chemistry*, 89(1-4):69–88.

Twardowski, M., Lewis, M., Barnard, A., and Zaneveld, J. (2005). In-water instrumentation and platforms for ocean color remote sensing applications. In Miller, R., Del Castillo, C., and Mckee, B., editors, *Remote Sensing Of Coastal Aquatic Waters*, pages 60–100. Springer Publishing, Dordrecht, Netherlands.

Twardowski, M. S., Claustre, H., Freeman, S. A., Stramski, D., and Huot, Y. (2007). Optical Backscattering Properties Of The 'Clearest' Natural Waters. *Biogeosciences*, 4(6):1041–1058.

Vaillancourt, R., Brown, C., Guillard, R., and Balch, W. (2004). Light Backscattering Properties Of Marine Phytoplankton: Relationships To Cell Size, Chemical Composition And Taxonomy. *Journal Of Plankton Research*, 26(2):191–212.

Valentine, R. and Zepp, R. (1993). Formation Of Carbon-Monoxide From The Photodegradation Of Terrestrial Dissolved Organic-Carbon In Natural-Waters. *Environmental Science & Technology*, 27(2):409–412.

Vodacek, A., Blough, N., Degrandpre, M., Peltzer, E., and Nelson, R. (1997). Seasonal Variation Of Cdom And Doc In The Middle Atlantic Bight: Terrestrial Inputs And Photooxidation. *Limnology And Oceanography*, 42(4):674–686.

Werdell, P. and Bailey, S. (2005). An Improved In-Situ Bio-Optical Data Set For Ocean Color Algorithm Development And Satellite Data Product Validation. *Remote Sensing Of Environment*, 98(1):122–140.

Werdell, P. J., Bailey, S. W., Franz, B. A., Harding, Jr., L. W., Feldman, G. C., and Mcclain, C. R. (2009). Regional And Seasonal Variability Of Chlorophyll-A In Chesapeake Bay As Observed By Seawifs And Modis-Aqua. *Remote Sensing Of Environment*, 113(6):1319–1330.

Williams, P. (1998). The Balance Of Plankton Respiration And Photosynthesis In The Open Oceans. *Nature*, 394(6688):55–57.

Zaneveld, J. (1995). A Theoretical Derivation Of The Dependence Of The Remotely-Sensed Reflectance Of The Ocean On The Inherent Optical-Properties. *Journal Of Geophysical Research-Oceans*, 100(C7):13135–13142.

Zaneveld, J. and Kitchen, J. (1995). The Variation In The Inherent Optical-Properties Of Phytoplankton Near An Absorption Peak As Determined By Various Models Of Cell Structure. *Journal Of Geophysical Research-Oceans*, 100(C7):13309–13320.

Zdanowski, M. and Donachie, S. (1993). Bacteria In The Sea-Ice Zone Between Elephant-Island And The South-Orkneys During The Polish Sea-Ice Zone Expedition, (December 1988 To January 1989). *Polar Biology*, 13(4):245–254.

Zhai, P.-W., Hu, Y., Trepte, C. R., and Lucker, P. L. (2009). A Vector Radiative Transfer Model For Coupled Atmosphere And Ocean Systems Based On Successive Order Of Scattering Method. *Optics Express*, 17(4):2057–2079.